TECHNISCHE UNIVERSITÄT MÜNCHEN

Department Chemie

Lehrstuhl für Biotechnologie

The human and *C.elegans* Hsp90 chaperone machinery in the context of steroid receptor clients

Kaziales Anna

Vollständiger Abdruck der von der Fakultät für Chemie der Technischen Universität München zur Erlangung des akademischen Grades eines

Doktors der Naturwissenschaften (Dr. rer. nat.)

genehmigten Dissertation.

Vorsitzender: Univ.-Prof. Dr. Johannes Buchner

Prüfer der Dissertation:

1. Priv.-Doz. Dr. Klaus Richter

2. Univ.-Prof. Dr. Matthias Feige

Die Dissertation wurde am 1. März 2021 bei der Technischen Universität München eingereicht und durch die Fakultät für Chemie am 26. Mai 2021 angenommen.

Publications

Part of this thesis is published or is currently in the process of being submitted for publication. The equal contribution of authors is indicated with a star.

- **Kaziales, A**., Barkovits, K., Marcus, K., and Richter, K. (2020) Glucocorticoid receptor complexes form cooperatively with the Hsp90 co-chaperones Pp5 and FKBPs. *Scientific Reports* 10, 10733.
- Rasmus Ree*, Laura Kind*, **Anna Kaziales**, Sylvia Varland, Minglu Dai, Klaus Richter, Adrian Drazic, and Thomas Arnesen. (2020) PFN2 and NAA80 cooperate to efficiently acetylate the N-terminus of actin. *Journal of Biological Chemistry*, Volume 295, Issue 49, 16713– 16731
- Maike Krause, Katharina Sessler, **Anna Kaziales**, Richard Grahl, Sabrina Noettger, Holger Barth, and Herbert Schmidt. (2019) Variants of Escherichia coli Subtilase Cytotoxin Subunits Show Differences in Complex Formation In Vitro. *Toxins*, 11(12): 703.
- (in preparation)

  Anna Kaziales, Florian Rührnößl, Johannes Buchner and Klaus Richter. Glucocorticoid resistance conferring mutation in the C-terminus of GR alters the receptor conformational dynamics.

Table of Contents

Abstract

The function of steroid receptors in the cell depends on the chaperone machinery of Hsp90, as Hsp90 primes steroid receptors for hormone binding and transcriptional activation. Several conserved Hsp90 cochaperones are known to additionally participate in receptor·chaperone assemblies but the precise events that take place upon receptor maturation are not understood in detail. It is also unknown to what extent the contribution of these cofactors is conserved in other eukaryotes. In the context of this thesis the reconstituted *C.elegans* and human chaperone assemblies were examined. The nematode phosphatase PPH-5 and the prolyl isomerase FKB-6 were found to facilitate the formation of glucocorticoid receptor (GR) complexes with HSP-90. Within these complexes, HSP-90 can perform its closing reaction more efficiently. By combining chemical crosslinking and mass spectrometry, contact sites within these assemblies were defined and were used to construct models for GR·HSP-90 and the trimeric GR·HSP90·FKB-6/PPH-5 complexes. A basis for a FRET system that can potentially provide details on the HSP-90 conformational cycle was set. Compared to the nematode Hsp90 system, the human system shows less cooperative client interaction and a stricter requirement for the co-chaperone p23 to complete the closing reaction of GR·Hsp90·Pp5/Fkbp51/Fkbp52 complexes. In both systems, hormone binding to GR is accelerated by Hsp90 alone and in the presence of its cofactors. These results show that cooperative complex formation and hormone binding patterns are, in many aspects, conserved between the nematode and human systems. Gaining insight into the conformational requirements for GR to bind ligand, coactivator, DNA and Hsp90β was attempted by observing the behavior of a glucocorticoid resistant mutant. This GR variant, harbors a single point mutation in the last C-terminal residues, L773P, that causes decreased affinity to hormone. Using *in vitro* and *in silico* methods, the conformational consequences of this mutation were assigned to particular GR elements. A particularly interesting part of these results was the monitoring of GR's conformational dynamics after binding to Hsp90β that became possible by HD/X. An aryl hydrocarbon receptor construct was successfully purified for further Hsp90 investigations. Lastly, whole genome data from microarray analyses upon selective Hsp90β inhibition and steroid receptor activation were collected in order to identify modified signaling pathways.

Zussamenfassung

Die Funktion von Steroidrezeptoren in der Zelle hängt von der Chaperon Maschinerie von Hsp90 ab, da Hsp90 Steroidrezeptoren in ihre aktive Konformation umwandelt. Es ist bekannt, dass mehrere konservierte Hsp90 Cochaperone zusätzlich an Rezeptor·Chaperon Anordnungen beteiligt sind, aber die genauen Ereignisse, die bei der Rezeptorreifung stattfinden, sind nicht im Detail bekannt. Es ist auch nicht bekannt, inwieweit der Beitrag dieser Cofaktoren in anderen Eukaryoten erhalten bleibt. Im Rahmen dieser Arbeit wurden die rekonstituierten C.elegans und menschlich Chaperon Anordnungen untersucht. Es wurde gefunden, dass die Nematodenphosphatase PPH-5 und die Prolylisomerase FKB-6 die Bildung von Glucocorticoidrezeptor (GR) -Komplexen mit HSP-90 erleichtern. Innerhalb dieser Komplexe kann HSP-90 seine Abschlussreaktion effizienter durchführen. Durch Kombination von chemischer Vernetzung und Massenspektrometrie wurden Kontaktstellen innerhalb dieser Anordnungen definiert und zur Konstruktion von Modellen für GR HSP-90 und die trimerischen GR HSP90 FKB-6/ PPH-5-Komplexe verwendet. Es wurde eine Basis für ein FRET-System festgelegt, das möglicherweise Details zum HSP-90-Konformationszyklus liefern kann. Im Vergleich zum Nematoden-Hsp90-System zeigt das menschliche System eine weniger kooperative Client-Interaktion und eine strengere Anforderung an das cohaperon p23, um die Abschlussreaktion von GR Hsp90 Pp5 / Fkbp51/ Fkbp52 Komplexen zu vervollständigen. In beiden Systemen wird die Hormonbindung an GR durch Hsp90 allein und in Gegenwart seiner Cofaktoren beschleunigt. Diese Ergebnisse zeigen, dass kooperative Komplexbildung und Hormonbindungsmuster in vielen Aspekten zwischen dem Nematoden und dem menschlichen System erhalten bleiben. Durch Beobachtung des Verhaltens einer Glucocorticoid-resistenten Mutante wurde versucht, einen Einblick in die Konformationsanforderungen für GR zur Bindung von Ligand, Coaktivator, DNA und Hsp90β zu erhalten. Diese Variante enthält eine Einzelpunktmutation im GR's C-terminalen Peptid, L773P, die eine verminderte Affinität zum Hormon verursacht. Unter Verwendung von *in-vitro* und in-silico Methoden wurden die Konformationsfolgen dieser Mutation bestimmten GR-Elementen zugeordnet. Ein besonders interessanter Teil dieser Ergebnisse war die Überwachung der Konformationsdynamik von GR nach Bindung an Hsp90β, die durch HD / X möglich wurde. Ein Arylkohlenwasserstoffrezeptorkonstrukt wurde erfolgreich für weitere Hsp90-Untersuchungen gereinigt. Zuletzt wurden Gesamtgenomdaten aus Microarray Analysen zur selektiven Hsp90β-Hemmung und Steroidrezeptoraktivierung gesammelt, um modifizierte Signalwege zu identifizieren.

1. Introduction

1.1 Allostasis, Homeostasis, Proteostasis

Homeostasis is conventionally thought of as a synchronic servomechanism that maintains the *status quo* for organismal physiology (1). The homeostasis concept has been extended in the recent years to better explain stress, recognizing that what is optimal under basal conditions is different under stress (1,2). The concept of allostasis, maintaining stability through change, is fundamental for organisms adjusting to predictable and unpredictable events (2). Allostatic systems are adaptive and have a broad range of operating levels: the autonomic nervous system, the immune system, the HPA axis and cardiovascular systems are all mobilized (3).

Nearly every biological process involves proteins, the most versatile and structurally complex macromolecules. Proteins face various challenges in reaching and maintaining their active or "native state": post-translational modifications, changes in cell physiology, the appearance or change in concentration of small-molecule ligands (4-6). A significant fraction of mammalian proteins are intrinsically unstructured and may adopt an active conformation only upon binding to other macromolecules or membranes (7-12). Due to the complexity of maintaining a healthy proteome, organisms have invested in an extensive network of factors that maintain proteome integrity and provide adaptation to changes in the environment (6,7,10,12). These proteins are able to prevent aberrant interactions and aggregation in the crowded cellular environment (10,13). The mechanisms that cells use for protein quality control and maintenance of proteome homeostasis, proteostasis, are crucial for organismal health and constitute some of the most fundamental and medically relevant problems in biology (5,7). There is a growing need to expand our knowledge of these phenomena because human disturbance, global climate change and pollution are all major perturbations of the environment (2). How vertebrates respond to the unpredictable in general will thus, have important conservation value for the future.(2)

1.2 Protein Folding

Proteins are chains of amino acids encoded in the nucleotide sequence of the respective gene and must fold, through a complex energy landscape, into precise three-dimensional conformations to fulfill their biological functions (7,11,12,14).

A major milestone in protein research was the thermodynamic hypothesis of Christian Anfinsen, who supported that all the information required for a polypeptide to properly fold is encoded in the amino acid sequence (15,16) Many small proteins readily refold *in vitro*, which highlights how the amino acid sequence, encoded in the DNA, contains the necessary information to dictate the three-dimensional structure of a protein (11,14)(12). The fact that proteins quickly fold to their native conformation despite the vast amount of possible configurations that would demand an enormously long time to sample, is known as Levinthal's Paradox (17,18). It soon became clear that not all proteins can refold *in vitro* but are subjected to unspecific aggregation, and insoluble cytosolic aggregates, inclusion bodies, were observed (4,11,14,19,20).

The set of conformations that a folding protein might adopt can be likened to a landscape: polypeptide chains explore a funnel-shaped potential energy surface towards the energy minimum corresponding to their native structure (Figure 1.1) (7,11,21-24). The folding problem has been a fundamental question in biology (6,10,25-28). Most recently, AlphaFold, an artificial intelligence algorithm developed by Google's DeepMind, achieved to solve one of the most important aspects of the folding problem: accurate prediction of protein structures that can match or outcompete state-of-the art-experimental results (29,30). Even though this step forward was broadly perceived as a watershed moment, the folding code question: what balance of forces encodes native structures, remains (24,30,31).

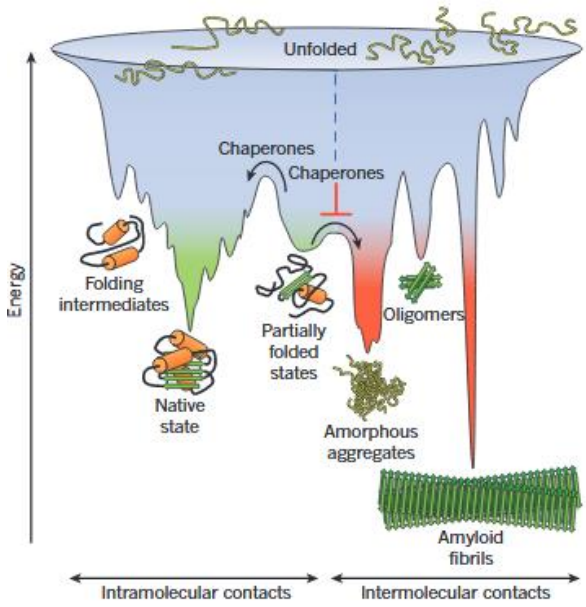

Figure 1.1. Competing reactions of protein folding and aggregation. Scheme of the funnel shaped free energy surface that proteins explore as they move towards the native state by forming intramolecular contacts. Adapted from (4,7).

Partially folded or misfolded protein states are at high risk of aggregation, since they have exposed hydrophobic elements accessible for intermolecular, besides intramolecular, contacts (6,7,11). Organisms invested in molecular chaperones to control and assist the folding of nascent or misfolded proteins, so that they don't fall in a "kinetic trap" of the complex energy landscape (7,10,11,32).

A healthy and adaptive proteostasis network does not only require the strict control of protein synthesis and folding but also conformational maintenance and regulation of abundance, localization, and degradation (6,11,33). Numerous diseases, such as Parkinson's disease, Huntigton's disease, amyotrophic lateral sclerosis and Alzheimer's disease, are associated to protein aggregation (4,5,33,34). Such diseases are age-related, due to the decline of proteostasis, along with the ability to upregulate chaperones in response to stressors that comes with aging and triggers disease manifestation, which further accelerates proteostasis decline (4,7,33,34).

1.3 Molecular Chaperones

A molecular chaperone by definition, is any protein that interacts with, stabilizes or helps another protein to acquire its functionally active conformation without being present in its final structure (7,11). The major chaperone families are classified according to their molecular weights (namely Hsp40, Hsp60, Hsp70, Hsp90, Hp100 and the small Hsps) and were initially discovered due to their involvement and elevated expression during the heat shock response (7,11,12). However, their roles in proteome maintenance and other cellular processes are essential also under physiological conditions (6,11,12). The Hsp60s (the chaperonins), Hsp70s and Hsp90s are molecular machines that use ATP hydrolysis and cofactor-regulated binding and release cycles to accomplish their folding missions (6,7,11). Chaperone binding to hydrophobic regions of a non-native protein prevents aggregation while ATP-triggered substrate release allows folding to proceed (7,32). The present work will focus on the chaperone machinery of Hsp90.

1.4 The Hsp90 molecular chaperone

Heat shock protein 90 (Hsp90) is an ATP-driven molecular machine, highly conserved and abundant in the cytosol and acts as the central hub of proteostasis (6,11,12,35). Susan Lindquist first proposed that Hsp90 acts as a capacitor for morphological variation (36). This chaperone machinery is involved in numerous essential biological processes, to name a few, signal transduction, chromatin remodeling, cellular trafficking, development and the immune response (6,32,35,37-39). A detailed network, constructed by Picard and coworkers, demonstrates the wide spectrum of Hsp90 activity (Figure 1) (38).

In humans, Hsp90 exists in two isoforms in the cytosol, Hsp90α– the stress-inducible, and Hsp90β–the constitutively expressed isoform. Besides cytosolic Hsp90s, the organelle-specific Grp94 and TRAP1 reside in endoplasmic reticulum (ER) and mitochondria (32,40). Hsp90 is recruited to hundreds of diverse client proteins (a full list of known Hsp90 interactors is maintained by the Picard lab: https://www.picard.ch/downloads/Hsp90interactors) that require energy-intense rearrangements. Unlike molecular chaperones, such as Hsp70, that

bind unfolded/nascent polypeptides, Hsp90 maintains client proteins in a nearly folded conformation poised to respond to an activation signal, such as hormone binding or phosphorylation (32,41). This diverse client set seems to be defined by the exposure of hydrophobic residues and general conformational instability (39).

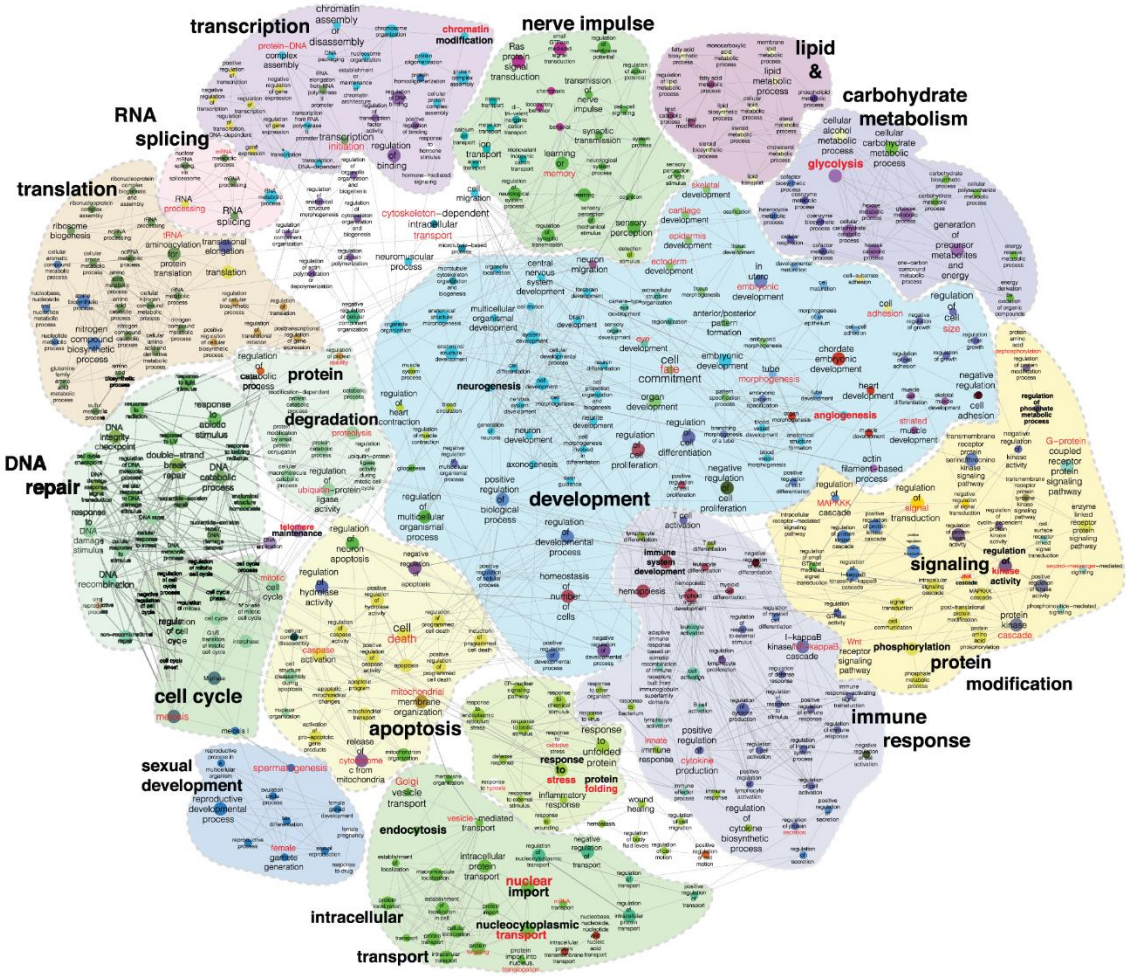

Figure1.2. Functional map of Hsp90 interactome, adapted from (38).

Hsp90 is a homodimer. Monomeric Hsp90 consists of three conserved domains: the N-terminal nucleotide binding domain (NBD), the middle domain (MD) and the C-terminal dimerization domain (CTD), all of which have been implicated in client and cofactor binding (Figure 1.3) (7,11,12,42-45). A flexible, charged linker modulates NBD·MD contacts while a C-

terminal (MEEVD) motif is important for interaction with cochaperones that contain tetratricopeptide repeat (TPR) domains (46-54).

All examined forms of Hsp90, from bacteria to *H. sapiens*, bind and hydrolyze ATP (12,55-57). Dimerization of Hsp90 occurs via the C-terminal domains and the *apo*-state of Hsp90 predominantly samples an open V-shaped conformation (11,58). Binding of ATP to the N-terminal domain triggers dimerization of the Hsp90 NBDs and leads to Hsp90 sampling a series of distinct conformations (Figure 1.3) (11,12,56-62).

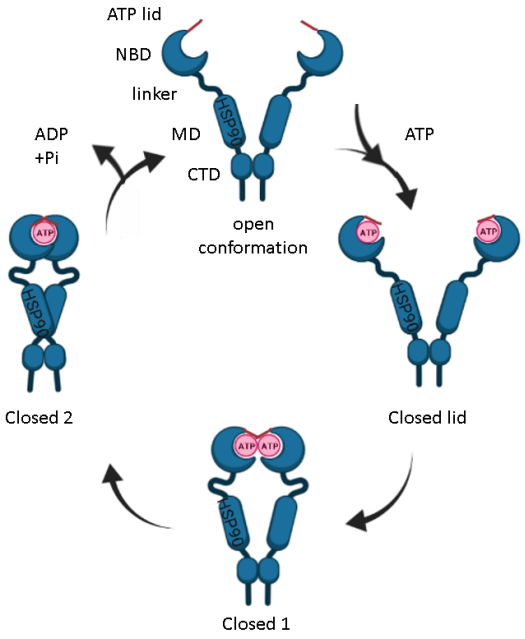

Figure 1.3. Hsp90 domains and conformational cycle. Hsp90 predominantly adopts a V-shaped conformation in the absence of ATP. Upon ATP binding, the N-terminal lid segment closes onto the ATP binding pocket. Conformational rearrangements occur in the NBD and the NBD domains dimerize to form closed state 1. This conformation is followed by the completely closed state 2, in which MD and NBD contact each other and stabilize the catalytic active conformation. Post ATP-hydrolysis, Hsp90 returns to the *apo*-state, releasing ADP and phosphate. Figure was generated with Biorender.

Hsp90 has a weak intrinsic ATP hydrolysis activity that is under allosteric regulation and directly affected by binding of cochaperones and client proteins (35,62-71). Several single

switches, dispersed in the chaperone structure have been reported but their coupling is not well understood (70,72-77). Verkhivker and coworkers, upon systematic examination of molecular and network signatures of these switches, recently supported that regulation of Hsp90 by cochaperones p23 and Aha1 and the p53 client protein may be determined by distinct intramolecular communication “spines” (63,78). It is by know well established that Hsp90 can adopt a number of structurally distinct conformations during the ATPase cycle and that it forms a variety of complexes with clients and cochaperones, but it is unclear how Hsp90 promotes the activation of a client protein (35,79).

1.5 Hsp90 cochaperones

More than 20 Hsp90 cochaperones have been identified in the eykaryotic cell (6). Client-specific cofactors tailor the Hsp90 machinery into a client-specific mode and regulate the conformational changes while providing further interaction sites for the clients (6,12,61,80-85). Cochaperones not only regulate the progression of the Hsp90 conformational cycle, but they may also be involved in client recognition (12,39,86). The large majority of Hsp90 cochaperones contain one or more structural domains composed of tetratricopeptide repeat (TPR) motifs, which bind to the conserved (MEEVD) peptide of Hsp90’s CTD (46,53,54,87). Despite their common binding mode, these cochaperones have diverse functions. Table 1.1 provides a summary of the major Hsp90 cofactors and their (known) functions.

Table 1.1. Major Hsp90 cochaperones of higher eukaryotes. Adapted from (12,45,81). Table refers to the human homologs of these conserved proteins.

Cochaperone	Function	TPR domain
Hop	adaptor for Hsp70 and Hsp90,ATPase inhibitor for Hsp90	✓
PP5	Phosphatase, dephosphorylates HSP90; maturation of clients	✓
Fkbp51, Fkbp52	peptidyl prolyl isomerase, involved in SHR activation	✓
p23	ATPase inhibitor, stabilization of the closed 2 state	
Cyp40	Peptidyl prolyl isomerase, involved in SHR activation	✓
Aha1	ATPase activator	
Tah1	component of the R2TP complex	✓
Cdc37	Kinase-specific cochaperone, ATPase inhibitor	
TTC4	genetic interaction with Cpr7; regulator of protein translation	✓
Sgt1	part of the ubiquitin ligase complex, involved in kinetochore assembly and plant immunity, adaptor for clients	
CHIP	E3 ubiquitin ligase, interaction with Hsp70	✓
Unc45	Myosin-dependent processes	✓

1.6 Hsp90 and steroid hormone receptors

Steroid hormones are vital regulators of reproductive, growth and homeostatic processes (88). The steroid hormone receptor (SHR) mode of action is well studied: they bind to hormone, undergo conformational changes and translocate to the nucleus, where they modulate gene expression (89). Like many signaling proteins, all mammalian steroid hormone receptors are strictly dependent on the chaperone machinery of Hsp90 to acquire their active conformation (88,90-92).

Hsp90-containing SHR complexes were first identified in the 1980s (93-96). In these studies, SHRs, such as the glucocorticoid (GR), mineralocorticoid (MR) or progesterone receptors (ER), were isolated from vertebrate cells and the associated proteins were identified and studied by western blot analyses. Hsp90 and several other proteins were detected in these complexes,

leading to the identification of Fkbp51, Fkbp52, Cyp40, Hop, p23, Hip and Pp5 as the components of SHR complexes (97-104). Later, studies reported on an ATP-dependent series of events, in which at least Hsp40, Hsp70, Hop, Hsp90 and p23 participate (88,90,105,106). It is well accepted that during chaperone complex assembly, the ligand-binding cleft of the receptor is opened to allow hormone binding, an event followed by dramatic conformational changes, so in the end, a mature receptor can translocate to the nucleus (106). This is supported by recent observations: Hsp90·Cdc37 separates the domains of Cdk4 kinase, leading to a less compact state and was also found to stabilize an open state of the RISC Argonaute protein, Ago2 (84,107).

Cochaperones differentially affect SHR·Hsp90 complexes, serving as control elements of their maturation process (44,53,59,105,108,109). The adaptor protein Hop transfers SHRs from Hsp70 to Hsp90 binding both chaperones through its two separate TPR domains (12,51,52,64,110). TPR cochaperones may bind competitively to the (MEEVD) motif of Hsp90 and for instance the immunophilins Fkbp51, Fkbp52, Cyp40 and phosphatase Pp5 can all be identified in mature SHR Hsp90·p23 complexes (111). Despite the high homology of Fkbp51 and Fkbp52, these cochaperones differentially associate with the different SHR complexes and their opposing effects were observed on GR activation by Hsp90 (11,59,90,111-113). Binding of hormone is observed to substitute Fkbp51 with Fkbp52 in GR·Hsp90 complexes (114).On the other hand, while Fkbp51 is a negative regulator of GR, it is reported to be a positive regulator of the androgen receptor (AR) (115-117). Evidence supports that Fkbp51 suppresses GR signaling and retains the receptor complex in the cytoplasm while Fkbp52 is involved in dynein interaction and translocation of the GR to the nucleus (118,119). Pp5 is recovered from both nuclear and cytoplasmic GR and overexpression of Pp5's TPR prevents the binding of Fkbp52 (120). It has been suggested that there is a hierarchical effect these TPR cofactors have on GR that follows the order Fkbp52> Pp5> Fkbp51 (121,122). Cochaperone p23 that slows down the ATPase activity and stabilizes the closed Hsp90 conformation was found to directly interact with GR through a helical motif in the protein tail (83).

Despite these (and many more) findings and the fact that SHR·Hsp90·cochaperone complexes have long been identified and played a key role in Hsp90 research as obligate clients, the answers to what is their exact mechanistic contribution or which transformations take place are missing.

1.7 The Glucocorticoid Receptor

As mentioned in the previous section, one of the most studied substrates of Hsp90 that plays a central role in the maintenance of basal and stress-related homeostasis, and the one most employed in the present work, is GR, encoded in *NR3C1* (123,124).

Glucocorticoids (GCs) are some of the most pervasive messengers and GR is expressed in nearly all cells, regulating a plethora of functions in health and disease (124). GR also regulates many functions of the central nervous system such as cognition, mood and sleep (125). Realization that these hormones have such a pervasive role led to widespread use of GC-like ligands to treatment of a wide variety of conditions, like adrenal insufficiency and inflammatory-related conditions (126).

GR shares the conserved within the SHR family domain architecture: an N-terminal transactivation domain (AF-1, aa 1-417), a zinc-finger DNA-binding domain (DBD, aa 418-487), a short hinge region (aa 488-520) and a ligand-binding domain (LBD, aa 521-777) (126). The GR LBD bound to the dexamethasone ligand (DEX) consists of in total 11 α-helices and 4 β-strands that form 2 short β-sheets (126). SHR crystal structures with agonist ligands like DEX, have shown that the C-terminal α-helix, the activation function-2 (AF-2), serves in forming the lid of the ligand binding pocket (Figure 1.4) (126). Structures with antagonist ligands show this element displaced (127).

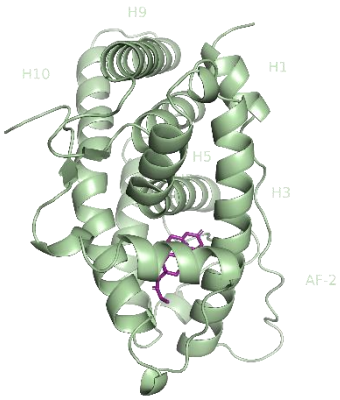

Figure 1.4. GR LBD agonist conformation (PDB ID 5NFP).

As discussed in the previous chapter, in the absence of ligand, GR is part of a multi-protein complex containing Hsp90 90 and other cochaperones. After participating in a series of chaperone assemblies and binding to ligand, a hyper-phosphorylated and transcriptionally active GR is transported to the nucleus (92). It then homo- or heterodimerizes, recruits coactivators/corepressors and/or other transcription factors, binds to glucocorticoid response elements (GREs) and modulates many distinct gene networks (124). These multifunctional proteins dock on GR through leucine-rich, amphipathic α-helices (LXXLL) (128). Moreover, the ligand-activated membrane-bound GR is reported to mediate non-genomic events, such as triggering the activation of kinase signaling cascades, including the mitogen.-activated protein kinase (MAPK) or the phosphatidylinositol 3-kinase (PI3K) pathways (129).

Regarding its interaction with the chaperone machinery, it is by now established that interaction with the Hsp70 system, preceding binding of GR to Hsp90, is an important phase of GR maturation, a step at which Hsp70 partially unfolds the GRLBD (104,105). It has been shown that while bound to Hsp70 and Hsp40, GR's ligand binding domain (LBD) lacks the essential structural determinants for ligand binding (105). Hsp90 and both nucleotide binding and hydrolysis are required to reverse the Hsp70 inhibition, likely by promoting Hsp70 release from GRLBD (105). GR bound to Hsp40 and Hsp70 is transferred to Hsp90 with the assistance of Hop. As soon as GR is delivered to Hsp90/ATP, Hsp70 and Hsp40 are released and a PPIase may bind (11). GR bound to Hsp90 exhibits high affinity for the hormone and p23 stabilizes the closed Hsp90 conformation (11). Post ATP hydrolysis, hormone-bound GR, cochaperones and ADP are released so Hsp90 can enter a new cycle. As mentioned in the previous section, the actual transformations on GR are yet to be clarified (11).

1.8 Glucocorticoid Resistance

Primary Generalized Glucocorticoid Resistance (PGGR) or Chrousos syndrome is a condition characterized by generalized, partial tissue insensitivity to glucocorticoids (130). Patients with PGGR have defective GC negative feedback loops, which lead to compensatory hyperactivation of the HPA axis (130-132). The elevated plasma adrenocorticotropic hormone (ACTH) causes adrenal hyperplasia and increased production of steroid precursors. The

molecular basis of this condition is attributed to mutations in the human glucocorticoid receptor-α gene (*NR3C1*), which impair one or multiple aspects of GR action. The impairment originates from the decreased affinity to hormone and thus, alters tissue sensitivity to GCs (130,133). To date, 24 different GC resistant mutants have emerged in the clinic, in the DBD or the LBD of GR, causing a broad spectrum of clinical manifestations of variable severity (130,132,134-137). Symptoms, when PGGR is pronounced, are relevant to mineralocorticoid and/or androgen excess, for instance hypofertility, hypertension, hypokalemic alkalosis, hirsutism, acne as well as profound anxiety and depression (130). In addition, some patients exhibiting GC resistance do not harbor a mutation in the *NR3C1* gene, which implies that other factors participating in GC signal transduction, might as well be responsible for impaired GC sensitivity (138). *In vitro* studies on such mutations in the context of Hsp90 may help explain the requirements for this remarkable molecule's transformation into a mature receptor.

PGGR was in a case caused by a heterozygous mutation (T→C) at nucleotide position 2318 (exon 9) of the hGRα gene, which results in substitution of leucine by proline at amino acid position 773 in GR's C-terminus (132). The affected young woman reported fatigue, anxiety and was diagnosed with hyperandrogenism and hypertension (132). Deletion of the last 14 residues is reported to be causing alterations in hormone binding specificity and significant reduction in the GR-mediated transactivation of target-genes (139,140). This conserved region is required for ligand binding; however the differential hormone-binding capacities of SHRs are not encoded by this element (139). The described point mutation will be addressed throughout this thesis.

1.9 Hsp90 inhibitors

Hsp90 is a chaperone responsible for the folding of clients directly associated with cancer progression, it was found upregulated in several types of cancer and inhibition of the machinery is thought to have promising therapeutic potential (79,141-143). In fact, proteins associated with all 10 hallmarks of cancer are dependent on the Hsp90 protein folding machinery, whose inhibition results in suppression of numerous oncogenic pathways (79,144). Hsp90 is certainly an essential protein, but the fact that non-cancer cells require a smaller pool of chaperone molecules, compared to cancer cells that exhibit Hsp90 "addiction", seems to

leave a promising therapeutic window (12,145,146). Within the tumor environment Hsp90 is thought to have an altered epichaperome compared to healthy cells that may potentially provide further vulnerability towards inhibition (145). In addition, ATP adopts an unusual binding mode in Hsp90's NTD allowing the targeting of Hsp90 chaperone activity by small molecules (143).

The first identified and perhaps most described inhibitors of Hsp90 are the macrocyclic geldanamycin and radicicol that have limited *in vivo* potential, while later, several studies have attempted to improve the pharmacological properties of these ansamycin and resorcinol scaffolds (79,143,146-153). Other synthetic molecules, for example pyrazole and purine scaffolds (e.g PU-H71) or inhibitors like epigallocatechin, novobiocin, sansalvamide A, and derivatives that target Hsp90's CTD domain to disrupt interactions with the TPR cochaperones have been reported (154-158). Other inhibitors like derrubone, withaferin A and celastrol aim to block binding of Cdc37 to Hsp90 and the small molecule gedunin selecitively blocks recruitment of p23 (159).

To date, development of Hsp90 inhibitors led 17 compounds that bind the NBD of the chaperone and decrease cellular levels of cancer-related factors to clinical trials (143,146). All of them have the major disadvantage that exhibit activity against all four Hsp90 isoforms (pan-inhibition), which causes the induction of the pro survival heat shock response and other toxic events (160,161). The development of isoform selective inhibitors may be a way to limit the detrimental effects of pan-inhibition and lately, studies towards this direction have been published (144,162,163). Recently, the first N-terminal isoform-selective inhibitor was rationally designed by taking advantage of the subtle differences in the ATP binding pockets of Hsp90α and Hsp90β (144). This inhibitor, KUNB31, exhibited 50-fold selectivity for Hsp90β, was selectively active against cancer cells while preventing Hsp90 induction and indicates that isoform-selective inhibition may indeed be a promising way to limit the toxicity of targeting Hsp90 with small molecules (144).

1.10 The aryl hydrocarbon receptor

The aryl hydrocarbon receptor is a member of the Pern-Arnt-Sim (163) superfamily of transcription factors, initially thought to be a sensor for xenobiotic substances and the regulator of enzymes such as the cytochrome P450s that metabolize such chemicals (164,165). AHR's involvement in toxicological responses against environmental contaminants like 2,3,7,8-tetrachlorodibenzo-p-dioxin (TCDD) and polycyclic aromatic hydrocarbons gave the receptor its name but later, a number of indoles provided by the diet, microorganisms, metabolism, and pollution emerged as AHR activators (164,166,167). Importantly, there is evidence that AHR plays important roles in homeostasis, the immune response, stem cell maintenance and cellular differentiation, upon binding to this increasing number of ligands (164-166).

AHR is localized in the cytoplasm in a complex with Hsp90, the TPR cochaperone AHR-interacting protein (AIP or Xap2 or Ara9), the Hsp90 cochaperone p23 and the c-SRC protein kinase (167-171). These studies provided with evidence that Hsp90 is required for ligand binding and AHR function *in vivo*, holding the receptor in a conformation of high affinity for its ligands (97,170,171). Upon ligand binding AHR undergoes conformational changes and translocates to the nucleus, where it controls the transcription of multiple target genes.

Hankinson and coworkers reported that AHR interacts with other transcription factors like NF-κB, c-Maf, the retinoic acid receptor, the estrogen receptor E2F and retinoblastoma protein (Rb) to modulate gene expression (164,172). AHR can also influence chromatin remodeling by interacting with the SWI/SNF chromatin-remodeling complex and the steroid receptor coactivator-1 complex (SRC-1) and by displacing histone deacetylase complexes (173,174). Additionally, it is involved in a number of epigenetic mechanisms like micro-RNA, retrotransposon and long non-coding RNA regulation and can act as an E3 ubiquitin ligase that targets sex steroid receptors for degradation (164,175). Opitz and coworkers identified the tryptophan catabolite kynurenine (Kyn) as an endogenous AHR ligand that is constitutively produced by human tumours, suppresses antitumour immune responses and promotes tumour survival and motility through the AHR (176). Emerging evidence suggest that AHR promotes clonogenicity and invasiveness of cancer cells while transgenic mice with a

constitutive active AHR spontaneously develop tumours (176-179). AHR repressor, AHRR, was found to act as a tumour suppressor in multiple human cancers (180).

AHR seems to be a convergence point of several signaling pathways in health and disease and importantly, to regulate cancer progression and responses to xenobiotics. Understanding its messages and interactions may, therefore, have therapeutic potential in the context of autoimmunity and cancer (164,165,176,181).

1.11 *C. elegans'* Hsp90 and nuclear receptors

Thanks to the conserved nature of the chaperone system, studies on model organisms have helped gain substantial knowledge on heat shock proteins and importantly, much knowledge on the Hsp90 machinery originates from the *S. cerevisiae* system. However, multicellular organisms have developed further client/cofactor sets. The nematode *C.elegans* is an organism that only has 959 differentiated cells, a defined developmental pathway and a similar to *H.sapiens* set of Hsp90 cofactors. It encodes one cytosolic Hsp90 isoform, DAF-21 and importantly, one large PPIase, FKB-6, highly homologous to human Fkbps (182,183). FKB-6 exhibits 42.3% sequence identity compared to human Fkp52, 41.3% to Fkbp51 while it harbors a calmodulin binding region at its C-terminus, like Fkbp52 (Supplementary Figure 1).

Research on DAF-12, one of the numerous nuclear receptors (NRs) of *C.elegans*, supports that its physiological hormone is a sterol derivative (dafachronic acid- bile acid-like) (184-186). Studies on DAF-12 provided the first evidence for any kind of lipophilic hormone in the nematode (185). It exhibits high homology with the Vitamin D receptor and it is believed, that a DAF-12/co-regulator complex functions as a hormone regulated switch, specifying fast life history (reproductive development, developmental advance, fat metabolism, accelerated aging) in the presence of ligand and slow life history (dauer diapause, delayed development, fat storage and retarded aging) in its absence (185-187).

Despite the astounding expansion of nuclear receptors in C. elegans that harbors 284 of them in its genome, in contrast to only 48 found in humans, only ~20 *C.elegans* NRs have described visible phenotypes, only 15 have distinct homologs in other species while it is unclear why do

worms have so many receptors (185). Due to the limited, especially structural data on the *C.elegans* Hsp90 system, it is yet not clear to what extent the contribution of Hsp90 and its cofactors is conserved in C.elegans NR processing. In the context of this thesis, a DAF-12 LBD construct was purified and was tested for HSP-90 interaction, aiming to study the nematode chaperone with a native NR client. Since this attempt was unsuccessful, GRLBD was used as a model substrate to examine the nematode Hsp90 system.

1.12 Protein Phosphatase 5

Protein Phosphatase 5 (Pp5) is a serine/threonine phosphoprotein phosphatase (PPP) that dephosphorylates numerous signaling proteins. It contains a conserved C-terminal αJ phosphatase domain and unlike other members of this family, such as PP1, PP2A and PP2B, also contains a TPR domain at its N-terminus (188,189). An interaction between these two domains maintains the enzyme in an auto-inhibited state that limits substrate entry to the active site of the phosphatase and results in a low basal activity *in vitro* (189) .Hsp90 and fatty acids, including arachidonic acid, stimulate phosphatase activity (190).

Experiments in yeast showed that deletion of the *ppt1* gene leads to hyperphosphorylation of Hsp90 *in vivo* and an apparent decrease in the efficiency of the Hsp90 chaperone system (191). Pp5 dephosphorylation activity is modulated by Hsp90, which disrupts auto-inhibition of the phosphatase (188). This interaction is dependent on the C-terminal MEEVD motif of Hsp90 that binds to the TPR domain of the phosphatase (188,191). Haslbeck et al recently showed how C-terminal Hsp90 fragments differentialy stimulate the phosphatase activity of PPH-5 (188). This study also suggests that ternary complexes with GR are cooperatively formed with full-length HSP-90 and PPH-5.

Separase is a highly conserved protease required for chromosome segregation and mutations in the *C.elegans* separase gene, *sep-1*, are embryonic lethal (192,193). A study aiming to identify factors that influence the activity of separase in cortical granule exocytosis and cytokinesis, identified a mutation in the protein phosphatase 5 (*pph-5*) gene, together with an in-frame deletion of 50 amino acids in the TPR region, as extragenic suppressors of separase (193). A more recent ENU mutagenesis suppressor screen, identified further intragenic

mutations, *pph-5* mutations, spanning across the TPR and phosphatase domains of PPH-5, and also a mutation on HSP-90's CTD (192). Depletion of *pph-5* caused no phenotypes on its own, but was effective in restoring localization of mutant separase to vesicles and suppressing cortical granule exocytosis and cytokinesis phenotypes (193).

Interestingly, recent studies on the human system uncovered a previously unrecognized function of Hsp90 in membrane remodelling that is required for exosome release (194). Although observations linking separase to membrane trafficking events have been made, it is still not clear how separase achieves this function (192,195). Identification of an HSP-90 mutation that can suppress separase, besides numerous mutations of PPH-5, supports the hypothesis that HSP-90 acts via its regulation of PPH-5 but the possibility that HSP-90 directly regulates separase independently of PPH-5, can not be excluded.

2. Objective

This thesis aimed to initially examine the conserved principles between the nematode and human Hsp90 chaperone assemblies on the molecular level. We were interested to see the consequences of binding of client and cofactors to Hsp90 assemblies and the extent to which the chaperone could progress its conformational cycle. This was addressed by reconstituting the Hsp90 chaperone assemblies from the *C.elegans* and human systems, which made clear that the two nematode cofactors, PPH-5 and FKB-6, facilitate GR·HSP-90 complex formation, an effect that is observed also for their human counterparts. Model structures of the nematode assemblies were constructed through a combination of crosslinking-MS and crosslink-guided molecular docking to get insight into the topology of these complexes, and answer whether an interaction between cofactor and client would be possible on the chaperone scaffold. Hormone binding properties of GR within these assemblies were also examined and show similar binding patterns that imply a high degree of conservation between the two systems.

A glucocorticoid resistance conferring mutation in the C-terminus of GR was employed in an attempt to understand the conformational requirements for GR to bind ligand, coactivator, DNA and the Hsp90β machinery. With this investigations the impairment could be assigned to specific GR elements while also observing the non-mutated GR mode of action. The events following hormone binding to GR and/or inhibition of the Hsp90 machinery were approached also on the whole-genome level. Microarray analyses were performed in order to identify modified pathways as a consequence of dexamethasone binding and selective Hsp90β inhibition, as this approach could reveal chaperone·SHR specific interactions on whole-genome resolution.

3. Materials & Methods

3.1 Materials & Equipment

Table 3.1. Reagents. All chemicals were of molecular biology grade and were dissolved/diluted in ddH_2O or DMSO.

Name	Source
LB-medium powder	Serva (Heidelberg, Germany)
Bacto Tryptone	Serva (Heidelberg, Germany)
Adenosin-5`-triphosphate (ATP)	Roche (Mannheim, Germany)
Adenosin-5`-[γ-thio]-triphosphate (ATPγS) tetralithium salt	Sigma (St. Louis, USA)
Adenosine-5´-diphosphate (ADP), Disodium salt	Roche (Mannheim, Germany)
5'–Adenylyl-ß,γ-imido-triphosphate (AMP-PNP)	Roche (Mannheim, Germany)
BS^3	Creative Molecules Inc.
DSSG	Creative Molecules Inc.
Acetonitrile	Sigma (St. Louis, USA)
Acrylamide (38 %)	Roth (Karlsruhe, Germany)
Agarose	Serva (Heidelberg, Germany)
Agar	Serva (Heidelberg, Germany)
Ammoniumperoxodisulfate	Serva (Heidelberg, Germany)
Bacto Tryptone	Serva (Heidelberg, Germany)
Bromophenol blue S	Serva (Heidelberg, Germany)
β-mercaptoethanol	Serva (Heidelberg, Germany)
bis-sulfo-succinimidyl-suberate(BS^3)	Creative Molecules (Scottsdale, USA)
CHAPS	Roth (Karlsruhe, Germany)
Coomassie brilliant blue	Serva (Heidelberg, Germany)
Corticosterone	Sigma (St. Louis, USA)
Clear G	Serva (Heidelberg, Germany)
Dexamethasone	Serva (Heidelberg, Germany)
Dimethylsulfoxid (DMSO)	Serva (Heidelberg, Germany)
1,4-Dithiothreitol (DTT)	Roth (Karlsruhe, Germany)
Ethanol, p.a	Merck, Darmstadt, Germany
Ethylenediamintetraacidic acid (EDTA)	Serva (Heidelberg, Germany)
Glycerol	Roth (Karlsruhe, Germany)
Glucose	Serva (Heidelberg, Germany)
Glycine	Serva (Heidelberg, Germany
Hydrochloric acid	Sigma (St. Louis, USA)
Imidazole	Sigma (St. Louis, USA)
Ispopropanol	Sigma (St. Louis, USA)
Isopropyl-β-D-thiogalaktopyranosid (IPTG)	Merck, Darmstadt, Germany
Kanamycin	Roth (Karlsruhe, Germany)
Lactose	Sigma (St. Louis, USA)
N-(2-Hydroxyethyl)-piperazine-N'-2-ethan-sulfonic acid (HEPES)	Roth, Karlsruhe, Germany
N, N,N',N'-Tetramethylethylendiamin (TEMED)	Serva (Heidelberg, Germany

NADH	Sigma (St. Louis, USA)
Phosphoenolpyruvate (PEP)	Sigma (St. Louis, USA)
Protease Inhibitor Mix HP	Serva, (Heidelberg, Germany)
Radicicol	Sigma (St. Louis, USA)
Sodiumdodecylsulfate (SDS)	Serva, (Heidelberg, Germany)
SYPRO orange	Invitrogen, (La Jolla, USA)
Tris-(Hydroxymethyl)-aminomethane (Tris)	Roth, Karlsruhe, Germany
$CaCl_2$	Roth (Karlsruhe, Germany)
$MgCl_2$	Roth (Karlsruhe, Germany)
KH_2PO_4	Roth (Karlsruhe, Germany)
$KHPO_4$	Roth (Karlsruhe, Germany)
KCl	Roth (Karlsruhe, Germany)
Na_2HPO_4	Roth (Karlsruhe, Germany)
NaCl	Roth (Karlsruhe, Germany)
NH_4HCO_3	Roth (Karlsruhe, Germany)
Trifluoroacetic acid (TFA)	Merck (Darmstadt, Germany
Yeast extract	Serva (Heidelberg, Germany)

3.1.2 Strains

Table 3.2. Bacterial strains

Organism	**Genotype**	**Source**
E.Coli Mach1	F- Φ80(ΔlacZ)ΔM15 ΔlacX74 hsdR(rK-mK+) ΔrecA1398 endA1 tonA	Invitrogen (Karlsruhe, Germany)
E.Coli BL21	F–*ompT hsdS*(rB–mB–) *dcm+* Tetr *gal endA Hte [argU* ileY leuW CamR]	Stratagene (La Jolla, USA)
E.Coli XL1 blue	*recA1 endA1 gyrA96 thi-1 hsdR17 supE44 relA1 lac*	Stratagene (La Jolla, USA)

3.1.3 Buffers and solutions

Table 3.3. Buffers and solutions

ATPase assay pre-mix	phosphoenolopyruvate	2.6 mM
	NADH	260 nM
	Lactate Dehydrogenase	0.5 U ml-1
	Pyruvate Kinase	0.024 U ml-1
	$MgCl_2$	5 mM
	in standard assay buffer	
Fairbanks A	Coomasie Brillianr Blue R	2.5 g
	Ethanol	250 mL
	Acetic acid	80 mL

	ddH_2O	to 1 L
Fairbanks D	Ethanol	250 mL
	Acetic acid	80 mL
	dd H_2O	To 1 L
Heparin loading buffer	Tris/HCl, pH 7.9	50 mM
	NaCl	50 mM
	Glycerol	10 % v/v
	β-mercaptoethanol	0.5 mM
	DEX	50 µM
Heparin elution buffer	Tris/HCl, pH 7.9	50 mM
	NaCl	1 M
	Glycerol	10 % v/v
	β-mercaptoethanol	0.5 mM
	DEX	50 µM
GR Dialysis buffer	Tris/HCl, pH 7.9	25 mM
	NaCl	100 mM
	Glycerol	10 % v/v
	CHAPS	0.05 % w/v
GR SEC	Tris/HCl, pH 7.9	25 mM
	NaCl	100 mM
	Glycerol	10 % v/v
	DTT	2 mM
	DEX	50 µM
GRLBDm resuspension buffer	Tris/HCl, pH 7.9	50 mM
	Urea	2 M
	β-mercaptoethanol	2 mM
	$MgCl_2$	5 mM
	Imidazole	10 mM
	NaCl	100 mM
	Glycerol	10 % v/v
His Trap loading Buffer for GRLBDm	Tris/HCl, pH 7.9	50 mM
	NaCl	500 mM
	Glycerol	10 % v/v
	Imidazole	10 mM
	β-mercaptoethanol	0.5 mM
	DEX	50 µM
His Trap loading Buffer for Hsp90 and cofactors	HEPES/KOH, pH 7.5	40 mM
	KCl	150 mM
His Trap elution Buffer for GRLBDm	Tris/HCl, pH 7.9	50mM
	NaCl	500 mM
	Imidazole	300 mM
	Glycerol	10 % v/v
	β-mercaptoethanol	0.5 mM
	DEX	50 µM

His Trap elution Buffer for Hsp90 and cofactors	HEPES/KOH, pH 7.5	40 mM
	KCl	150 mM
	Imidazole	300 mM
Ion exchange loading buffer	HEPES/KOH (pH variable)	40 mM
Ion exchange elution buffer	HEPES/KOH (pH variable)	40 mM
	KCl	1M
Laemmli Buffer (5x)	Tris/HCl, pH 6.8	312.5 mM
	SDS	10 % w/v
	β-mercaptoethanol	25 % v/v
	Glycerol	50 % v/v
	Bromophenol blue	0.05 % w/v
SDS running buffer	Tris/HCl, pH 6.8	25 mM
	Glycine	200 mM
	SDS	0.1 % w/v
SDS-PAGE stacking gel	Tris/ HCl, pH 6.8	125 mM
	SDS	0.2% (w/v)
	Acrylamide	5 % (w/v)
	TEMED	5 µL/ 2 gels
	APS	60 µL/ 2 gels
SDS-PAGE separation gel	Tris/ HCl, pH 6.8	62.5 mM
	SDS	0.2% (w/v)
	Acrylamide	12.5 % (w/v)
	TEMED	5 µL/ 2 gels
	APS	60 µL/ 2 gels
Standard assay buffer	HEPES	20 mM
	KCl	50 mM
	MgCl2	5 mM
TAE buffer (50x)	Tris/ acetic acid, pH 8	2 M
	EDTA/NaOH, pH 8	50 mM
PBS	KH_2PO_4	5.44 g
	Na_2HPO_4	7.11 g
	NaCl	2. 34 g
	1 M $MgSO_4$	1 mL
	ddH_2O	To 1 L

3.1.4 Media

Table 3. 4. Auto-induction medium for protein expression was prepared according to Studier (196). All media, unless they were commercially available, were autoclaved and supported with the appropriate antibiotic.

Name	**Substance**	**Concentration**
Gibco™ CO_2 Independent Medium	Commercially available	+ 10 % (v/v) fetal bovine serum + 20mL/L Gibco® GlutaMAX™
Dulbecco's Modified Eagle Medium (DMEM)	Commercially available	+ 10 % fetal bovine serum
LB	LB medium	20 g/L
Stock solutions		
50x	Na_2HPO_4	1.25 M
	KH_2PO_4	1.25 M
	NH_4Cl	2.5 M
	Na_2SO_4	0.25 M
ZY	Bacto tryptone	1% (w/v)
	Yeast extract	0.5 % (w/v)
50x 5052	Glycerol	25% (v/v)
	Glucose	2.5 % (w/v)
	α-lactose	10 % (w/v)
1 M MgSO4	$MgSO_4 \cdot 7H_2O$	1 M
1000x trace elements	$FeCl_3 \cdot 6H_2O$	50 mM
	$CaCl_2 \cdot 2H_2O$	20 mM
	$MnCl_2 \cdot 4H_2O$	10 mM
	$ZnSO_4 \cdot 7H_2O$	10 mM
	$CoCl_2 \cdot 6H_2O$	2 mM
	$CuCl_2 \cdot 2H_2O$	2 mM
	$NiCl_2 \cdot 6H_2O$	2 mM
	$Na_2MoO_4 \cdot 2H_2O$	2 mM
	H_3BO_3	2 mM
ZYM5052 media for protein expression (/L)		
	50x solution	20 mL
	50x 5052 solution	20 mL
	1M $MgSO_4$	2 mL
	Bacto tryptone	1% (w/v)
	Yeast extract	0.5 % (w/v)
	1000x trace elements	0.2 mL (0.6 mL for GRm)
	ddH_2O	968 mL

3.1.5 Oligonucleotides

Table 3.5. Oligonucleotides. All oligonucleotides were purchased from Eurofins (Ebersberg, Germany).

Name	Sequence	Application
DAF-12 DBD F	GGAATTGCTAGCCGACGACGTCAGAAAACATGTAGAG	Protein expression
DAF-12 DBD R	GGAATTGGATCCTCAGGATCTTTTATTACACGTTCCCG	Protein expression
DAF-12 LBD F	GGAATT GCTAGC AACAAAACTCCAGCTGATATTATG	Protein expression
DAF-12 LBD R	GGAATTGGATCCCTATTTGATTTTGAAAAATTCTCC	Protein expression
GR L773P F	CAAAAAACTTCCGTTTCATCAAAAGTG	mutagenesis
GR L773P R	ATATTTCCATTTGAATATTTTGGTATC	mutagenesis
GR D590A F	CTTACACCTGGCAGACCAAATGAC	mutagenesis
GR D590A R	TTCCTGAAACCTGGTATTG	mutagenesis
AHR1 F	GAATTGCTAGCATGGATGTTGCATTAAAATC	Protein expression
AHR1 R	GAATTGGATCCTTATTCTCCAGTGGTAAAC	Protein expression
AHR2 F	GAATTCATATGATGAATTTCCAAGGGAAG	Protein expression
AHR3 F	GAATTCATATGATGGAGAGGTGCTTCATATGTCGTCTAAG	Protein expression
AHR3 R	GAATTCTCGAGTTAACTAGTGCCATTTTTAGTCCTTAGTGG	Protein expression
VDR1 F	GAATTCATATGATGGAGG CAATGGC	Protein expression
VDR1 R	GAATTGGATCCTCAGGAGATCTCATTG	Protein expression
VDR LBD F	GAATTCATATGATGTCCTCCTGCTCAGATC	Protein expression
2698 F	ACTGTGGAACTGACTGTTCTCCACAGACTCT	AUC, EMSA
2698 R	AGAGTCTGTGGAGAACAGTCAGTTCCACAGT	AUC, EMSA
GATC PET RP	CTAGTTATTGCTCAGCGG	sequencing
GATC T7	TAATACGACTCACTATAGGG	sequencing

3.1.6 Enzymes and Kits

Table 3.6. Enzymes and Kits

Name	Source
Antarctic Phosphatase	New England Biolabs (Ipswich, USA)
DNaseI	Sigma Aldrich (St. Luis, USA)
GoTaq polymerase	New England Biolabs (Ipswich, USA)
Lactate dehydrogenase	Roche (Mannheim, Germany)
Phusion DNA Polymerase	New England Biolabs (Ipswich, USA)
Pyruvate Kinase	Roche (Basel, Switzerland)
Restriction Enzymes	New England Biolabs (Ipswich, USA)
T4 DNA Polymerase	New England Biolabs (Ipswich, USA)
T4 ligase	New England Biolabs (Ipswich, USA)
Trypsin	Roche (Basel, Switzerland)
Q5® Site-Directed Mutagenesis Kit	New England Biolabs (Ipswich, USA)
Wizard® Plus SV Minipreps DNA Purification Kit	Promega (Madison, USA)
Wizard® SV Gel and PCR Clean-Up System	Promega (Madison, USA)
Annexin V	Promega (Madison, USA)

3.1.7 Fluorophores

Table 3.7. Fluorophores

Name	Excitation	Emission	Source
ATTO 488	500 nm	520 nm	ATTO-TEC (Siegen, Germany)
ATTO 550	554 nm	576 nm	ATTO-TEC (Siegen, Germany)
Fluorescein Dexamethasone	490 nm	525 nm	Thermo Fischer Scientific
SYPRO Orange	470 nm	570 nm	Life Technologies (Carlsbad, USA)
Clear G	490 nm	530 nm	Serva (Heidelberg, Germany

3.1.8 Plasmids

Table 3.8. Plasmid vectors.

Name	Source
AHSA-1	Eppstein lab
AHR1	This work
AHR2	This work
AHR3	This work
HaloGRLBDm	JB strain collection
SumoGRDBDLBD (GRm)	JB strain collection
SumoGRDBDLBD D590A	This work
SumoGRDBDLBD L773P	This work
DAF-12 DBD	This work
DAF-12 LBD	This work
DAF-21	KR strain collection
DAF-21 C63	purchased
DAF-21 C63 V499A	This work
FK1	Siyuan Sima
FK2	Siyuan Sima
FKB-6	KR strain collection
Fkbp51	JB strain collection
Fkbp52	JB strain collection
Hsp90β	JB strain collection
PPH-5	KR strain collection
PPH-5 P375Q	Lukas Schmauder
PPH-5 tm2979	Vera Wanka
Pp5	KR strain collection
STI-1	KR strain collection
VDR1	This work
VDR2	This work
Xap2	JB strain collection

3.1.9 Equipment

Table 3.9. Instruments, devices and other equipment

Name	Origin
Instruments	
Analytical Balances (1409 MP, BL310, BP121 S)	Satorius (Goettingen, Germany)
Analytical Ultracentrifuges (AUC)	Beckmann Coulter (Krefeld, Germany)
Carry 100/50 UV-VIS spectrometer	Varian (Palo Alto, USA)
CD spectrometer	Jasco J-715 (Hessen, Germany)
Cell Disrupter	Constant Systems (Warwick, UK)
Biometra BioDOC II	Biometra (Goettingen, Germany)
AUC Fluorescence Detector	Aviv Biomedical (Lakewood, USA)
Preparative Centrifuges (Avanti J25, rotors JA-10, JA/25.50)	Beckmann (Krefeld, Germany)
Mx3000P QPCR light cycler	Agilent Technologies (Santa Clara, USA)
Stereo Microscope	Leica (Wetzlar, Germany)
Nano Drop ND-2000	Peqlab (Erlangen, Germany)
Pharmacia FPLC system	Pharmacia (Stockholm, Sweden)
Fluorescence Spectrometer FP 8000	Jasco (Hessen, Germany)
Fluoromax 4 Spectrofluorimeter	(Horiba Jobin Yvon, Bensheim, Germany)
Q Exactive Hybrid-Quadropole Orbitrap mass spectrometer	Thermo Fischer Scientific
Purification Columns	
HiTrap Heparin HP	GE Healthcare (Little Chalfont, UK)
HisTrap HP, 5mL	GE Healthcare (Little Chalfont, UK)
Resource Q column, 6 mL	GE Healthcare (Little Chalfont, UK)
Superdex 75 or 200 prep grade, 130 or 240 mL	GE Healthcare (Little Chalfont, UK)
Other	
Autoclave Varioclav EP-Z	HP Medizintechnik (Oberschleißheim, Germany)
Amicon Ultra Centrifugal Filters	Merck-Millipore (Darmstadt, Germany)
Gel Electrophoretic Device	GE Healthcare (Freiburg, Germany)
Dialysis Tubes Spectra Por 6-8 kDa	Thermo Fischer Scientific
Incubator	New Brunswick Scientific (Nuertingen, Germany)
Magnetic Stirrer Heidolph MR2000	Heidolph (Staufen, Germany)
Microconcentrators	Merck-Millipore (Darmstadt, Germany)
Pur A Lyzer dialysis kit	Sigma Aldrich (St. Luis, USA)
Superloops	GE Healthcare (Freiburg, Germany)
Thermomixer	Eppendorf (Hamburg, Germany)
Pharmacia EPS 3500, 301 1001	GE Healthcare (Freiburg, Germany)
Ultrafiltration Cell and Discs	Merck-Millipore (Darmstadt, Germany)
BiometraBioDOC II	Biometra (Göttingen, Germany)
Quartz Cuvettes	Hellma (Müllheim, Germany)

3.1.10 Software, Databases, Tools

Table 3.10. Software, Databases, Tools

Name	Source
Adobe Illustrator CS3	Adobe Systems (San Jose, USA)
Avogadro	https://avogadro.cc/
Biorender	https://biorender.com
BIOVIA discovery studio	BIOVIA (California, USA)
BLAST	NCBI
CGenF	MacKerell et. al, University of Maryland
Chimera	University of California San Franscisco
ClustalOmega	https://www.ebi.ac.uk/Tools/msa/clustalo/
ClusterEx	Klaus Richter
CUPSAT	http://cupsat.tu-bs.de/
Cytoscape	National Resource for Network Biology
Deuteros	Politis Lab, King's College London
DiffUZ	Klaus Richter
PLGS and DynamX	Waters Inc.
EPD the Eykaryotic promoter database	Swiss Institute of Bioinformatics
ExPAsy	Swiss Institute of Bioinformatics
FoldX	http://foldxsuite.crg.eu/
GeneMANIA	https://genemania.org/
GEO microarray repository	NCBI, https://www.ncbi.nlm.nih.gov/gds/?
HADDOCK 2.2 expert interface	Bonvin Lab, University of Utrecht (Utrecht, Netherlands)
MaxQuant 1.5	https://www.maxquant.org/
Microsoft Office 2010	Microsoft (Redmont, USA)
NEB cutter	http://nc2.neb.com/NEBcutter2/
Origin Pro 8.6	OriginLab
PDB, Protein Data Bank	https://www.rcsb.org/
pLink	Chinese Academy of Sciences, Beijing, China
pyMol	Schrödinger, Inc.
SedFit	Peter Schuck
Transcriptome Analysis Console (TAC)	Thermo Fischer Scientific
Uniprot	https://www.uniprot.org/
xMass	Klaus Richter

3.2 Methods

3.2.1 Molecular Biology

Storage and Cultivation of E.coli

E.coli was cultured in LB or ZYM 5052 media and selection was achieved by adding 35 µg/mL kanamycin or 100 µg/mL ampicillin, depending on the plasmid's resistance. Cells were incubated in liquid media or on plates at 37 °C and cultures were inoculated with single colonies. For cultures growing in LB media, growth was monitored by measuring the optical density at 600 nm. For storage, a cryo- vial with 0.5 mL of overnight culture was supplied with 0.5 mL 60 % sterile glycerol, was shock frozen in liquid nitrogen and stored at -80°C.

Transformation of E.coli

100 ng DNA were added to 200 µl competent *E.coli* cells and incubated for 15 minutes on ice. A 60 second heat shock at 42 °C was performed and cells were incubated for 15 more minutes on ice. Cells were supplied with LB medium and incubated at 37°C for 45 minutes. Subsequently, cells were spun down with 7000 rpm for 1 minute, the pellet was resuspended in 60µl LB medium, plated on LB plates with the appropriate antibiotic and incubated overnight at 37 °C.

Plasmid DNA isolation from *E.coli* cells and determination of DNA concentration

DNA was isolated from 5 mL *E. coli* overnight pre-cultures, supported with appropriate antibiotic and using the Wizard Plus SV Mini-Prep kit, according to the manufacturer. DNA concentration was determined by absorbance (UV-Vis) spectroscopy at a wavelength of 260 nm using a Nanodrop ND-1000 UV-Vis spectrophotometer. The DNA sequence was verified by NGS at GATC/Eurofins (Konstanz, Germany).

Polymerase Chain Reaction (PCR)

The polymerase chain reaction (PCR) was used to amplify genomic DNA of interest to generate protein constructs. GoTaq or Phusion DNA Polymerase and the respective buffers provided with the enzymes, were used according to the manufacturer. A concentration of 1 ng/µL template, 1 pmol/µL forward and reverse primer and 2mM dNTPs were used. Due to the high GC content in all possible AHR and VDR primers, a two-step PCR was performed as described in Table 3.12.

Thermocycling conditions for a routine PCR were as in the following table:

Table 3.11. Thermocycling conditions for a routine PCR

step	T (°C)	Time
Initial Denaturation	98°C	30 seconds
25-35 Cycles	98°C	5-10 seconds
	45-72°C	10-30 seconds
	72°C	15-30 seconds per kb
Final Extension	72°C	5-10 minutes
Hold	4-10°C	∞

Table 3.12 Two-step PCR conditions

step	T (°C)	Time
Initial Denaturation	98°C	30 seconds
25-35 Cycles	98°C	5-10 seconds
	72°C	15-30 seconds per kb
Final Extension	72°C	2 minutes
Hold	4-10°C	∞

The PCR products were confirmed by agarose gel electrophoresis and were purified using the Wizard SV Gel and PCR Clean-up system according to the manufacturer.

Agarose gel electrophoresis

DNA was separated on 1 % agarose gels (w/v) prepared with the addition 1 g agarose in 100mL TAE buffer, heating of the solution followed by addition of 1µL Clear G DNA stain upon casting the gel. Separation, including a DNA standard for size determination, was carried out with 120 V for 20 minutes.

Cloning

The appropriate enyzmes for digestion, dephosphorylation and ligation were used according to the supplier. Plasmid vectors and inserts were digested for 4 hours at 37 °C and vectors were dephosphorylated for 1 additional hour by the Antarctic Phosphatase in the same reaction mixture, to prevent self-ligation. After purification of the products with the Wizard® SV Gel and PCR Clean-Up System, overnight ligation was performed at 4 °C with the T4 ligase.

Site Directed Mutagenesis

Single point mutations were incorporated with the Q5® Site-Directed Mutagenesis kit by NEB according to the manufacturer. Primers were designed with 5´ ends annealing back-to-back with the NEB online design software, NEBaseChanger™. After PCR, the amplified material is ligated with the KLD (Kinase-Ligase-DpnI) enzyme mix and transformed into *E.coli*.

Human Cell Culture

Human HEK293 cells were cultured according to the cell line provider, in Dulbecco's modified Eagle's medium (DMEM), supplemented with 10% fetal bovine serum and penicillin-streptomycin and were incubated in a 5% CO_2 incubator.

Cells used in the Annexin V assay were cultured in CO_2-independent medium supplemented with 10% fetal bovine serum, Glutamine and penicillin-streptomycin and were seeded in 96-well plates the day prior to the experiment.

Annexin V assay

Annexin V assays to detect early apoptosis were carried out utilizing the RealTime-Glo™ Annexin V Apoptosis kit according to the manufacturer's instructions. Cells seeded in 96-well plates the day prior to the experiment were treated with identical handling with the appropriate DMSO, DEX and KUNB31 concentrations, mixed with the assay mix and luminescence was recorded in a plate reader for 55 hours at 37 °C.

RNA extraction

Total RNA was extracted from HEK293 cells according to the "Purification of total RNA from animal cells using the spin technology protocol of the RNeasy Micro Kit (QIAGEN, Hilden, Germany). In brief, the harvested cells were washed with PBS. Dry cell pellets were flash-frozen and shipped on dry ice. After adding 700µl buffer RLT containing 1% beta-mercaptoethanol and thawing, the samples were mixed by vortexing and homogenized with QIAshredder spin columns. Next 1 volume of 70% ethanol was added and the samples were applied to RNeasy MinElute spin columns followed by an on-column DNase digestion and several wash steps. Finally total RNA was eluted in 14 µl of nuclease free water. Purity and integrity of the RNA was assessed on the Agilent 2100 Bioanalyzer with the RNA 6000 Nano LabChip reagent set (Agilent, Palo Alto, CA, USA). Sample processing was performed at a Genomics Core Facility, "KFB - Center of Excellence for Fluorescent Bioanalytics" (Regensburg, Germany; www.kfb-regensburg.de) as a fee-for-service.

GeneChipTM microarray assay

Sample preparation for microarray hybridization was carried out as described in the Applied BiosystemsTM GeneChipTM Whole Transcript (WT) PLUS Reagent Kit User Guide (Thermo Fisher Scientific, Waltham, MA, USA). In brief, 200 ng of total RNA was used to generate double-stranded cDNA. 12 µg of subsequently synthesized cRNA were purified and reverse transcribed into single-stranded (ss) cDNA, whereas unnatural dUTP residues were incorporated. Purified ss cDNA was fragmented using a combination of uracil DNA glycosylase (UDG) and apurinic/apyrimidinic endonuclease 1 (APE 1) followed by a terminal labeling with biotin. 3,8 µg of fragmented and labeled ss cDNA were hybridized to Applied BiosystemsTM GeneChipTM Human Gene 2.0 ST arrays for 16 h at 45° C and 60 rpm in an Applied BiosystemsTM GeneChipTM hybridization oven 640. Hybridized arrays were washed and stained in an Applied BiosystemsTM GeneChipTM Fluidics Station FS450, and the fluorescent signals were measured with an Applied BiosystemsTM GeneChipTM GeneChip Scanner 3000 7G System. Fluidics and scan functions were controlled by the Applied BiosystemsTM GeneChipTM Command Console v5.0 software. Sample processing was performed at a Genomics Core Facility, "KFB - Center of Excellence for Fluorescent Bioanalytics" (Regensburg, Germany; www.kfb-regensburg.de) as a fee-for service.

3.2.4 Protein Biochemistry

Protein expression and Cell disruption

All proteins in the present study were expressed in *E.coli* BL21 codon+ cells utilizing pet28 vectors harboring a hexa-histidine His_6-tag. GR constructs harbored a Halo (GRLBD) or SUMO (GRm) tag, in addition to the His_6-tag, that was cleaved by the appropriate protease before purifying to homogeneity.

For expression of Hsp90 and cofactors, the respective vectors were transformed into BL21 codon+ *E.coli* and a 5 mL overnight pre-culture was inoculated. 2L of LB media in 5L flasks supported with Kanamycin, were inoculated with the overnight pre-culture and were grown

at 37 °C until an OD_{600} of 0.6-0.8 was reached. The cells were subsequently induced with 0.5 mM IPTG and the desired proteins were expressed over night at 25°C.

For GR, MR, AHR, VDR and DAF-12 constructs, 1L ZYM 5052 media per baffled 5L flask with the appropriate antibiotic was inoculated with 1mL overnight preculture, supported with 1% glucose. After 4h of growth at 37 °C, the appropriate steroid was added (for GR and MR), the cultures were transferred to 18°C, and proteins of interest were expressed overnight.

Cells were harvested by centrifugation with 7000 rpm (JA10 rotor, 15 min, 4°C). After harvesting, cells were homogenized in the appropriate buffer, supported with protease inhibitor HP and DNAse I and were mechanically disrupted at 1.8 kbar using a hydraulic press. Cell debris was removed by centrifugation at 20000 rpm (J25.50 rotor, 45 min, 4°C) and cleared lysate was injected in a 150 mL superloop for further purification.

Ni-NTA affinity chromatography

HisTrap HP columns are packed with Ni Sepharose affinity resin that provides a convienent way for purifying the proteins harboring a His_6-tag. All proteins purified in this study were first subjected to a Ni-NTA step including: 50 mL wash with 100% HisTrap loading buffer, a 120 mL washing step with HisTrap loading buffer containing 5% HisTrap elution buffer, and elution within 60 mL of 100% HisTrap elution buffer. Purification was carried out at at 4 °C with 1.5 mL/min.

Heparin affinity chromatography

Heparins are negatively charged, polydispersed linear polysaccharides, which have the ability to bind a wide range of biomolecules including hormone receptors (197). Heparin is not only separating proteins according to affinity but is also an ion exchanger and can help achieving a high-resolution purification. GRm, after proteolytic cleavage of the SumoTag, was loaded onto a 150 mL superloop and injected into a HiTrap Heparin HP. After the injection and a 50 mL washing step with heparin loading buffer, GRm was eluted with a salt gradient within 200 mL using heparin elution buffer. Purification was carried out at 4 °C with 1.5 mL/min.

Anion exchange

Anion exchange chromatography separates the different species based on their affinity to the ion exchanger. Resource Q/S columns are packed with strong ion exchangers and yield high-resolution purifications. This step was, with the exception of GRm that was subjected to Heparin chromatography, performed for each protein purification, after isolation of the His_{6}-tagged proteins and prior to SEC.

Size exclusion chromatography (SEC)

SEC is a chromatography step used to separate proteins according to their molecular weight. Protein fractions pooled after anion exchange or heparin affinity chromatography were (upon concentration if needed) injected (5-10mL volume) to a Superdex 16/600 or 26/600 column. The appropriate storage buffer with a flow of 0.4 mL/min flow was used to purify proteins to homogeneity according to their size. After this purification step performed at 4 °C, proteins were concentrated and shock-frozen for storage at -80°C.

Sodium dodecyl sulfate polyacrylamide gel electrophoresis (SDS-PAGE)

Cell extracts and purified proteins were analysed by SDS-PAGE according to Laemmli. Samples were mixed with 5x Laemmli buffer and were boiled at 95 °C prior to gel loading. Acrylamide concentration of the gels, unless otherwise noted, was 12.5 %. SDS-PAGE was carried out at a constant current of 35 mA per gel for 40 min. Gels were stained with Coomassie blue according to Fairbanks. The molecular weight of the proteins was compared to a protein standard.

Protein Labeling

Proteins were randomly labeled at cysteine or lysine residues using the maleimide- or succinimide- functionalized ATTO 488 dye respectively. 0.1 mg ATTO 488 dissolved in DMSO was added to 1 mg of protein with a final maximal DMSO concentration of 1%. The reaction was carried out for one hour at room temperature and was quenched with 100 mM DTT. Free label was removed by dialysis against 25 mM Tris, 100 mM NaCl, 50 µM DEX (for GR), and 0.5 mM DTT.

The degree of labeling was determined using the following equation:

$$\mathrm{C[M]} = \left(\frac{A_{280} - A_{max} * \mathrm{CF}}{\varepsilon(\mathrm{POI})}\right) * \text{dilution factor}$$

$$\text{Degree of labelling} = \frac{A_{505}}{\varepsilon_{ATTO488} * \mathrm{c[M](POI)}} * \text{dilution factor}$$

c[M](POI)= concentration of protein of interest in M, A_{280}= absorbance at 280 nm, A_{max}= absorbance maximum of dye, CF= correction factor of the dye, for ATTO 488 CF = 0.1, ε_{POI}= molar extinction coefficient of the protein of interest in $cm^{-1}M^{-1}$, $\varepsilon_{ATTO488}$= molar extinction coefficient of the dye in $cm^{-1}M^{-1}$

Crosslinking experiments

The crosslinking reactions were carried out in 20 mM HEPES, 20 mM KCl, 5 mM MgCl2, pH 7.5 for 10 minutes at room temperature, using the bis-sulfo-succinimidyl-suberate crosslinker (BS3-H12/D12) (Creative Molecules, Scottsdale, USA) in a 50-fold excess over protein, as described previously (59,188). The crosslinking reaction was quenched by the addition of 5 × Laemmli buffer. Samples were analysed on SERVAGel Neutral pH 7.4 gradient gels and bands representing the crosslinked species were excised.

Analytical Ultracentrifugation (AUC)

Sedimentation analysis was performed with a ProteomeLab Beckman XL-A analytical ultracentrifuge (Beckman, Krefeld, Germany) with an AVIV fluorescence detection system (Aviv Biomedical Inc., Lakewood, USA). Ultracentrifugation was carried out at 42000 rpm, 20 °C, in standard assay buffer (and 50 µM dexamethasone for GR, when fluoresecently labelled F-DEX was not employed). Samples containing 600 nM of randomly labelled GRLBDm (in Cys residues) and 3 µM of the unlabelled chaperones and cofactors of interest, unless stated otherwise, were prepared while nucleotides were added at a concentration of 2 mM. AUC experiments monitoring F-DEX, utilized 400nM F-DEX and 2 µM of the unlabelled proteins of interest, unless stated otherwise. These measurements were carried out in 20 mM HEPES, 20 mM KCl, 5 mM $MgCl_2$, pH 7.5. Data analysis was performed by calculating differences between scans from a selected time range and averaging over several of these differentials. dF/dt data were then normalized against the initial fluorescence intensity. To ensure comparable sample handling, plots were generated from samples measured in the same experiment with automated data processing in the in-house software diffUZ. $s_{20,w}$ values were derived from a bi-Gaussian fitting of the dF/dt plots.

Sedimentation experiments, in which all proteins should be detected without specific labelling were performed with the UV/VIS detector at 280 nm.

Small angle X-ray scattering (SAXS)

SAXS measurements were carried out on a Rigaku BioSAXS-1000 instrument with an H7007 microfocus generator equipped with a Cu target at 40kV and 30mA, as described previously (198). The measurements were performed for each sample at three different concentrations and upon subjecting the purified proteins to SEC. SAXS measurements were performed by Ralf Stehle.

Electrophoretic Mobility Assays

The gel electrophoresis mobility shift assay (EMSA) is used to detect protein complexes with DNA, during which the species of interest are subjected to electrophoresis under native conditions (199). EMSAs in this study were carried out using commercially available Novex™ TBE Gels, 10%. DNA 2698 was purchased as forward and reverse oligonucleotide and was hybridized by heating at 98 °C. Electrophoresis was carried out in TAE buffer and as indicated by the manufacturer. After electrophoresis, the gels were stained with Clear G DNA stain by incubating the gel in 20mL+ 5 µL Clear G for 20 minutes, and upon scanning of the gel with a Typhoon scanner at green fluorescence to specifically detect DNA, gels were also stained with Coomasie to detect the protein bands.

Absorbance UV-Vis spectroscopy

Proteins absorb UV light with maxima at 200 and 280 nm due to their backbone and aromatic amino acids. Protein concentration was determined on a NanoDRop ND1000, using the storage or dialysis buffer as blank. Concentration was calculated based on Beer and Lambert's law:

$$A = \varepsilon \times b \times c$$

With $A =$ absorbance, $\varepsilon =$ extinction coefficient of POI in $cm^{-1}M^{-1}$, $b =$ cell length in cm, $c =$ protein concentration in M. The protein extinction coefficient was calculated with the Expasy ProtParam tool.

ATPase assays

ATP turnover was monitored with a Cary 50 spectrometer, using an ATP-regeneration system at 30 °C and in standard assay buffer (200,201). After recording a baseline, 2mM ATP were added and activity was recorded for 40minutes. Background Hsp90 ATPase activity was determined by addition of radicicol (10 µM) and recording the signal for further 10 minutes.

ATPase activity was determined using the following equation:

$$\text{ATPase activity}[\text{min}^{-1}] = \frac{\frac{\Delta A_{340\text{nm}}}{\Delta t}}{(\varepsilon_{\text{NAD+}} - \varepsilon_{\text{NADH}}) * c(\text{ATPase})}$$

With: $\varepsilon_{NAD+} - \varepsilon_{NADH} = 6200$, A= absorbance,t= time, , c = protein concentration in M.

Fluorescence spectroscopy

Intrinsic tryptophan fluorescence spectra were recorded with a Fluoromax 4 in a 1cm quartz cuvette, at 20 °C and 1-8 µM protein concentration. Samples were excited at 280 nm and emission spectra were recorded between 300 and 400 nm. Slits were set to 5nm.

Fluorescence polarization

Fluorescence polarization was monitored with a Jasco FP-8500. fluorescence spectrometer (Jasco, Groß-Umstadt, Germany) equipped with polarizers. 1 µM apo-GRLBDm, after extensive dialysis to remove dexamethasone as described, was added to various chaperone mixtures with a chaperone and cofactor concentration of 3 µM (44). Binding kinetics to 50 nM fluorescently labelled dexamethasone were recorded at 20 °C in 20 mM HEPES, 20 mM KCl, 5 mM $MgCl_2$, 2 mM ATP, pH 7.5. Hormone binding rates were determined by fitting association kinetics to exponential models and the error bars represent the standard deviation of three independent measurements.

Förster resonance energy transfer measurements (FRET)

HSP-90 C63 V499A labelled with ATTO488 likely at Cys 63 was mixed with HSP-90 labelled under identical conditions with ATTO 550 in standard assay buffer. Fluorescence was monitored with a JASCO FP-8500 (Jasco, Groß-Umstadt, Germany) fluorescence spectrometer recording the kinetics of donor and acceptor dye simultaneously.

H/DX MS

Hydrogen/Deuterium exchange mass spectrometry was performed on a fully automated system equipped with a Leap robot (HTS PAL; Leap Technologies, NC), a Waters ACQUITY M-Class UPLC, an H/DX manager (Waters Corp., Milford, MA) and a Synapt G2-S mass spectrometer (Waters Corp., Milford, MA), as described previously (202,203). 30 µM GRm were diluted 1:20 with deuterium oxide in 25 mM Tris, 100mM NaCl 10 % (v/v) glycerol, pH 7.9 and incubated for 0.17min, 1 min, 10 min, 30 min and 2hr. For measurements with the Hsp90 chaperone the protein sample contained 15 µM Hsp90 and 15 µM GRm and the buffer contained 2mM ATP. The exchange was quenched by 1:1 dilution with quenching buffer (200 mM Na2HPO4 × 2 H2O, 200 mM NaH2PO4 × 2H2O, 250 mM Tris (2-carboxyethyl)phosphine, 3 M GdmCl, pH 2.2) at 1°C. Digestion was carried out a Waters Enzymate BEH Pepsin Column (2.1 × 30 mm) at 20°C. Peptides were trapped and separated on a Waters AQUITY UPLC BEH C18 column (1.7 µm, 1.0 × 100 mm) with a acetonitrile /H2O gradient containing 0.1% (v/v) formic acid at 0 °C to minimize back-exchange. Eluting peptides were directly subjected to the Synapt TOF mass spectrometer by electrospray ionization. Data analysis was conducted with the Waters Protein Lynx Global Server PLGs (version 3.0.3) and DynamX (Version 3.0) software package. Measurements and DynamX analysis were performed by Florian Rührnößl.

Circular dichroism spectroscopy

Circular dichroism spectroscopy was used to ensure proper folding of the proteins used in the present study

Proteins were measured at 0.1 mg/mL protein concentration using 0.1 cm cuvettes. CD spectra were recorded at 20 °C for a wavelength range of 260-200 nm using a Jasco J-715 spectropolarimeter coupled to a Peltier element. Spectra were accumulated 12 times at 20 °C and were normalized for mean residue ellipticity using the following equation:

$$\Theta_{MRW} = \frac{MRW \times \Theta}{10 \times c \times d}$$

The mean residue weight (MRW) is calculated from the MW/(N– 1) with N = number of amino acids. Θ_{MRW}= mean residue ellipticity in deg $cm^2 dmol^{-1}$, Θ= measured ellipticity in deg, d = cell length in cm, MW= molecular weight in g/mol, c= protein concentration in M.

Thermal transitions were recorded at 220nm for a temperature range of 20-90 °C with a heating rate of 1°/min.

In-gel digestion

Protein bands were washed and destained by three times alternating 10 min treatments with buffer A (10 mM ammoniumhydrogencarbonate, pH 8.3) and buffer B (buffer A:100% acetonitrile from Merck KGaA, Darmstadt, Germany in a ratio of 50:50 (v/v)), as described previously76,77. After the second incubation with 50 mM ammonium bicarbonate, samples were treated with 50 µl 10 mM DTT (AppliChem GmbH, Darmstadt, Germany) for 1 h at 56 °C and with 50 µl 50 mM IAA (Merck KGaA, Darmstadt, Germany) for 45 min at room temperature before the destaining protocol was continued. Finally, gel pieces were dried in a vacuum concentrator (RVC2-25CD plus, Martin Christ Gefriertrocknungsanlagen, Osterode am

Harz, Germany). Digestion was initiated by adding 8 µl of trypsin solution (0.015 µg/µl, Serva, Heidelberg, Germany) and was performed overnight. The digestion was stopped, and peptides were eluted by incubating the gel pieces two times for 15 min with 30 µl of a 1:1 solution containing 100% acetonitrile and 0.1% (v/v) TFA (Merck KGaA, Darmstadt, Germany) in an ice-cooled ultrasonic bath. Samples were dried in a vacuum concentrator and resuspended in 20 µl 0.1% (v/v) TFA. Afterwards, the peptide concentration was determined by amino acid analysis (AAA) as described by Plum et al.(204). Measurements were performed by Katalin Barkovits at Ruhr University Bochum.

NanoLC-ESI–MS/MS

200 ng tryptically digested samples were measured by nanoLC-ESI–MS/MS as described previously (205). An UltiMate 3,000 RSLC nano LC system (Thermo Fischer Scientific, Bremen, Germany) was utilized for nano HPLC analysis using the following solvent system: (A) 0.1% FA; (B) 84% ACN, 0.1% FA. Samples were initially loaded on a trap column (Thermo Fischer Scientific, 100 µm × 2 cm, particle size 5 µm, pore size 100 Å, C18) with a flow rate of 30 µl/min with 0.1% TFA. After sample concentration and washing, the trap column was serially connected with an analytical C18 column (Thermo Fischer Scientific, 75 µ m × 50 cm, particle size 2 µm, pore size 100 Å), and the peptides were separated with a flow rate of 400 nl/min using a solvent gradient of 4% to 40% B for 95 min at 60 °C. After each sample measurement, 1 h of column washing was performed for equilibration. The HPLC system was on-line connected to the nano-electrospray ionization source of a Q Exactive HF mass spectrometer. The mass spectrometer was operated in a data-dependent mode with the spray voltage set to 1,600 V in positive mode and a capillary temperature of 275 °C. Full scan MS spectra (mass range 350–2000 m/z) were acquired in the Orbitrap analyzer at a mass resolution of 60,000. The twenty most intensive ions per spectrum were subsequently fragmented using collision-induced dissociation (35% normalized collision energy) and scanned in the linear ion trap. The m/z values triggering MS/MS were set on a dynamic exclusion list for 30 s. Measurements were performed by Katalin Barkovits at Ruhr University Bochum.

3.2.6 Computational Methods

Identification of crosslinked peptides

Initial data analysis was performed with MaxQuant 1.5 to obtain lists of all peptides and peaks from the raw data files (206). These tables were then searched with xMASS as described previously, yielding crosslinks in four categories with either crosslinker attached at one (Type 1) or both ends (Type 2) on one peptide, crosslinker bridging peptides from the same protein (Type 3) or crosslinker bridging peptides from different proteins (Type 4) (188). These crosslinked products could be filtered for the same intensity of the peaks separated by 12.07 Da, co-elution from the column, fragmentation spectrum in MS2 and other potential solutions with a similar score. In parallel, the software pLink was used to search the same datasets with the default parameter settings (207).

Homology Modeling

Homology models for *C.elegans* PPH-5 and FKB-6 were generated using the Chimera interface to MODELLER. FKB-6 and PPH-5 were modelled based on human FKBP51 (PDB 5NJX) and rat PP5 (PDB 4JA9) respectively (208-211).

C.elegans Hsp90 was modelled by Klaus Richter with the Chimera interface to MODELLER and using the ADP-bound HtpG from *E.coli* as template (58).

Integrative Modeling & Molecular Docking

Disvis is an algorithm developed by the Bonvin lab that visualizes and quantifies the information content of distance restraints between macromolecular complexes and provides a first overview of the interaction space (212,213). Disvis can be used to filter out false positive restraints so the validity of the crosslinked products was confirmed using this algorithm.

Docking was performed in the expert interface of HADDOCK. Lysine residues identified in crosslinking products were defined as active residues, enforcing a distance restraint of 30 Å between their Cβ-atoms, to direct the docking calculations. Structures from the best binary solutions were used to proceed with docking the third protein and assemble the trimeric complexes.

Molecular Dynamics Simulations

Molecular Dynamics simulations were performed with GROMACS v2018 in the CHARMM36 force field, obtained from the MacKerell lab website and were based on the Protein-Ligand tutorials provided by Justin A. Lemkul, Ph.D., Virginia Tech Department of Biochemistry. Simulations were all based on the crystal structure with PDB ID 5NFP solved by Hemmerling et al. The L773P mutation was generated with the FoldX algorithm. Dexamethasone topology was generated with the CGenFF server. CHARMM is an all-atom force field and since hydrogens are not assigned in crystal structures, the Avogadro progam was used to assign the dexamethasone hydrogen atom coordinates. The cgenff_charmm2gmx.py script from the MacKerell lab was used to format the ligand topology for GROMACS. The protein ligand topology was built by including the ligand parameters and topology in the protein topology. The unit cell was defined as a dodecahedron (gmx editconf) and was solvated in TIP3P water (gmx solvate). The protein net charge was neutralized (gmx genion) by adding the appropriate Na^+ and Cl^- ions and the energy minimization step was performed (gmx em) in maximum 50000 minimization steps (nsteps), ensuring the geometry and solvent orientation in the starting structure are reasonable. The ligand was restrained (gmx genrestr) and grouped with the protein for the purpose of temperature coupling whereas the ions and solvent were grouped together. The first equilibration phase is conducted under an NVT ensemble (constant Number of particles, Volume, and Temperature, also referred to as 'isothermal-isochoric) (gmx nvt) and stabilizes the temperature of the system to 300K (here in 2 steps of 100ps each). Pressure equilibration is conducted in 2 steps of 100ps each, under an NPT ensemble, where the number of particles, pressure and temperature are constant (isothermal-isobaric ensemble). After the two equilibration phases, position restraints are

released and production MD was run for data collection for either 100ns or 1ns. MD trajectories were analyzed with the GROMACS toolset.

GeneChipTM microarray data analysis

Summarized probe set signals in log2 scale were calculated by using the RMA algorithm with the Applied BiosystemsTM GeneChipTM Expression Console v1.4 Software (214). After exporting into Microsoft Excel, average signal values, comparison fold changes and significance P values were calculated. Microarray data were analysed with the software TACx. Gene lists were filtered for p-value and fold change as indicated in the respective tables.

4. Results

4.1 Glucocorticoid receptor complexes form cooperatively with the Hsp90 co-chaperones Pp5 and FKBPs

Parts of this section have been published in **Kaziales, A**., Barkovits, K., Marcus, K., and Richter, K. (2020) Glucocorticoid receptor complexes form cooperatively with the Hsp90 co-chaperones Pp5 and FKBPs. *Scientific Reports* 10, 10733.

Open and closed states of GRLBDm complexes with HSP-90 can be formed with the nematode PPH-5.

GR-complexes with nematode HSP-90 can accommodate the protein phosphatase PPH-5, which binds via its TPR-domain to HSP-90 and is then active to dephosphorylate the DNA-binding domain of the HSP-90 bound GR (188). Given that no further information is available on this protein complex, also in other model systems, we were interested to see how the function and affinity are regulated and whether the HSP-90 conformation is restricted. We therefore tested whether the GRLBDm·HSP-90·PPH-5 complex can be influenced by the presence of nucleotides that induce the closed state of HSP-90. GRLBDm was fluorescently labelled with ATTO 488 and sedimentation behavior of the protein complexes it is forming was followed by analytical ultracentrifugation (AUC) coupled to fluorescence detection. GRLBDm alone sediments with 2.8 S, while in the presence of nematode HSP-90 it forms a complex with 6.1 S. Upon addition of PPH-5 to GRLBDm·HSP-90, a strong shift to higher $s_{20,w}$, 7.2 S, was observed for the ternary complex, as reported previously (Fig. 4.1).(188) Furthermore, the addition of PPH-5 led to a significant reduction of free GRLBDm at 2.7 S compared to HSP-90 alone, implying that the presence of PPH-5 increases the affinity of HSP-90 for GRLBDm (Fig. 4.1).

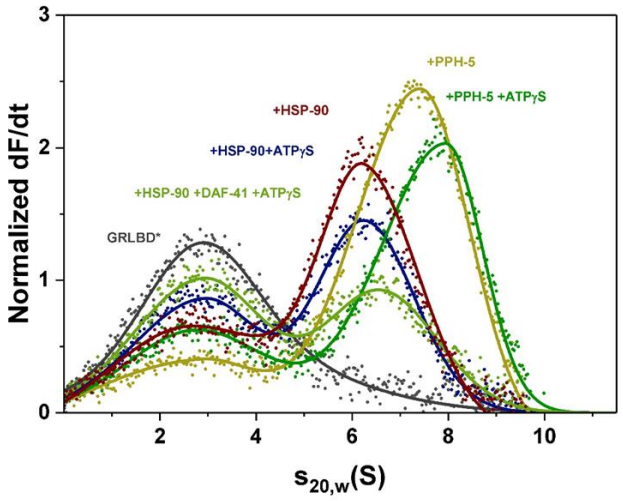

Figure 4.1. Sedimentation velocity AUC analysis of labelled GRLBDm, GRLBDm·HSP-90, GRLBDm·HSP-90/ATPγS, GRLBDm·HSP-90·PPH-5, GRLBDm·HSP-90/ATPγS·PPH-5 complexes.

Then the slowly hydrolysable ATP analog, ATPγS, was utilized to test whether the closing reaction of the nematode Hsp90 protein is possible. The presence of ATPγS indeed leads to an increased sedimentation coefficient ($s_{20,w}$) for the ternary complex from 7.2 S to 7.9 S, implying that GRLBDm·HSP-90·PPH-5 can be influenced by the nucleotide and may become more compact. The increased $s_{20,w}$ matches the behavior of other Hsp90-assemblies, in which the nucleotide-induced closing reaction is observable (62,215). Despite the increased sedimentation coefficient, the amount of bound GRLBDm decreased and the concentration of free GRLBDm at 2.8 S increased, implying that the ATPγS-induced closing reaction slightly decreases the affinity of the chaperone complex to its client (Fig. 4.1). We also tested the nucleotide influence in the absence of PPH-5. Also under these conditions, ATPγS reduces the affinity of HSP-90 for GRLBDm, but the shift representing the closing movement cannot be observed and the $s_{20,w}$ is unchanged at 6.2 S (Fig.4. 1). This implies that PPH-5 supports the nucleotide-induced compaction of nematode HSP-90·GRLBDm complexes and simultaneously increases the affinity of the chaperone machine to this client.

HSP-90 co-chaperones differentially influence GRLBDm complexes.

Having observed that PPH-5 forms a complex with HSP-90 and GRLBDm and supports the nucleotide-induced rearrangement of the chaperone, we aimed at testing whether other cofactors of the nematode HSP-90 system are influencing the assembly of the GRLBDm·HSP-90 complex. The cofactors STI-1, FKB-6 and AHSA-1, all of which had been shown to interact with HSP-90 in the absence of client proteins and to modulate GR activity in the vertebrate or yeast systems, were purified (46,64,67,99,101). Addition of STI-1 strongly reduces binding of the GRLBDm to the HSP-90 protein, while AHSA-1 binds in addition, but does not affect the affinity for GRLBDm (Figure 4.2A).

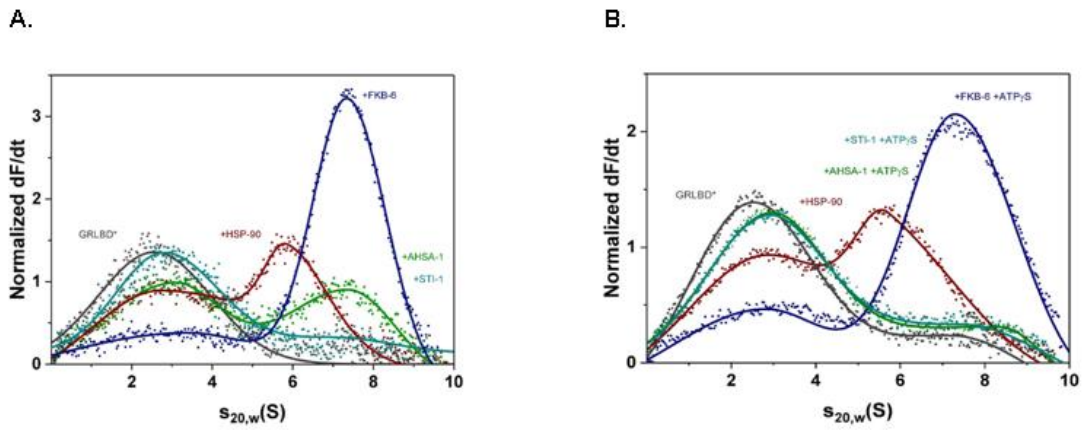

Figure 4.2 A) Influence of AHSA-1, STI-1 and FKB-6 cofactors on the formation of *GRLBDm·HSP-90 complexes analyzed by sedimentation velocity AUC. B) The same experimental setup with AHSA-1, STI-1 and FKB-6 was performed in the presence of ATPγS to initiate the closing reaction of HSP-90.

Interestingly, the addition of FKB-6 leads to a marked increase in affinity and to formation of HSP-90·GRLBDm·FKB-6 ternary complex (Figure 4.2A). Thus, the large PPIase FKB-6, like the phosphatase PPH-5, is apparently capable of strengthening the interaction between GRLBDm and the HSP-90 dimer. We then tested whether these cofactors' interactions are also sensitive to the nucleotide bound state of the HSP-90 protein, by adding ATPγS to the cofactor

containing GRLBDm·HSP-90 complexes (Figure 4.2B). This leads to a further diminishing of the complex peak in the case of AHSA-1 and continued depletion in the case of STI-1. In contrast, the FKB-6 containing complex is still intensely formed and its sedimentation coefficient is increased from 6.9 to 7.3 S. This implies that, in the presence of FKB-6, as in the presence of PPH-5, nematode HSP-90 is able to perform its nucleotide-induced rearrangements.

Hsp90 proteins from the human and *C.elegans* system do not readily respond to nucleotides inducing the closing reaction, as it has been observed for the yeast protein

Having observed the ability of the nematode Hsp90 protein to perform its closing reaction in the presence of the cochaperone PPH-5 or FKB-6 but not when in binary complexes with the GR client, a question that arised was if this is also the case for the isolated chaperone protein. To answer this the human, nematode and yeast Hsp90 proteins were subjected to AUC coupled to interference optics in the presence of nucleotides. The shift reported in previous research for the yeast chaperone was readily observable when Hsp82 was bound to either AMPPNP or ATPγS, hinting at a more compact chaperone conformation (Figure 4.3 C)(215). This behavior was not observed under the same conditions for the nematode or human protein (Figure 4.3 A, B).

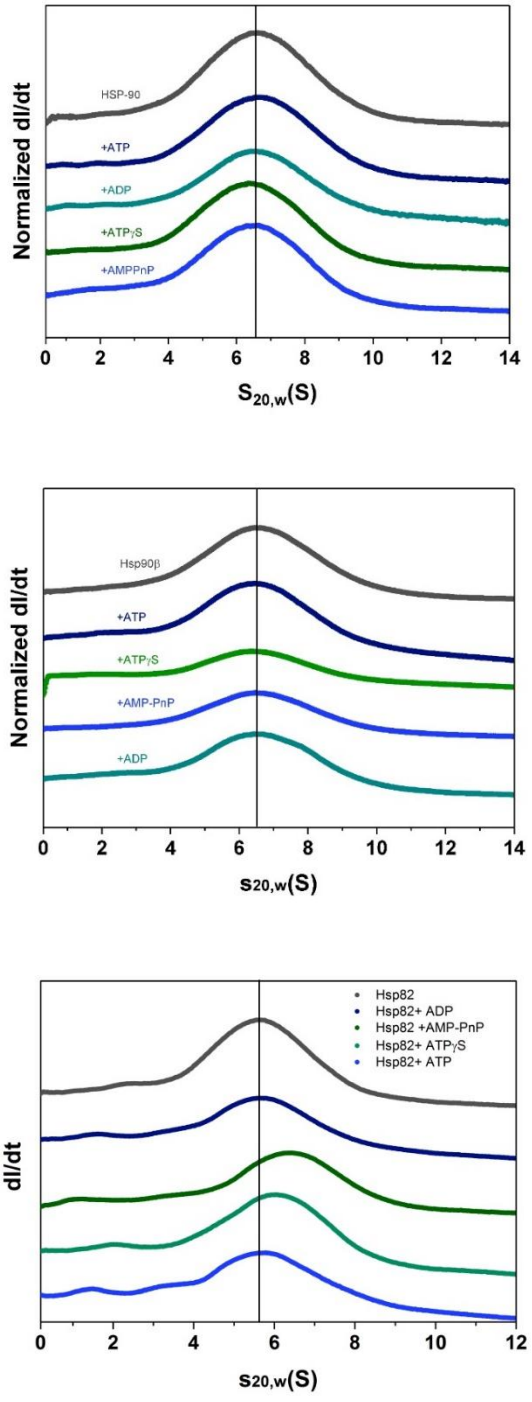

Figure 4.3. Sedimentation velocity AUC coupled to interference optics shows that the shift in s-value readily observable for the isolated yeast Hsp90, Hsp82, in the presence of nucleotides that induce the closing reaction (AMPPNP and ATPγS) is not observable under the same conditions for the *C.elegans* or human chaperone proteins.

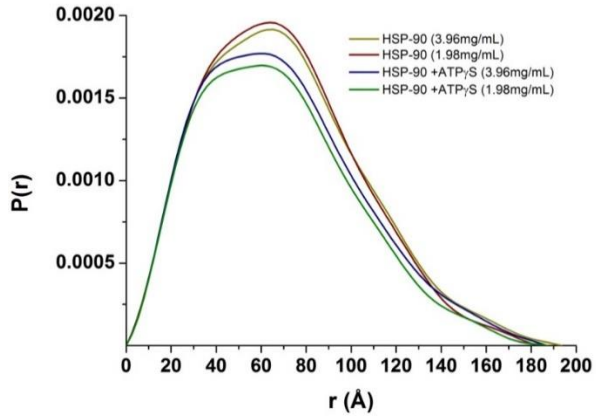

Figure 4.4 Pair distance distributions obtained by SAXS measurements of nematode HSP-90 in the absence and presence of ATPγS.

Examining the closing reaction of nematode HSP-90 protein by small angle X-ray scattering in the presence and absence of ATPγS, shows only a slight shift of the distribution hinting to higher population of more compact HSP-90.

Cep23/DAF-41 binds to closed GRLBDm·HSP-90·FKB-6/PPH-5 complexes with no influence on the affinity for the client.

Given that PPH-5 and FKB-6 support GR complex formation, we aimed at testing how the cofactor Cep23/DAF-41 influences the affinity of the Hsp90 machinery for GRLBDm. The interaction of the Hsp90 machinery with p23 critically depends on nucleotide binding to Hsp90 and the closed conformation of the chaperone (61,216-219). This interaction reflects a late step during the maturation cycle of GR, at the point where the active hormone binding site is formed (220).

AUC experiments were performed to evaluate the effect of DAF-41 in the presence of ATPγS. The ternary GRLBDm HSP-90·DAF-41 complex displayed a reduced affinity for the client compared to HSP-90 alone, as judged from the free GRLBDm fraction (Figure 4.5 A, B). Binding of GRLBDm to HSP-90·PPH-5 decreased in the presence of ATPγS. The addition of Cep23/DAF-

41 did not change this affinity, as almost the same amount of GRLBDm molecules were retained in the chaperone complex. Cep23/DAF-41 binding to the complex can nevertheless be seen from the significant increase in the complex's sedimentation coefficient towards 8.3 S (Fig. 4.5 A). This was also tested for the PPIase FKB-6 (Fig. 4.5 B).

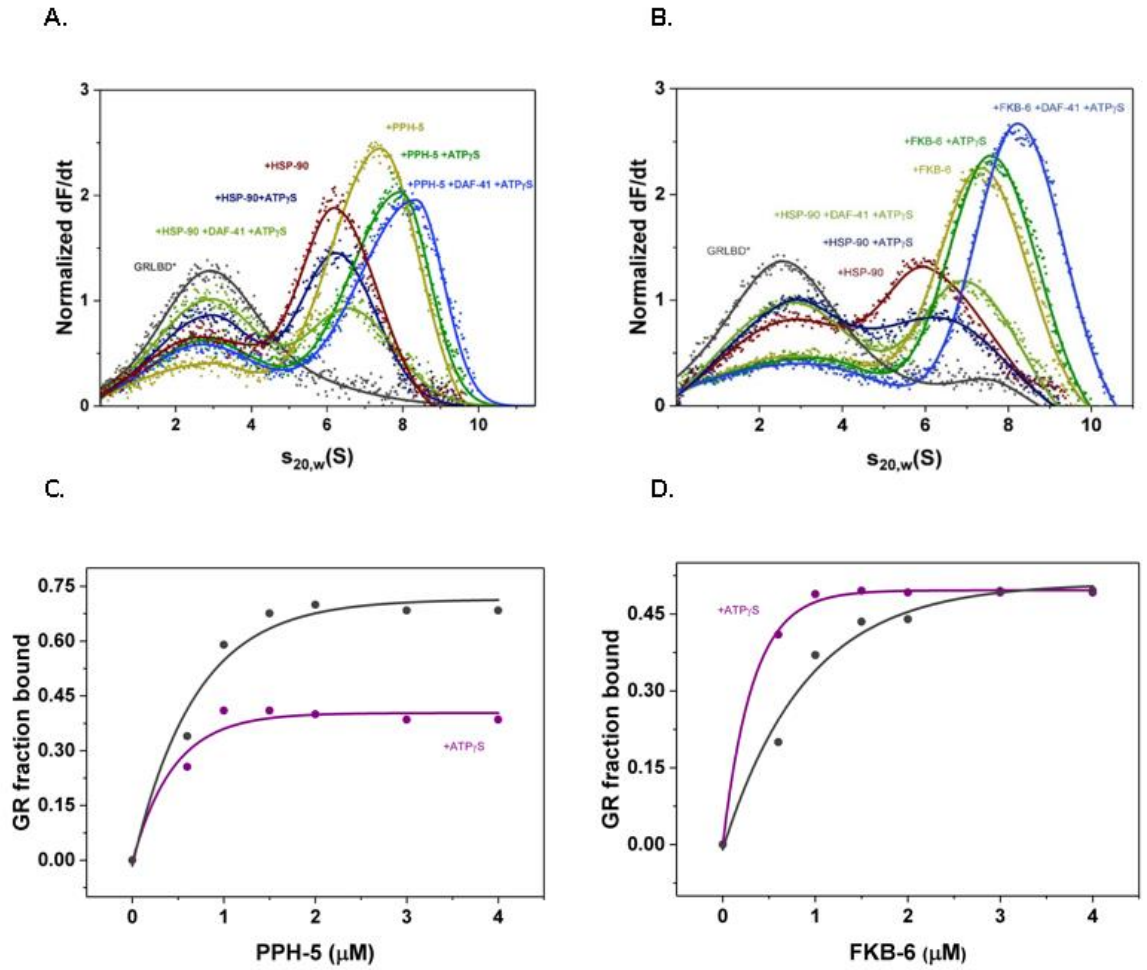

Figure 4.5 Cep23/DAF-41 can be included in *GRLBDm·HSP-90·PPH-5/FKB-6 complexes. (A) Sedimentation velocity AUC analysis of *GRLBDm, *GRLBDm ·HSP-90, *GRLBDm·HSP-90/ATPγS, *GRLBDm·HSP-90/ATPγS·DAF-41, *GRLBDm·HSP-90·PPH-5, *GRLBDm·HSP-90/ATPγS·PPH-5, *GRLBDm·HSP-90/ATPγS·PPH-5·DAF-41 complexes. (B) The same experimental set-up performed accordingly for *GRLBDm·HSP-90 complexes in the presence of FKB-6 and/or Cep23/DAF-41 as described in the plot. In both cases addition of Cep23/DAF-

41 leads to an increase in the average sedimentation coefficient of the complex forming species. C,D

Here, as well, DAF-41 bound in addition, while maintaining the affinity for GRLBDm. It therefore seems that Cep23/DAF-41 has a similar effect on both TPR-cofactor complexes, not influencing the affinity for the client further than the TPR cofactor itself, while interacting with the closed HSP-90 conformation. Titration experiments, supplementing GR·HSP-90 with increasing TPR cofactor concentrations in the presence and absence of ATPγS, indicate that the observed cooperativity in complex formation is stronger for open HSP-90 complexes with PPH-5 (Figure 4.5 C). FKB-6 slightly favors a more compact chaperone but the same amount of GR molecules is included in the complex at saturating FKB-6 concentrations (Figure 4.5 D).

Insight into ternary complex topology

To determine a representative topology of the ternary GRLBDm·HSP-90 complexes with PPH-5 and FKB-6, binding interfaces were examined by chemical crosslinking and mass spectrometry. The protein complexes were treated with the isotopically labelled crosslinker H_{12}/D_{12}-BS^3 and analysed by SDS-PAGE. The complex-representing bands (Fig. 4.6) were subjected to tryptic digestion, followed by high resolution mass spectrometry.

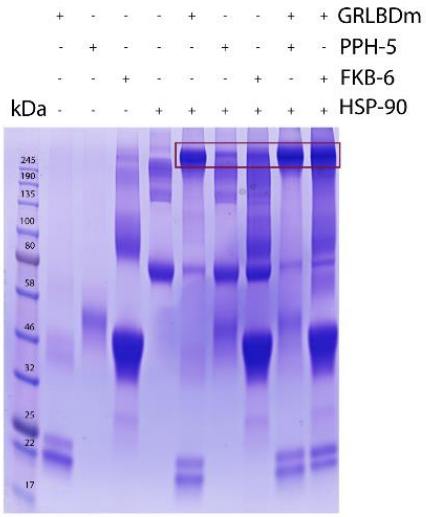

Figure 4.6 Crosslinked protein complexes with composition as indicated in the figure were analysed by SDS-PAGE. Binary or ternary complex representing bands, as highlighted by the frame, were excised and analysed by mass spectrometry

The analysis, carried out independently by the in-house software xMASS and pLink, aimed at detecting inter-protein crosslinked peptides, reporting on potential contact sites of the proteins (188,207).This data suggests that GRLBDm is positioned in the middle (M) domain of HSP-90, as we identified peptides of GRLBDm crosslinked to the lysines 326, 329 of HSP-90 (Tables 4.1, 4.2). Additional contacts were detected, linking GRLBDm to the C-terminal dimerization domain (CTD) at positions 551,555 and 601. These crosslinking sites were identified in both the PPH-5 (Table 4.1) and FKB-6 complexes (Table 4.2).

Table 4.1. Inter-protein crosslinked peptides detected for GRLBDm·HSP-90·PPH-5 complexes. Shown are the crosslinked products detected by mass spectrometry for GRLBDm·HSP-90·PPH-5 complexes, using two different search algorithms, xMASS and pLink. Amino acid positions refer to full length, non-tagged proteins as numbered in the Uniprot database. Scan number refers to the MS2 scan with the most hits for the specified peptide. Shown are also the number of hits for this scan, the per cent spectral intensity as well as the agreement between xMASS and pLink.

Peptide 1	Peptide 2	Lys 1	Lys 2	MS2 scan	Hit number in scan	Hit % spectral intensity	Independent analysis
Peptide HSP-90	**Peptide GR-LBD**						
APFDLFENKK	ELGKAIAK	326	699	24,061	30	99	✓
DSSTMGYMAAKK	QVIAAVKWAK	601	576	22,378	84	92	✓
APFDLFENKK	MTYIKELGK	326	695	27,214	84	88	✓
SKNSIK	MTYIKELGK	329	695	10,548	29	99	✓
VEKVGVSNR	WAKAIPGFR	555	579	20,877	28	96	✓
DILEKK	WAKAIPGFR	551	579	25,527	18	99	✓
Peptide HSP-90	**Peptide PPH-5**						
DRVEVDKNDK	LHkK	624	205	5,506	26	95	
MIKLGLDIGDDEIEDSAVPSSCTAEAK	QKFEAAISTDHDKK	663	147	25,861	73	99	
VEVDKNDKTVK	FEAAISTDHDKkTVAETLDINAMAIEDSYDGPR	624	158	32,007	36	99	
Peptide GR-LBD	**Peptide PPH-5**						
QVIAAVKWAK	MYGFEGEVKAK	576	319	22,754	42	85	✓
WAKAIPGFR	MYGFEGEVKAK	579	319	25,375	64	99	✓

Table 4.2. Inter-protein crosslinked peptides detected for GRLBDm·HSP-90·FKB-6 complexes.

Peptide 1	Peptide 2	Lys 1	Lys 2	MS2 scan	Hit number in scan	Hit % spectral intensity	Independent analysis
Peptide HSP-90	**Peptide GR-LBD**						
APFDLFENKK	ELGKAIAK	326	699	24,087	38	83	✓
DSSTMGYMAAKK	QVIAAVKWAK	601	576	22,389	92	74	✓
APFDLFENKK	MTYIKELGK	326	695	27,231	89	91	✓
SKNSIK	MTYIKELGK	329	695	13,803	77	60	✓
VEKVGVSNR	WAKAIPGFR	555	579	20,880	31	55	✓
DILEKK	WAKAIPGFR	551	579	25,458	18	44	✓
Peptide HSP-90	**Peptide FKB-6**						
MKENQTQIYYITGESK	VPATWEMTAEEKLDAAKQAK	455	250	23,025	30	82	
KCMELIDEVAEDKDNFK	MSGEKIDITPKK	402	11	20,677	23	86	✓
DNFKK	YKR	406	278	25,623	18	98	

PPH-5 contains a TPR domain located at its N-terminus and a C-terminal αJ subdomain (188,221). Based on the identified crosslinking sites from the ternary GRLBDm·HSP-90·PPH-5 complex, the phosphatase appears bound to HSP-90 in a similar arrangement, as previously reported for the binary HSP-90·PPH-5 assembly (188). PPH-5 apparently adopts a head-to-tail topology relative to the chaperone, bringing the N-terminal TPR motifs towards the C-terminus of HSP-90. Crosslinking sites can be identified in the M and CTD domains of HSP-90 (Fig. 4.7 A, Table 4.1). Importantly, crosslinked products between PPH-5 and GRLBDm can also be found, hinting at an interaction on the chaperone scaffold that possibly sets the basis for the observed cooperativity during complex formation. Lysines 576 and 579 of GRLBDm are linked to lysine 319 that resides in the catalytic domain of the phosphatase. Performing a similar study with the cofactor FKB-6, crosslinking sites can be identified that help position the cofactor relative to GRLBDm and HSP-90. FKB-6 contains two peptidyl prolyl isomerase (FKBP) domains (FK1, FK2) and a C-terminal tetratricopeptide repeat (TPR) region (Fig. 4.8 A). We identified contacts between the chaperone and FK1 and TPR domains of FKB-6, as summarized in Table 4.2. The identified crosslinked product that pairs lysine 11 of FKB-6 and lysine 402 of HSP-90, indicates a contact between the FK1 domain of FKB-6 and HSP-90's M domain (Fig. 3C). It has been defined that the TPR cofactors interact with the Hsp90 machinery via its C terminal MEEVD motif which, lacking lysine residues, cannot be observed as a crosslinking product (52,54). We then aimed at confirming the relevance of the FKBP domains to complex formation based on biochemical experiments.

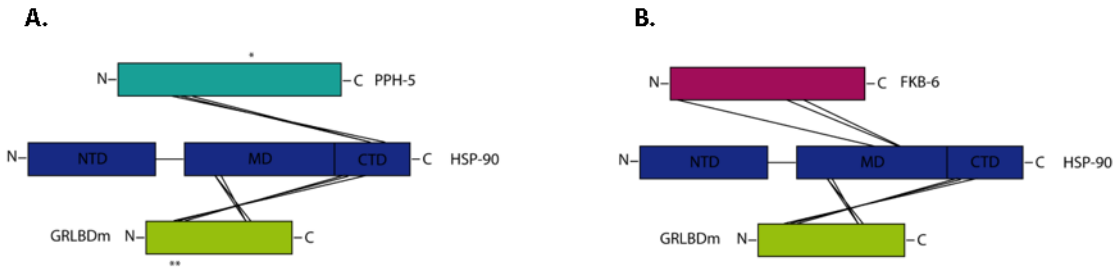

Figure 4.7 (A) Schematic representation of the inter-protein crosslinked products detected between HSP-90, GRLBDm and PPH-5. Lines represent the contacts between the two proteins and the chaperone whereas asterisks represent the crosslinked products detected between PPH-5 and GRLBDm. (B) Schematic representation of the inter-protein crosslinked products detected between HSP-90, GRLBDm and FKB-6.

Domain specific binding of FKB6 to GR-HSP-90

To this end FKB-6 variants that contain the TPR and either the FK1 (FK1-FKB-6) or the FK2 domain (FK2-FKB-6) were generated. Sedimentation velocity AUC experiments with FKB-6 truncated constructs revealed that deletion of the FK1 domain maintains robust binding to GRLBDm·HSP-90 whereas, upon removal of FK2, the ternary complex formation, occurs with sharply reduced affinity (Fig. 4.8 B). Thus, both FK domains apparently contribute to the interaction, with the FK2 domain having a stronger influence on the cooperative complex formation.

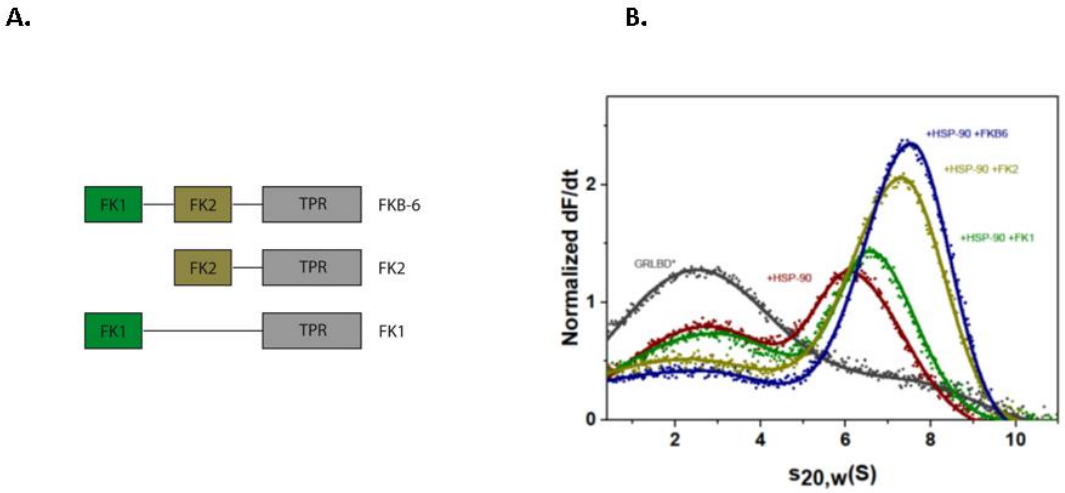

Figure 4.8: A) Schematic representation of the full length and truncated FKB-6 variants. B) Domain specific binding of FKB-6 and FKB-6 deletion constructs to GR-LBDm·HSP-90 analysed by sedimentation velocity AUC.

Representative topology for the trimeric complexes

When a distance restraint, like the ones derived from chemical crosslinking coupled to mass spectrometry, is imposed on a protein complex, the accessible interaction space reduces (212,213). This space further reduces when multiple restraints are enforced, as it can be observed from the decreasing number of possible complexes each time a crosslink-derived restraint is imposed between GRLBD and HSP-90 (Table 4.3). The DisVis algorithm was developed by Bonvin and coworkers to inform the user on the sum of complexes compliant with a given number of restraints, accompanied by a density that shows the maximum number of consistent restraints at every position in space (212) (213). This output is an indication of whether all data is consistent and can be combined without violations, allowing the identification of false positives and the visualization of the interaction space (212,213). The interaction space between GRLBD and HSP-90 upon imposing each of the 7 restraints is visualized in Figure 4.10, showing GR's center of mass positioned on the HSP-90 MD. Table 4.4 supports that there are no false-positives within the set, since all 7 restraints derived from crosslinking-MS for GRLBD·HSP-90 can be enforced at the same time while the violation percentage is near zero once all of them are introduced.

Table 4.3. Table shows the number of accessible GR·HSP-90 complexes consistent with at least N distance restraints after each restraint is imposed. Upon imposing 7 distance restraints on GR-HSP-90, there are still binding options possible, showing that this data does not enclose severe violations.

Number of consistent restraints	Number of accessible complexes consistent with at least N restraints	Fraction of accessible complexes consistent with at least N restraints
0	103640079	1.000000
1	3277242	0.031621
2	1779790	0.017173
3	830283	0.008011
4	53149	0.000513
5	9120	0.000088
6	2272	0.000022
7	503	0.000005

Table 4.4 Each row represents the number of consistent restraints whereas column represents how often that restrain is violated.

	Res1	Res2	Res3	Res4	Res5	Res6	Res7
1	0.7225	0.7793	0.8883	0.7293	0.8787	0.6024	0.5832
2	0.6153	0.6089	0.9160	0.6037	0.7922	0.4973	0.4636
3	0.6671	0.3552	0.9161	0.6656	0.6418	0.3463	0.3296
4	0.4394	0.5467	0.1538	0.4389	0.1987	0.5238	0.4747
5	0.6541	0.0782	0.2373	0.6286	0.0156	0.0811	0.0007
6	0.2468	0.0129	0.3026	0.1428	0.0000	0.0735	0.0000
7	0.0000	0.0000	0.0000	0.0000	0.0000	0.0000	0.0000

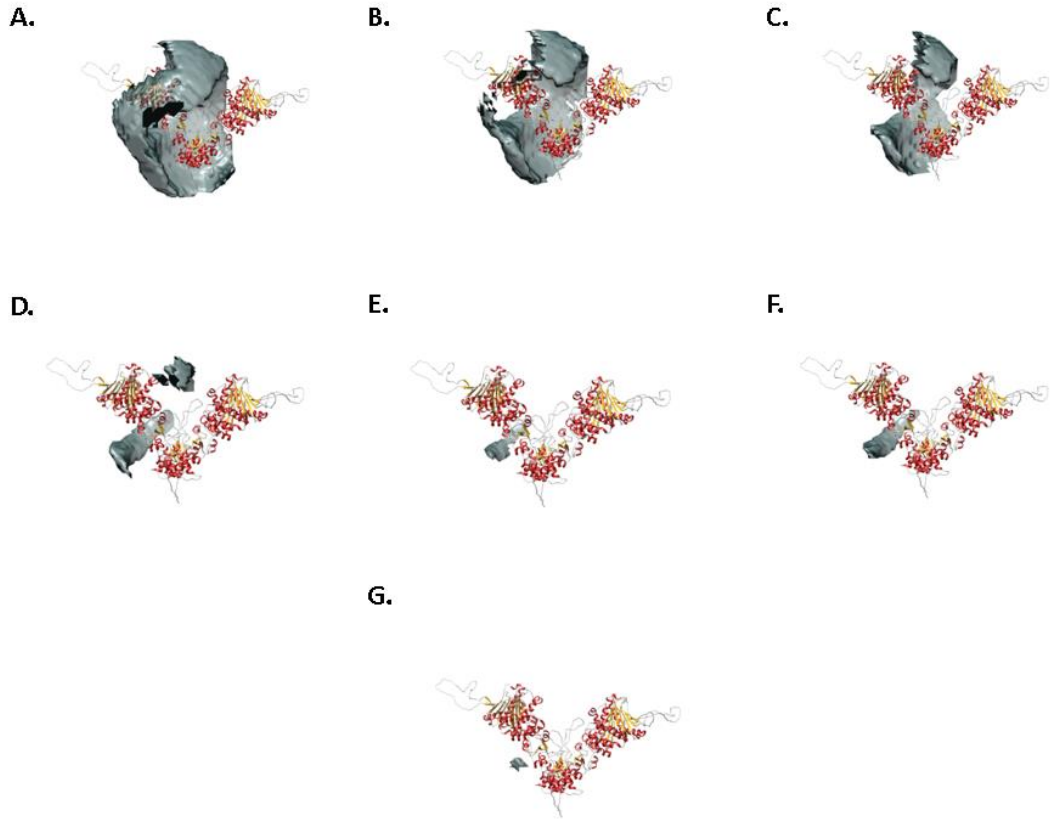

Figure 4.10. Crosslinking-MS-derived spatial restraints position GR center of mass on HSP-90 MD. Disvis output density representing the center of mass of GRLBD (grey, scanning chain) consistent with N restraints at every position in space. The interaction space between the proteins is markedly reduced after imposing each restraint.

All identified interprotein crosslinks were filtered with DisVis for false-positive hits prior to molecular docking and validated pairs were then used as distance restraints, set between 0 and 30 Å (Cβ – Cβ), to direct docking calculations with HADDOCK and generate model structures of the chaperone assemblies (222,223). A graphic overview of the strategy followed in order to obtain the structural models is presented in Figure 4.9.

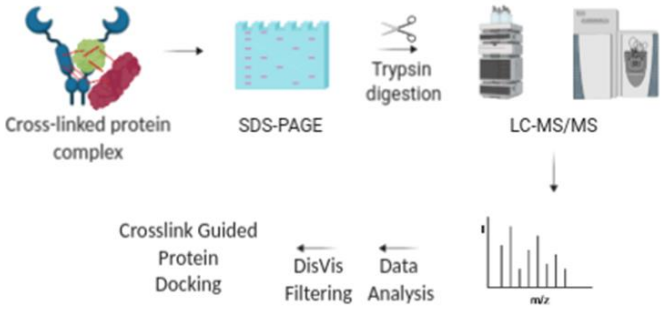

Figure 4.9 Schematic workflow followed to generate complex topologies. Chemically crosslinked protein complexes were analysed by SDS-PAGE and the bands of interest were excised, tryptically digested and subjected to mass spectrometry. Data analysis was performed with xMass and validated with DisVis. The validated restraints were imposed on molecular docking calculations with HADDOCK, utilizing the crystal structure 5NFP for GRLBD and homology models constructed for the HSP-90 and cochaperone proteins. Figure was generated with Biorender.

The representative topologies generated according to this method are depicted in Figure 4.11.

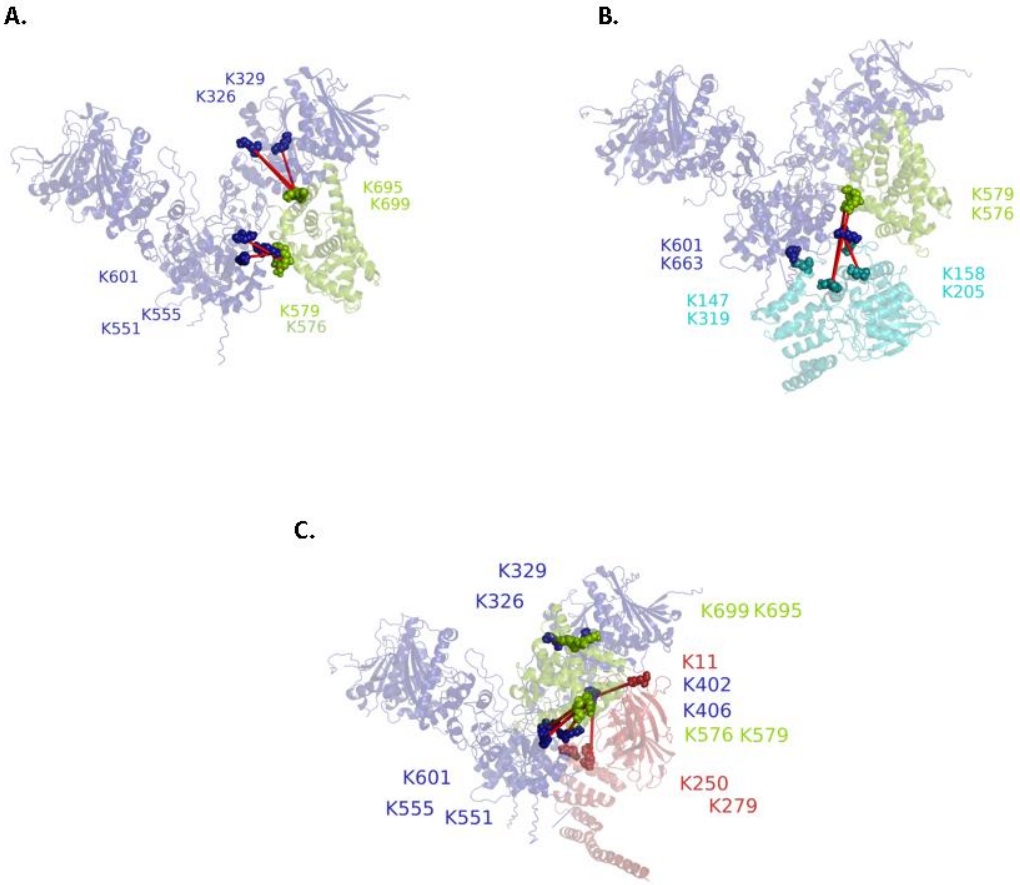

Figure 4.11. Structural representation of HSP-90 complexes, generated by crosslink guided molecular docking. (A) Structural representation of the binary GR-LBDm·HSP-90 complex. HSP-90 is shown in blue, GRLBD in green and spheres represent the crosslinked lysine residues. (B) Structural representation of the trimeric GRLBD·HSP-90·PPH-5 complex. HSP-90 is shown in blue, GRLBD in green and PPH-5 in cyan. (C) Structural representation of the trimeric GRLBD·HSP-90·FKB-6 complex. HSP-90 is shown in blue, GRLBD in green and FKB-6 in red.

Rates of hormone-binding to GR-LBDm are modulated by the Hsp90-state.

Although Hsp90 is required for hormone binding in vivo, it is known that GRLBD is capable of ligand binding in vitro in the absence of Hsp90 (44,105). It is unclear how the Hsp90 system primes GR for ligand binding, while cofactor-induced effects have been observed (224). We therefore tested to what extent the observed complexes are competent in hormone binding. A fluorescein-labelled variant of dexamethasone (F-DEX) was used to monitor the kinetic of hormone binding to GRLBDm by fluorescence polarization. We recorded the binding kinetics first in the absence and presence of HSP-90 and then supplemented with ATP, ATPγS, ATPγS/DAF-41. In these reactions ATP presence is crucial to accelerate hormone binding, as any other state of HSP-90 retains binding close to control levels (Fig. 4.12 A).

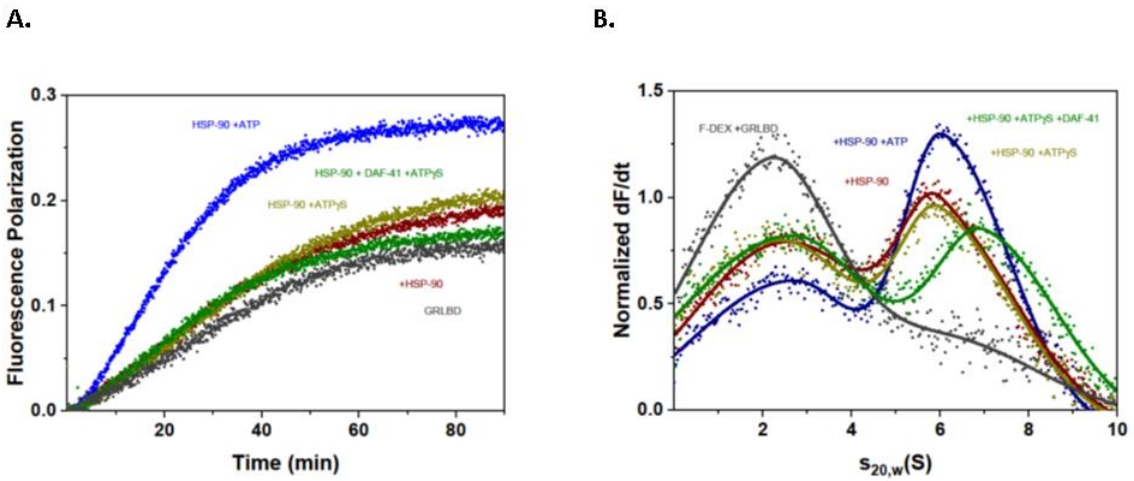

Figure 4.12 Hormone binding to GRLBDm is modulated by HSP-90/ATP. (A) Association kinetics of F-DEX to GRLBDm (grey) in the presence of *C.elegans* HSP-90 and nucleotides as indicated in the plot. (B) Sedimentation velocity analysis of F-DEX bound to GRLBDm in the presence of *C.elegans* HSP-90 and nucleotides as indicated in the plot.

The combination of HSP-90, Cep23/DAF-41 and ATP (Supplementary Fig. S2) seems to stimulate hormone binding to the same extent as HSP-90 and ATP alone, leaving uncertain whether an interaction with Cep23/DAF-41 has taken place, as this interaction is known to be better stabilized by ATPγS and not so much by ATP (219).By employing F-DEX in analytical ultracentrifugation measurements, only the F-DEX-bound complexes can be observed, allowing us to confirm the formation of protein complexes from an independent approach. F-DEX alone does not sediment in these experiments, but F-DEX bound to GRLBDm is readily observable at 2.8 S. Complex formation with chaperones then leads to the detection of larger species based on the bound fluorescent hormone. Judging from the reduction in the amount of monomeric F-DEX-bound receptor, the HSP-90 complex with hormone-bound GRLBDm is formed most efficiently, if ATP is also present (Fig. 4.12 B). This implies that the rate increase may correlate with the formation of this complex. Testing the influence of the TPR-cofactors PPH-5 and FKB-6 on the hormone binding to GRLBDm, a further modulation of the binding rates compared to GRLBDm·HSP-90·ATP (Fig. 4.13 A, Figure 4.17) was observed.

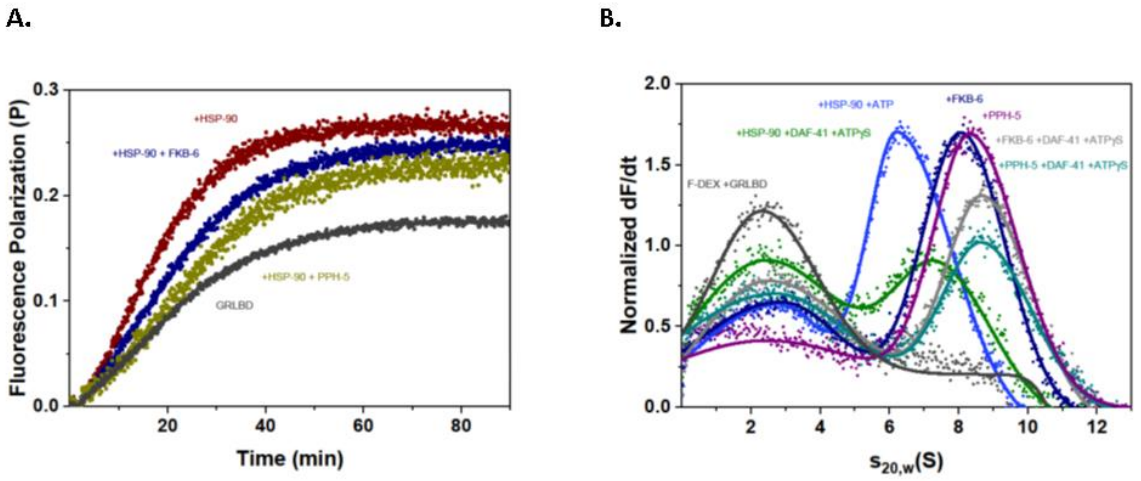

Figure 4.13 Hormone binding to GRLBDm is modulated by HSP-90, ATP and TPR-cofactors (A) Influence of TPR-cofactors on the hormone-binding rates of GRLBDm as determined from fluorescence polarization kinetics. All samples contained HSP-90 and ATP plus the indicated cofactors. Statistical significance was assessed by a two-sample t-test and a level of significance of 0.05. Error bars represent the standard deviation of three independent

measurements (n = 3). B) Sedimentation velocity analysis of F-DEX bound to GRLBDm in the presence of *C. elegans* HSP-90/ATP and cofactors as indicated in the plot.

The rate of hormone binding is slightly reduced but remains accelerated compared to control reactions. To get clarity on the complex formation, theses assemblies were further investigated by AUC experiments with F-DEX. *C. elegans* hormone-binding competent ternary complexes with the cofactors were formed as efficiently as with HSP-90/ATP in the case of FKB-6 and slightly more efficiently with PPH-5, as judged from the reduction of monomeric F-DEX-bound receptor at 2.7 S (Fig. 4.13 B). Based on this data, ATP-binding to HSP-90 seems to accelerate the binding of hormone to GRLBDm and slighter modifications to this rate are observable, when cofactors enter the complex (Fig. 4.17). Given that residual hormone might be present in the binding pocket, it cannot be excluded that the observed rates represent exchange kinetics and not binding rates. Nevertheless, such acceleration shows that nematode HSP-90 has the ability to influence the hormone binding properties of GRLBDm.

4.2 Hsp90β's conformation is more restricted in the human Hsp90 system.

We then aimed at understanding, to what extent the main principles are also conserved in the human system. The complexes assembled from the nematode proteins in this study correspond to those identified for the human system in the 1990s, but only limited in vitro data on the GR-complexes are available to date. To compare the two systems, the corresponding human proteins were purified and the experiments described for the nematode system were repeated. The human system is known to behave differently from the nematode HSP-90 regarding its ATP-turnover and conformational flexibility (225,226). GRLBDm forms protein complexes with the protein phosphatase Pp5 and Hsp90β (Fig. 4.14 A). In contrast to the nematode system, no ATPγS induced changes in the human GRLBDm·Hsp90β·Pp5 complex are observable and also no changes in $s_{20,w}$ are observed for the binary GRLBDm·Hsp90β complex after ATPγS addition. Only upon binding of p23 is a strong increase in $s_{20,w}$ observed and the closed form is obviously stabilized (Fig. 4.14 A). Interestingly, we find a cooperative action of ATPγS, p23 and Pp5, which leads to a strong increase in affinity and binding of almost all GRLBDm to the complex. It here seems that a closed Hsp90β complex with the phosphatase Pp5 is very favorable, but only achievable if p23 stabilizes the closed conformation (Fig. 4.14 A). We then tested both human PPIase homologs, Fkbp51 (Fig. 4.14 B) and Fkbp52 (Fig. 4.14 C). Both PPIases support GR-binding to the chaperone complex, albeit the cooperative effect is reduced compared to the nematode system. In contrast to the nematode FKB-6 complexes, the response of GRLBDm·Hsp90β·Fkbp51/52 complexes to ATPγS is not observable. The presence of ATPγS, however, slightly decreases the affinity for the client. As in the complexes with Pp5, binding of p23 eventually leads to the compaction of the PPIase-containing protein complex (Fig. 4.14 B, C), indicating that ATPγS may not be sufficient to initiate the closing reaction in the human system. The same experiment was performed with the ligand binding domain of the MR labelled with ATTO448 (Supplementary Figure 3). Here, the same requirement for p23 was observed so that the trimeric MRLBD·Hsp90β·Fkbp51/52 complex can adopt a more compact state. ATPγS or ATPγS/p23 did not affect the affinity under these conditions but MR showed a pronounced higher affinity for Fkbp51 compared to Fkbp52.

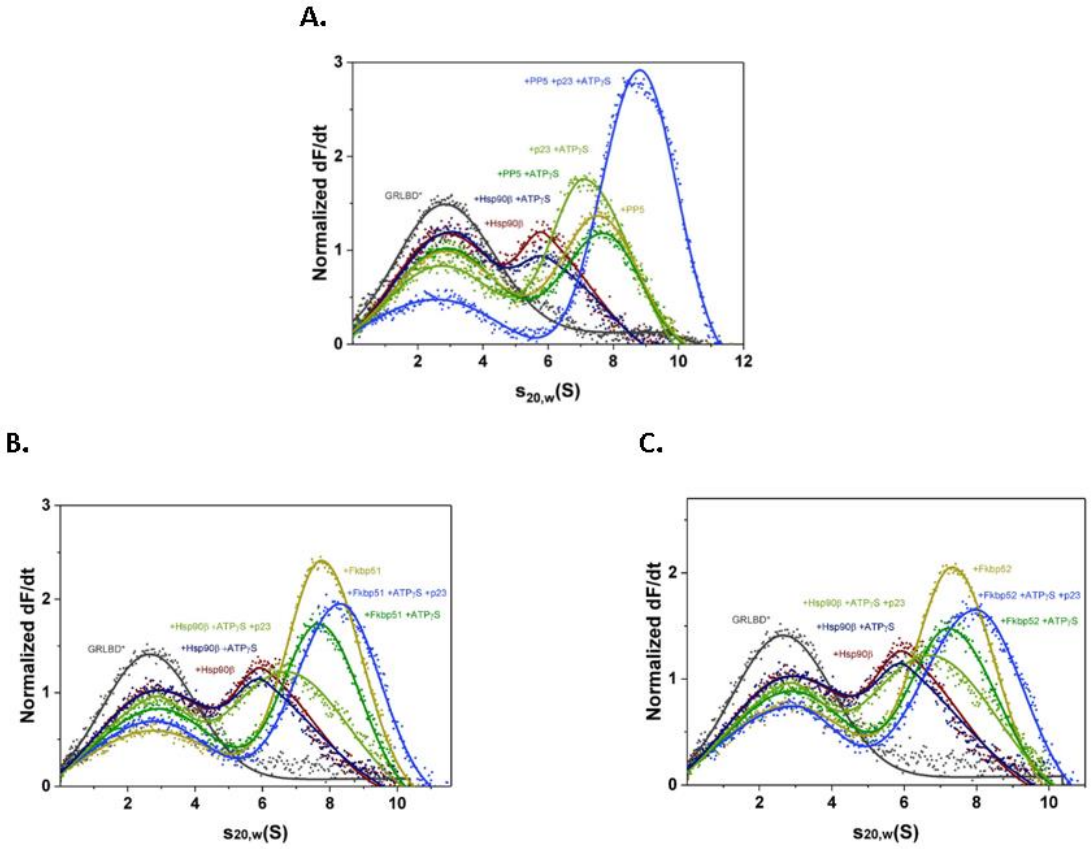

Figure 4.14. Hsp90β's conformation is more restricted in the human Hsp90 system. (A) Sedimentation velocity AUC analysis of *GRLBDm, *GRLBDm·Hsp90β, *GRLBDm·Hsp90β/ATPγS, *GRLBDm·Hsp90β/ATPγS·p23, *GRLBDm·Hsp90β·Pp5, *GRLBDm·Hsp90β/ATPγS·Pp5, *GRLBDm·Hsp90β/ATPγS·Pp5·p23 complexes. (B) Sedimentation velocity analysis of *GRLBDm·Hsp90β complexes with Fkbp51 and/or p23 set-up accordingly. (C) Sedimentation velocity analysis of *GRLBDm·Hsp90β complexes with Fkbp52 and/or p23 set-up accordingly.

This data shows that the nematode and human chaperone systems share a conserved interaction pattern with the TPR-cofactors involved in the processing of steroid receptors. The human Hsp90β however, shows a reduced ability to form the closed state under the examined conditions and seems to strictly require the cofactor p23 to perform this conformational change. Similar patterns between the two systems can also be observed for the interaction with the hormone. As in the nematode system, only Hsp90β/ATP can accelerate the binding

rate beyond control levels (Fig. 4.15 A). AUC data show that F-DEX-bound protein complexes are formed more efficiently with ATP and also the more compacted ATPγS/p23-bound states of Hsp90β (Fig. 4.15 B). Regarding the influence of human TPR-cofactors, only the hormone-bound quaternary complexes with ATPγS/p23 and either Fkbp51 or Fkbp52 form as efficiently or stronger than the binary GRLBDm·Hsp90β/ATP complex, judging from the reduced F-DEX-bound GRLBDm at 2.8 S (Fig. 4.16 B). Thus, like in the nematode system, ATP binding to Hsp90β appears to accelerate the exchange of hormone in GRLBDm and further modifications to the exchange kinetics are observable, when TPR-cofactors enter the complex (Figure. 4.16, 4.17).

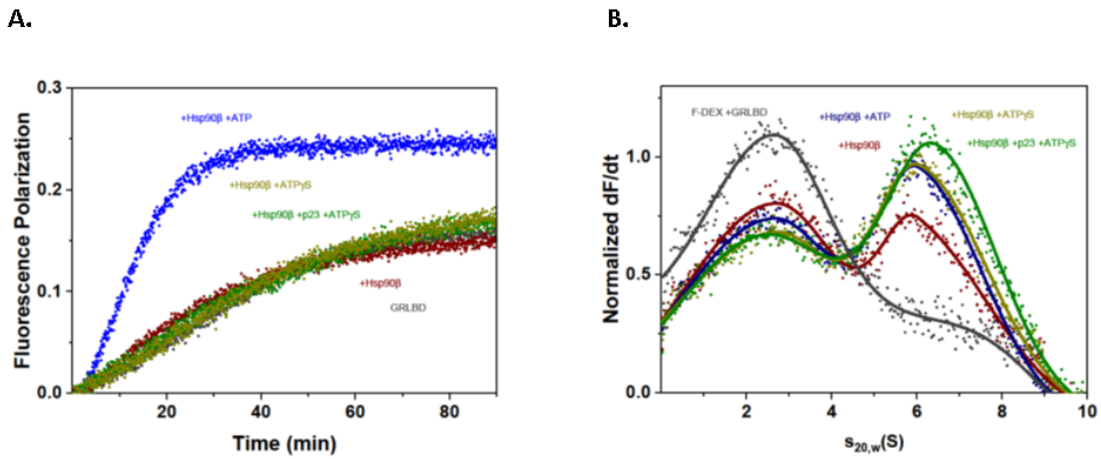

Figure 4.15. Association kinetics of F-DEX to GRLBDm in the presence of human Hsp90β and nucleotides as indicated in the plot. (E) Sedimentation velocity analysis of F-DEX association to GRLBDm in the presence of human Hsp90β and nucleotides as indicated in the plot.

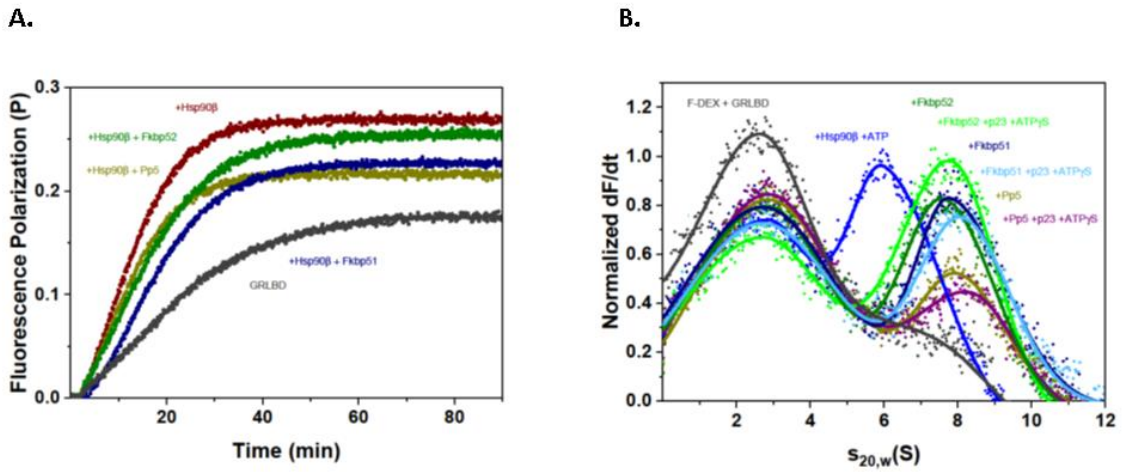

Figure 4.16 A) Association kinetics of F-DEX to GRLBDm in the presence of human Hsp90β/ATP and cofactors as indicated in the plot. B) Sedimentation velocity analysis of F-DEX association to GRLBDm in the presence of human Hsp90β/ATP and cofactors as indicated in the plot.

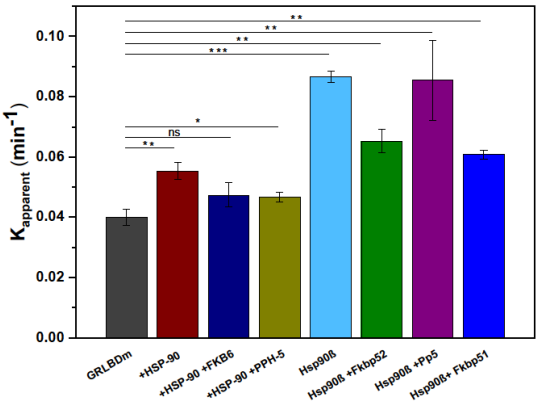

Figure 4.17 Influence of TPR-cofactors on the hormone-binding rates of GRLBDm as determined from fluorescence polarization kinetics. All samples contained HSP-90 and ATP plus the indicated cofactors. Statistical significance was assessed by a two-sample t-test and a level of significance of 0.05. Error bars represent the standard deviation of three independent measurements (n = 3).

4.3 PPH-5 mutants suppressing separase

The separase suppressing mutants P375Q and tm2979 (tm 2979 was purified by Vera Wanka) of the PPH-5 protein were purified and their folding status was assessed by CD spectrometry. All three proteins are folded, and the point mutant P375Q is exhibiting a highly similar secondary structure content to the WT PPH-5. The tm2979 that lacks 55 aa in the TPR region, is expected to lack secondary elements as observed in its spectrum but is nevertheless folded (Figure 4.18).

.

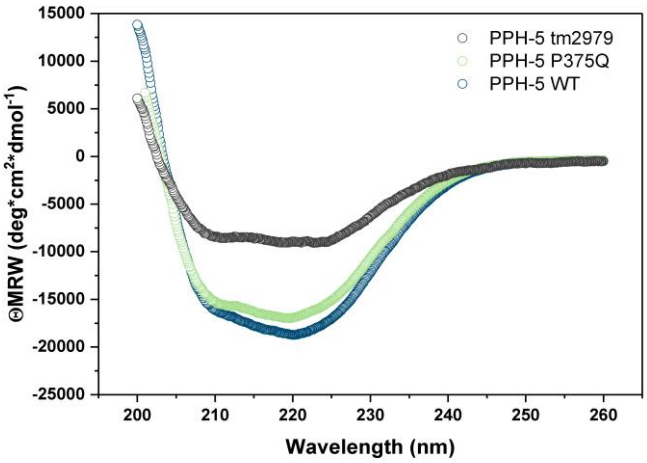

Figure 4.18. CD spectra of PPH-5 WT, P375Q and tm2979 normalized for mean residue molar ellipticity.

Since GR complexes with PPH-5 and HSP-90 form cooperatively, the two PPH-5 mutants were tested by analytical ultracentrifugation in their ability to support GR·HSP-90 complex formation. PPH-5 tm2979 could not bind to the GR chaperone complex, whereas PPH-5 Q375E did not facilitate complex formation as observed for WT PPH-5, judging by the fraction of monomeric GR at 2.7 S that remains unchanged when PPH-5 Q375Q is present (Figure 4.19 B). The titration data are plotted together in Figure 4.19 C, which shows the difference between PPH-5 WT and Q375E in facilitating GR·HSP-90 complex formation.

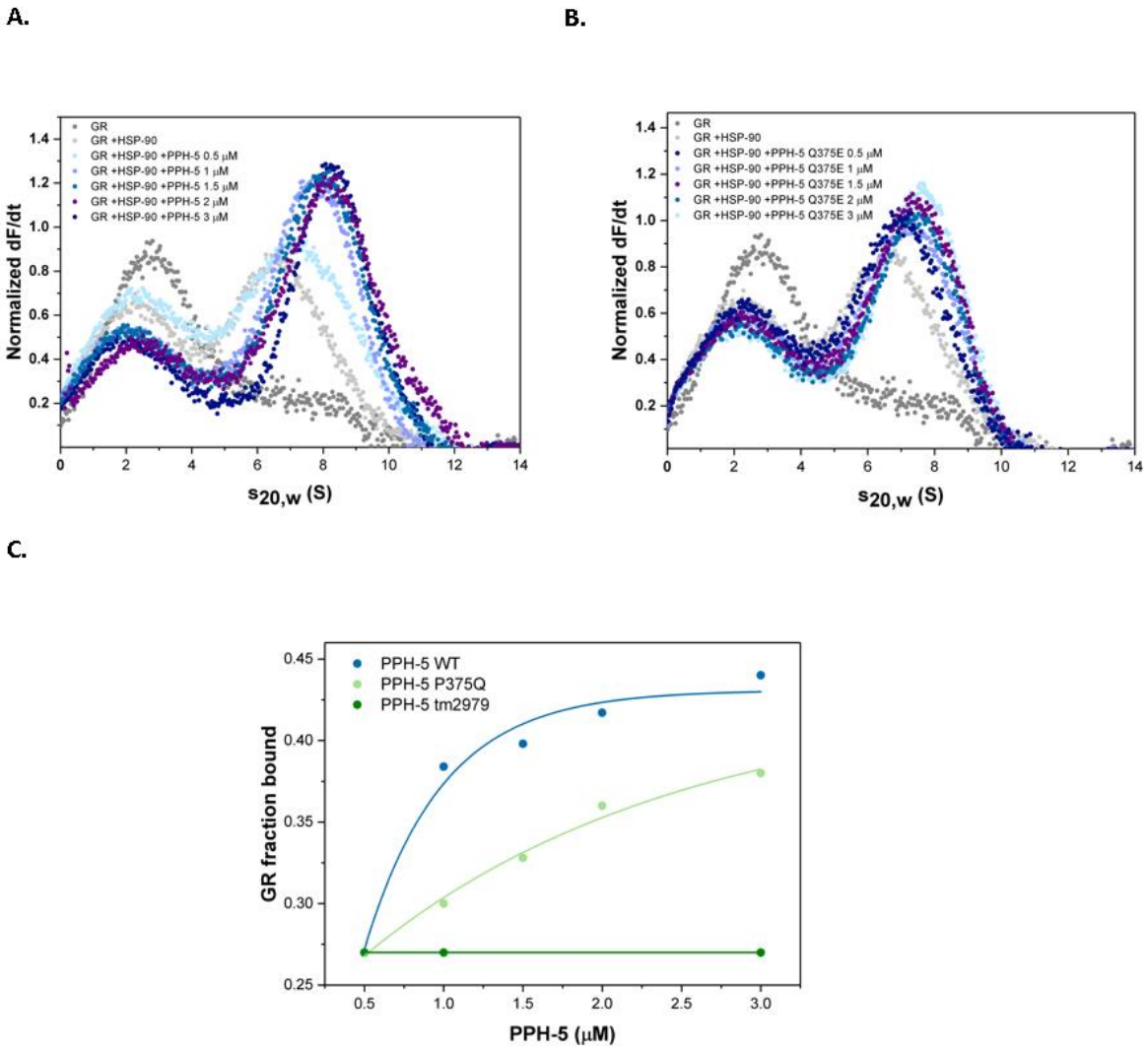

Figure 4.19 Sedimentation velocity AUC titrations to follow cooperative complex formation between GRm·HSP-90 and separase suppresing PPH-5 mutants tm2979 and P375Q. B) Titration experiments replotted for the GR fraction that is bound by quantifying the peak of monomeric GR at 2.8 S.

By mapping position 375 and also the other identified separase mutations in the structure generated for the trimeric GR·HSP-90·PPH-5 complex by crosslink-guided molecular docking, it is apparent that this mutation is within the PPH-5 HSP-90 interface (Figure 4.20). Moreover this position is in very close proximity to residues identified in crosslinked products with GRLBD, a contact site from which, the observed cooperativity in complex formation may originate. Moreover, the HSP-90 separase mutant, M661K, resides at the interface between

HSP-90 and the TPR domain of the phosphatase. The other separase mutations concern also the PPH-5 HSP-90 binding interace, are proximal to the catalytic site of the phosphatase or in the interdomain region. It therefore seems, that separase supressing mutations on PPH-5 and HSP-90 are relevant to the interaction between the two proteins and even though this pathway is not described, it is likely that separase is at some level regulated by an Hsp90·PPH-5 assembly.

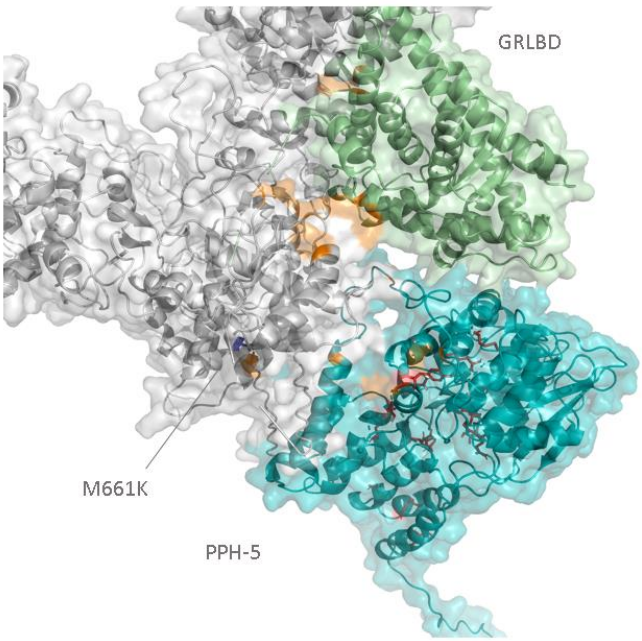

Figure 4.20. Separase suppresing mutations of PPH-5 mapped on the crosslink-guided model generated for trimeric GRLBD·HSP-90·PPH5. Orange surface show crosslinked products identified in the previous section, red sticks show the separase supressing mutations on PPH-5 while M661K mutation on HSP-90 C-terminus is shown in blue.

Introduction of these mutations in PPH-5 will help, along with in vivo investigations and purifying separase , understand from where the seperase suppresing effect originates.

Mutagenesis was performed *in silico* using the homology model that was generated for PPH-5 and HSP-90 to predict the total energy each point mutation would cost to the protein and select candidates for recombinant protein expression (Table 4.4). Point mutation E76A that was reported to enhance PPH-5 function was also included .

Table 4.4. FoldX total energy readout upon each point mutation using homology models of PPH-5 and HSP-90.

Mutation	Total Energy	Mutation	Total Energy
I32N	1.30134	R300C	2.91288
Y52N	0.522996	N309K	0.617836
G66E	-2.09618	M311R	1.84407
E76A	0.193242	Y322I	3.14326
L77P	6.93067	H351R	9.49498
A105F	18.4384	P375Q	1.65629
M211K	4.87787	C414Y	6.37089
H243R	1.61504	H426Q	1.10568
G244E	29.9024	C441Y	4.12925
D270A	-2.12336	**Open HSP-90**	1.73962
D270N	-1.8615	**Closed HSP-90**	0.874285

4.4 FRET system to follow the conformational cycle of nematode HSP-90

The Hsp90 chaperone processes client proteins while undergoing an ATP hydrolysis cycle with distinct open and closed intermediate states. Structural analyses have provided insight to these intermediates while a FRET system has previously been developed for the yeast Hsp90 protein (61,62) This way, the authors dissected the ATPase cycle kinetically and found out that conformational transitions are orders of magnitude slower than ATP hydrolysis and are, therefore, the limiting events during the Hsp90 cycle (62). Also, the effect of cochaperones in modulating the conformational cycle can be monitored with this approach.

Nematode HSP-90 harbors 8 cysteine residues which makes the design of a FRET construct with the appropriate labeling challenging, compared to the yeast chaperone that does not harbor cysteine residues. To create a FRET system that specifically addresses the N-domain kinetics, the engineered cysteine would need to be selectively labelled but this would be challenging with 8 other cysteines present. Based on multi-species sequence alignments, these residues were mutated to the most conserved in the other species residue in this position (plasmid vector designed by Klaus Richter). E63 was also mutated to a cysteine as, in analogy with the yeast chaperone, this position is surface exposed and not likely to be directly involved in Hsp90 function (62).

The exact changes in the nematode Hsp90 sequence can be seen in Figure 4.21.

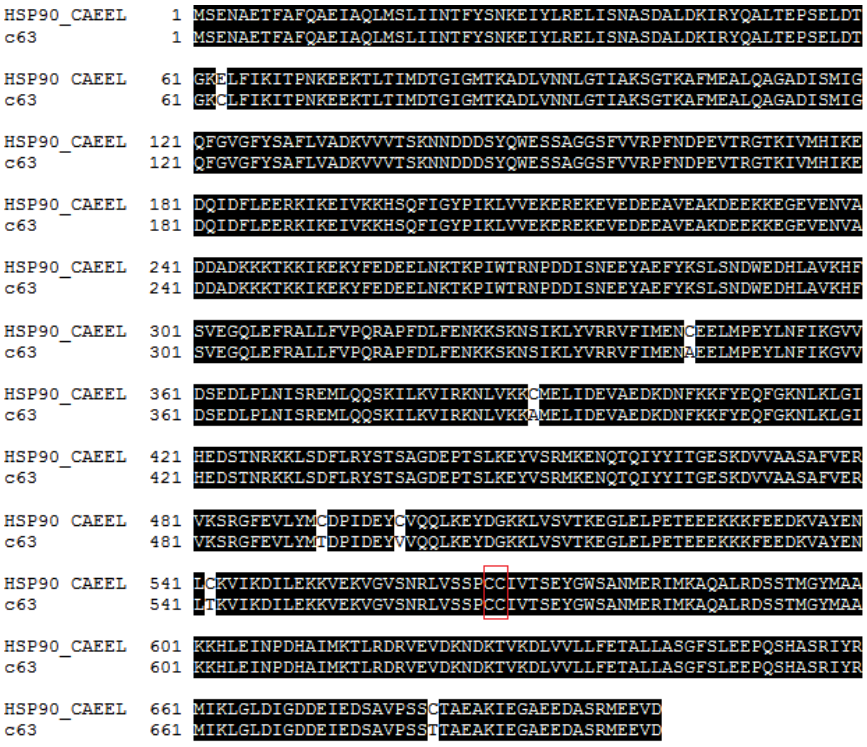

Figure 4.21 Sequence alignment for HSP-90 construct C63 and WT HSP-90. Cysteine residues are shown in black.

The C63 construct was purified from *E.coli* and yielded a folded (Figure 4.22 A) and functional in client and cochaperone binding (Figure 4.22 D) Hsp90 protein with substantially reduced thermal stability (Figure 4.22 B, C). Each cysteine mutation was also generated *in silico* with the FoldX algorithm to examine the energy penalty they cost to the protein (Table 4.5). It became apparent that C499V required a higher energy penalty compared to the other mutations (with the exception of the engineered cysteine at position 63 that is slightly destabilizing) that seem to be energetically favorable. This residue was then mutated to alanine and apparently, this position has a very pronounced effect on protein stability, since the alanine construct was thermally as stable or much more stable than WT as determined by TSA and CD thermal transitions respectively.

Table 4.5. Total energy reported by FoldX software upon mutation of each cystein to the appropriate amino acid to construct HSP-90 C63.

	Mutation	Total Energy
NBD	E63C	+0.66
	C345A	-0.15
	C391A	-0.22
MD	C492T	-0.26
	C499V	+1.21
	C542T	-0.36
CTD	C682T	-0.38

Purified HSP-90 C63 with an alanine at position 499 was labelled with ATTO 488 (donor) and with ATTO 550 (acceptor) dyes under identical conditions to test whether a FRET signal develops upon mixing the differentially labelled construct. Indeed, upon mixing a marked decrease in fluorescence intensity was observed in the donor channel accompanied by an increase in the acceptor channel, consistent with the formation of heterodimers harboring the FRET pair.

Next, cofactors and ATPγS were added to see whether structural changes could be detected as changes in the FRET signal. As shown with sedimentation velocity AUC, ATPγS does not suffice to induce the closing reaction in the nematode system, as it does with the yeast chaperone, so a mixture of FKB-6,p23 and ATPγS was added to the mixed HSP-90 C63 to induce the closing reaction of the chaperone. Indeed, upon addition of this mixture, a further modulation can be observed: the donor channel fluorescence increases while the acceptor channel fluorescence further decreases (Figure 4.23). Part of the conformational changes here seem to have already occured until mixing is achieved, so rapid mixing by stopped flow instrumentation would be needed for thoroughly performing this analysis. This could not be achieved within the timeline of the present thesis but the data presented here show that this may be a promising FRET construct for future investigations.

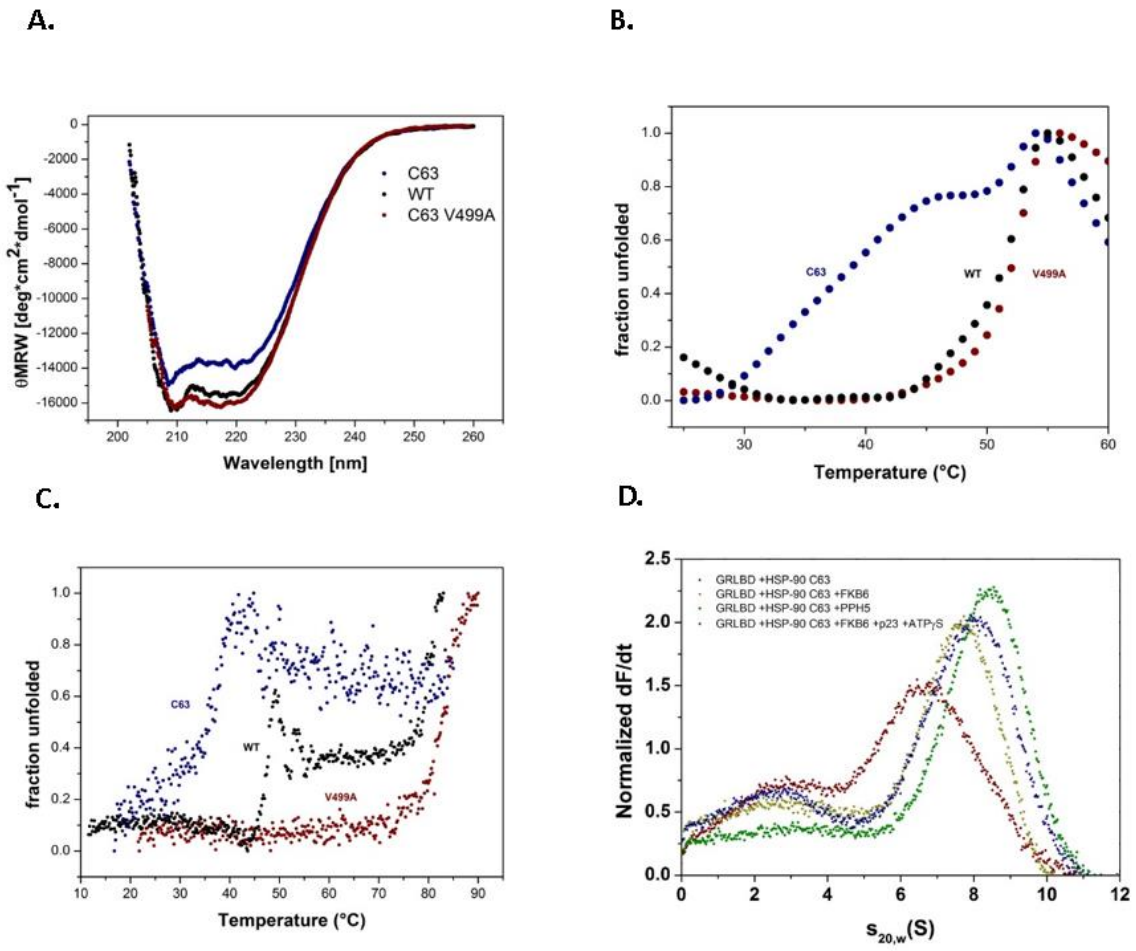

Figure 4.22. HSP-90 C63 and V499A are folded and stable proteins retaining client and cochaperone binding. Biophysical characterization of HSP-90 C63 and V499A by A) CD spectroscopy B) thermal shift assays C) CD thermal transitions and D) sedimentation velocity AUC in the presence of GR client and nematode cofactor proteins.

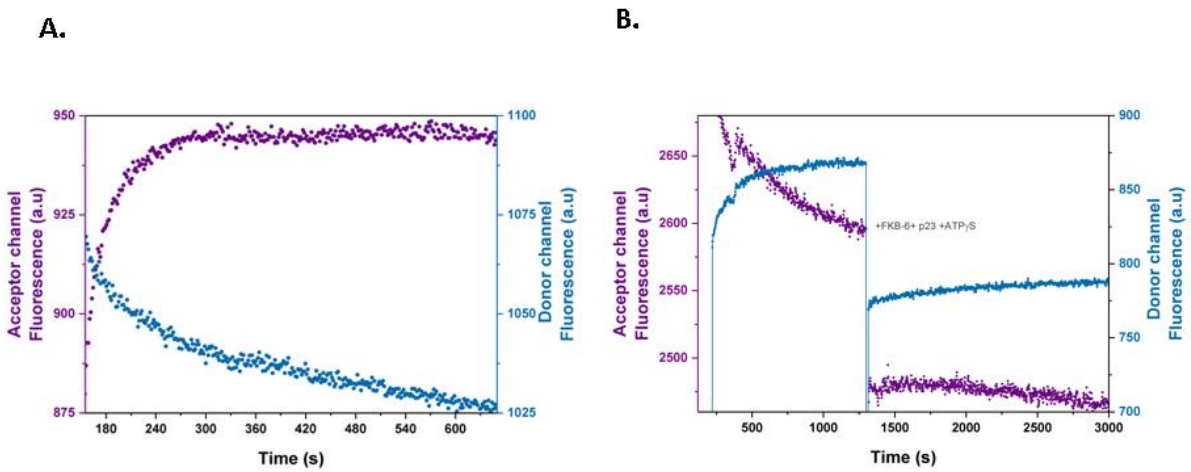

Figure 4.23. A) Kinetics developed upon mixing of HSP-90 C63V499A differentially labelled with the FRET pair ATTO488 (acceptor channel) and ATTO 550(donor channel) B) p23/ATPγS-induced conformational changes can be observed.

4.5 GRm L773P: A glucocorticoid resistance conferring mutation in the C-terminus of the glucocorticoid receptor

Point mutation L773P does not have overt effects on GRm.

Given that the wild type GR protein is rather unstable, the GRm variant, which is stabilized by mutagenesis and has previously been used to shed light on the GR·Hsp90 interaction, was employed (44,59,72,188,227). To study the influence of the point mutation the GRm construct that contains the DBD, hinge region and LBD of GR was purified. Leucine 773 was mutated to proline by site directed mutagenesis and both proteins, GRm and GRm L773P, were purified from *E.coli* in the presence of the stabilizing ligand dexamethasone (DEX), according to GRm purification that has been described previously (44).

The two GR variants were initially characterized to see whether there are pronounced differences in the mutant receptor and its oligomerization behavior and structural stability. Both receptor variants are monomeric and sediment with 2.8 S (Figure 1A), as deteremined by analytical ultracentrifugation (AUC) coupled to absorbance detection. Far-UV circular dichroism spectroscopy displayed a similar, high α-helical content for the two variants (Figure 1C). Both variants are stable up to 45 °C and then start unfolding in a cooperative transition, as determined by CD thermal transitions (Figure 1B). The GRm L773P melting temperature was determined to be approximately 3°C lower than that of the GRm variants'. Examination of the constructs by fluorescence spectroscopy shows that GRm exhibits a higher intrinsic tryptohane fluorescence that is not accompanied by a shift of the peak (Figure 4.2.2D). GRLBD harbors 5 tryptophane residues, mapped on its structure with blue sticks (Figure4.2.3). The difference in fluorescence intensity likely represents a more exposed Trp residue in the mutant construct.

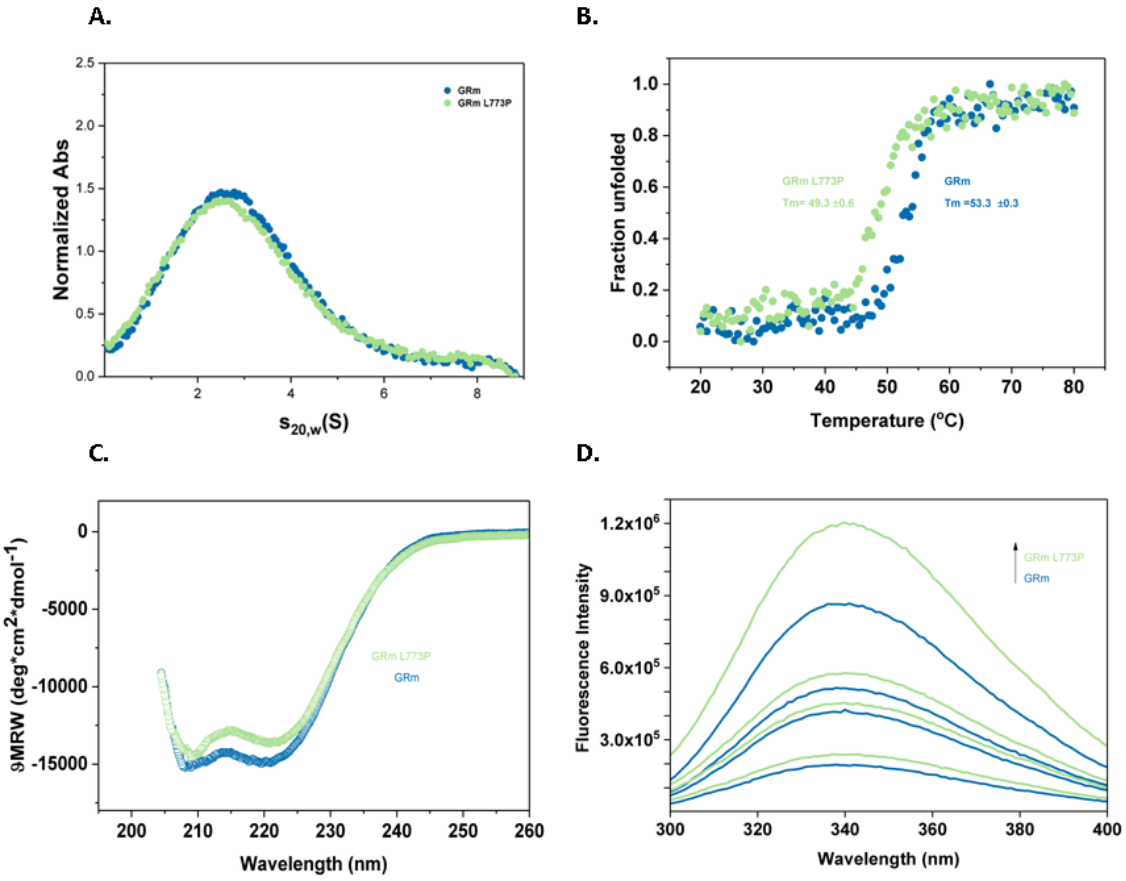

Figure 4.25: A) Both GRm variants are monomeric in solution as determined by AUC coupled to absorbance optics. B) CD thermal transitions show that GRm L773P has a T_m 3°C lower than GRm. C) CD spectra display similar α-helical content for the two GRm variants. D) Hormone exchange kinetics show substantially reduced rate for GRmL773P exchange.

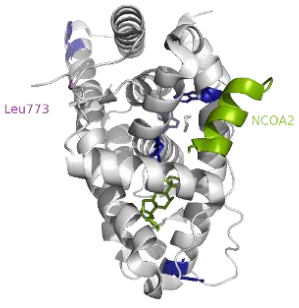

Figure 4.26. Tryptophane residues are mapped as blue sticks onto GRLBD structure (PDB 5NFP).

GRm L773P exhibits reduced hormone binding that is restored by Hsp90β and altered binding to a coactivator-derived peptide.

To further compare the two GRm variants, hormone-binding was followed by fluorescence polarization, recording GRm binding to fluorescein-labeled dexamethasone (F-DEX). Under these conditions, GRm L773P exhibited a 2.4-fold decrease in the apparent hormone-binding rate that could also be reflecting the ligand exchange kinetics, since residual dexamethasone is likely bound to extensively dialysed GR. Nevertheless, binding of F-DEX is taking place with a significantly reduced rate for GR L773P (Figure 4.27). Following GR binding το F-DEX in the presence of Hsp90β and ATP shows that the chaperone can accelerate the reaction kinetics of GRm L773P to an extent, even greater than for the leucine GRm variant (Figure 2A). This implies that interaction properties between GRm and Hsp90 are modified by the mutation.

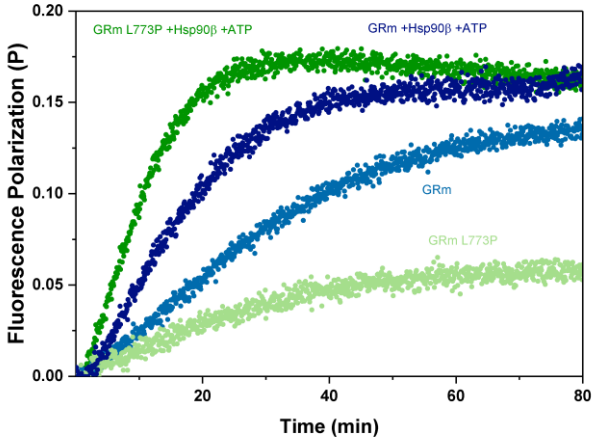

Figure 4.27. Fluorescence polarization measurements shows that hormone binding to GRm L773P takes place with significantly reduced speed while Hsp90β and ATP can accelerate the reaction kinetics to an extent, even greater than for GRm.

Then the interaction with a nuclear receptor coactivator 2-derived (NCOA2) peptide (residues 740−753), which binds the AF-2 helix of GR via its LLxxLL motif was examined. For this assay, the peptide was labelled with ATTO 488 and binding to GR could be observed by AUC coupled to fluorescence detection. The unbound NCOA2 peptide, sediments with approximately 1 S

and the complexes it is participating in, are observed at larger s-values. Both GRm variants could bind to the peptide, as observed at 2.7 S, with the L773P mutant exhibiting a slightly less efficient binding (Figure 4.28). However, when the chaperone Hsp90β is present, it is only possible for GRm to bind to Hsp90β and the peptide simultaneously, in a complex sedimenting with an $s_{20,w}$ of 7 S (Figure 4.28 B). In contrast, the L773P variant seems to only be bound to Hsp90β and to not fulfill the conformational requirements to form such ternary GR·NCOA2·Hsp90β complex (Figure 4.28).

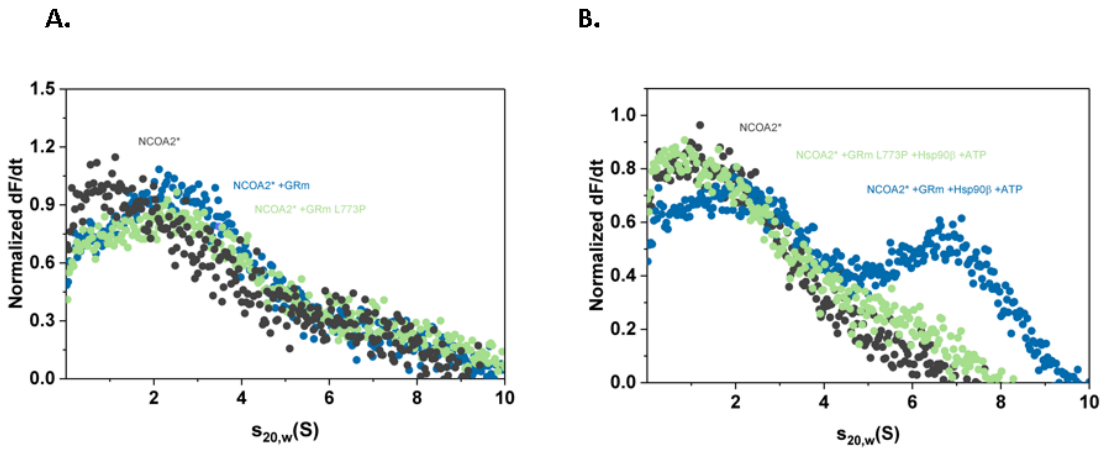

Figure 4.28. Sedimentation velocity AUC following binding of A) GR to a labelled NCOA2-derived peptide. B) same experimental set-up in the presence of Hsp90β and ATP.

GRm L773P·binds with reduced affinity to Hsp90β and Hsp90β-containing GRmL773P complexes are competent in hormone binding.

The two GRm constructs were examined by sedimentation velocity AUC coupled to absorbance optics for their interaction with Hsp90β. Under these conditions, in 1:1 stoichiometry, GRm L773P barely binds the chaperone, unlike the GRm·Hsp90β complex that readily forms and can be observed at 7 S (Figure 4.29 A).

Then F-DEX was employed in AUC coupled to fluorescence optics to assess the affinity of hormone-bound GR·chaperone assemblies. Under these conditions, the fraction of

monomeric GR that bound the ligand at 2.8 S was the same for both variants (Figure 4.29 B). Further, both variants can bind to Hsp90β, as observed by the respective peaks at 6.5 S and in both cases, ATP increases the hormone-bound GR·Hsp90β population (Figure 4.29 B). Judging from the reduction of the monomeric GR peaks, observed at 2.8 S, GRmL773P·Hsp90β complexes bound to hormone are represented by a lower population than for GR both in the presence and absence of ATP. Nevertheless, presence of Hsp90β stimulates hormone binding in both cases, compared to monomeric GR, and in both cases, when ATP is added nearly all hormone-bound GR is in complex with Hsp90β.

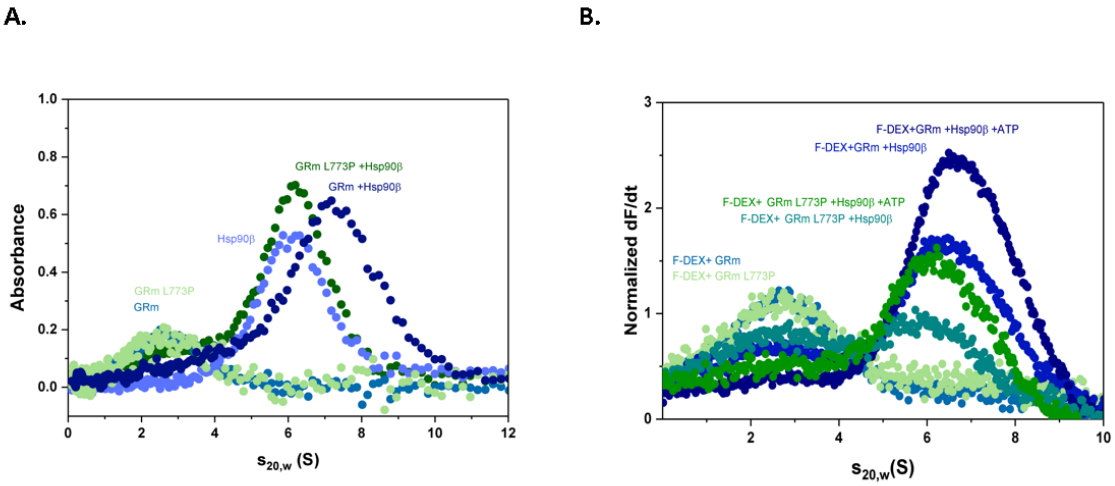

Figure 4.29. GRm L773P·binds with reduced affinity to Hsp90β and Hsp90β-containing GRmL773P complexes are competent in hormone binding. A. Sedimentation velocity absorbance AUC shows that GRmL773P hardly binds Hsp90 in a 1:1 ration, in contrast to GRm. B) Sedimentation velocity AUC shows that GRmL773P·Hsp90β binds hormone to a lower extent than GRm both in the absence and presence of ATP but both GR·Hsp90β assemblies are competent in hormone-binding.

It has recently been reported that GR decelerates the Hsp90 conformational cycle and ATPase activity decreases. Therefore, a regenerative ATPase assay was used to find out whether the modulation of the ATPase rate is also observable with the GRm L773P variant. Interestingly, GRm L773P suppresses the reaction rate even further than the GRm variant does (Figure 4.30).

Based on these results, it is to be expected that the changes imposed by the single-point mutation lead to altered interaction with the chaperone system.

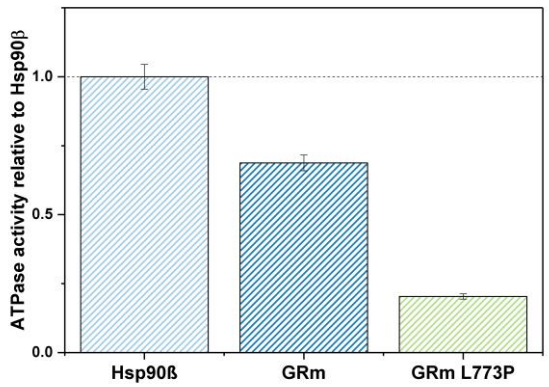

Figure 4.30. ATPase activity of Hsp90β is significantly lower in the presence of point mutant GRm L773P than in the presence of GRm. This plot shows the mean, relative to Hsp90β alone, ATPase activities in the presence of GRm and GRmL773P from three independent measurements with error bars representing the SD.

GRm L773P exhibits altered DNA binding properties

Having observed the differences in hormone and coactivator binding, the DNA binding competency of the two constructs was examined. A 32bp GRE element from the *fkbp5* promoter was chosen, utilizing the eykaryotic promoter database, and was used for AUC experiments with absorbance optics. This experiment shows that both constructs are able to bind to DNA, as shown by the peaks at ~4S, but the species observed for GRmL773P has a slightly smaller s-value (Figure 4.31). This implies either a lower affinity for the DNA or a different monomer: dimer ratio.

This was further examined with electrophoretic mobility assays (EMSA) under native conditions. GR without DNA was not able to run in the gel under these conditions but once DNA was added, the species formed could be separated by electrophoresis. It is clear from this assay that only GRmL773P forms a species matching the size of monomeric GR in complex

with the 32bp DNA (~50kDa), in addition to a species matching the size of dimeric GRm in complex with DNA. This band is hardly observable for GRm, which at all concentrations tested, formed a species that matches the size of dimeric GR+DNA (Figure 4.2.6).

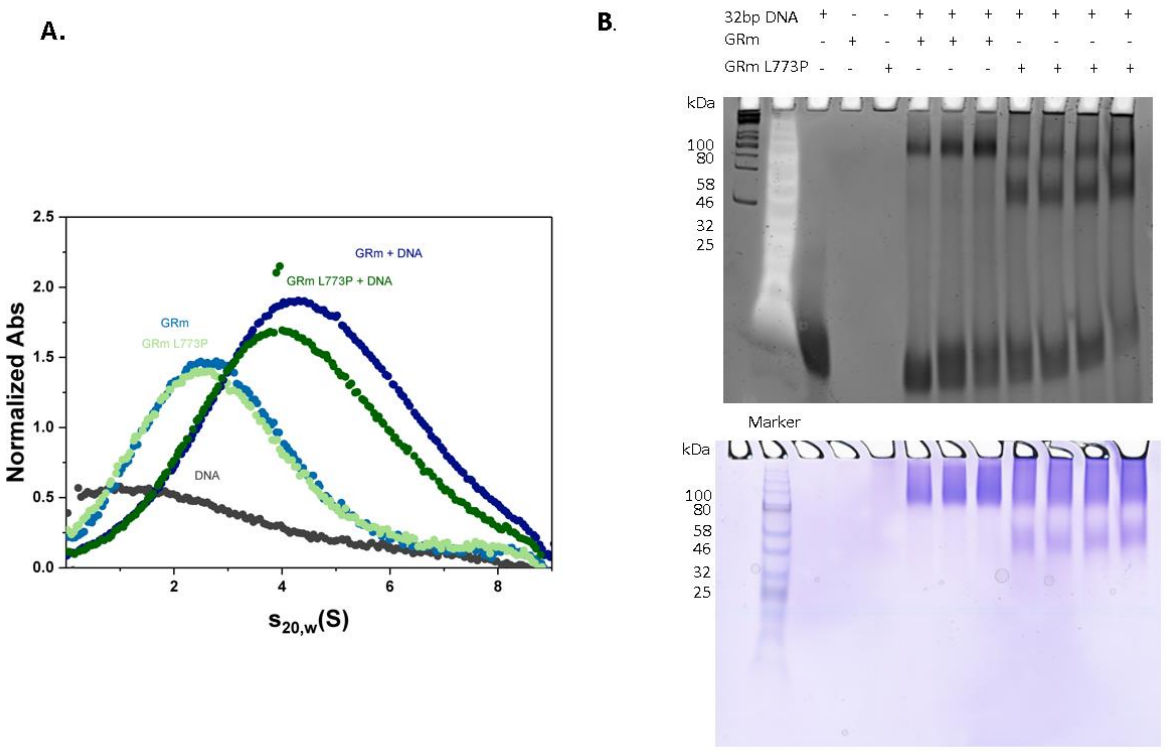

Figure 4.31. A) Sedimentation velocity AUC experiment showing that both GRmL773P (olive) and GRm (navy) are competent in DNA binding and a slightly reduced s-value for GRmL773P+DNA. B) EMSA assay under native conditions shows a high population of monomeric GRmL773P bound to DNA that is hardly visible for GRm, which forms dimers in the presence of DNA.

L773P point mutation alters the dynamics of several GR elements in the presence of dexamethasone

To understand the complex interaction patterns that seem influenced by the single-point mutation, the two GRm variants were subjected to hydrogen/deuterium exchange coupled to mass spectrometry (H/DX-MS) in the presence of dexamethasone. This analysis can reveal the conformational consequences of this point mutation to GRm and point to the elements that make this GRm variant glucocorticoid resistant.

High sequence coverage was obtained for both constructs (Figure 4.32) and by plotting the H/DX fractional uptake, both proteins seem dynamic, highlighting the ligand-induced plasticity of GR.

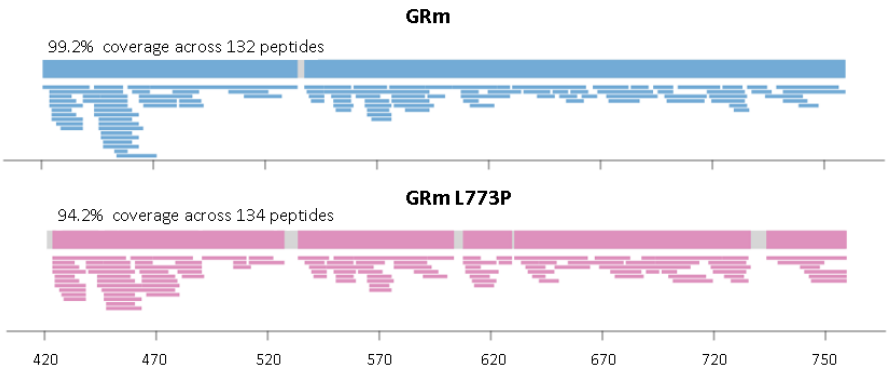

Figure 4.32: Sequence coverage obtained in HD/X MS measurements for the GRm and GRmL773P as visualized by Deuteros.

Several GR elements exhibit altered dynamics in the mutant receptor (Figure 4.34 A). Wood's plots, constructed for different time points with the Deuteros software and using the hybrid significance test. (p-value< 0.01), indicate that significant differences develop over time and affect H3, H4/5, H9 and H10 of GR LBD. Especially the proximal to the mutation site β-sheet 2, consisting of the strand located between H8 and H9 and the C-terminal strand following AF-2, exhibits higher fractional uptake (deprotection) in the mutant protein. Importantly, the DBD and hinge region of the receptor display altered dynamics (Figure 4.34 A, B-D)

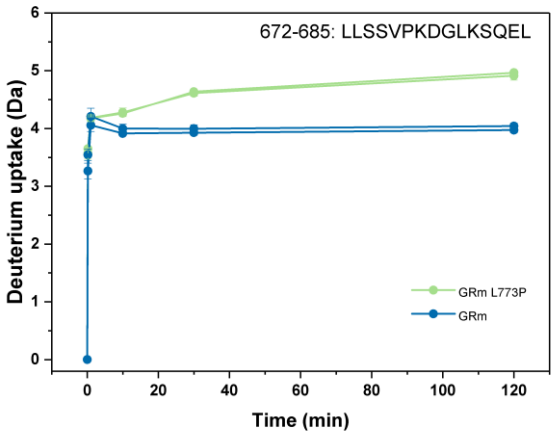

Figure 4.33. Deuterium uptake of GR peptide 672-685, corresponding to β-sheet 2 of GRLBD.

To further illustrate the affected regions, the differential HDX data was projected on the LBD of GR, utilizing the structure solved by Hemmerling et al (PDB 5NFP, Figure 4.34 D, E). It is here, readily observable that the differences observed, concern the interfaces between these neighboring GR elements and that the changes extend far beyond the mutation site.

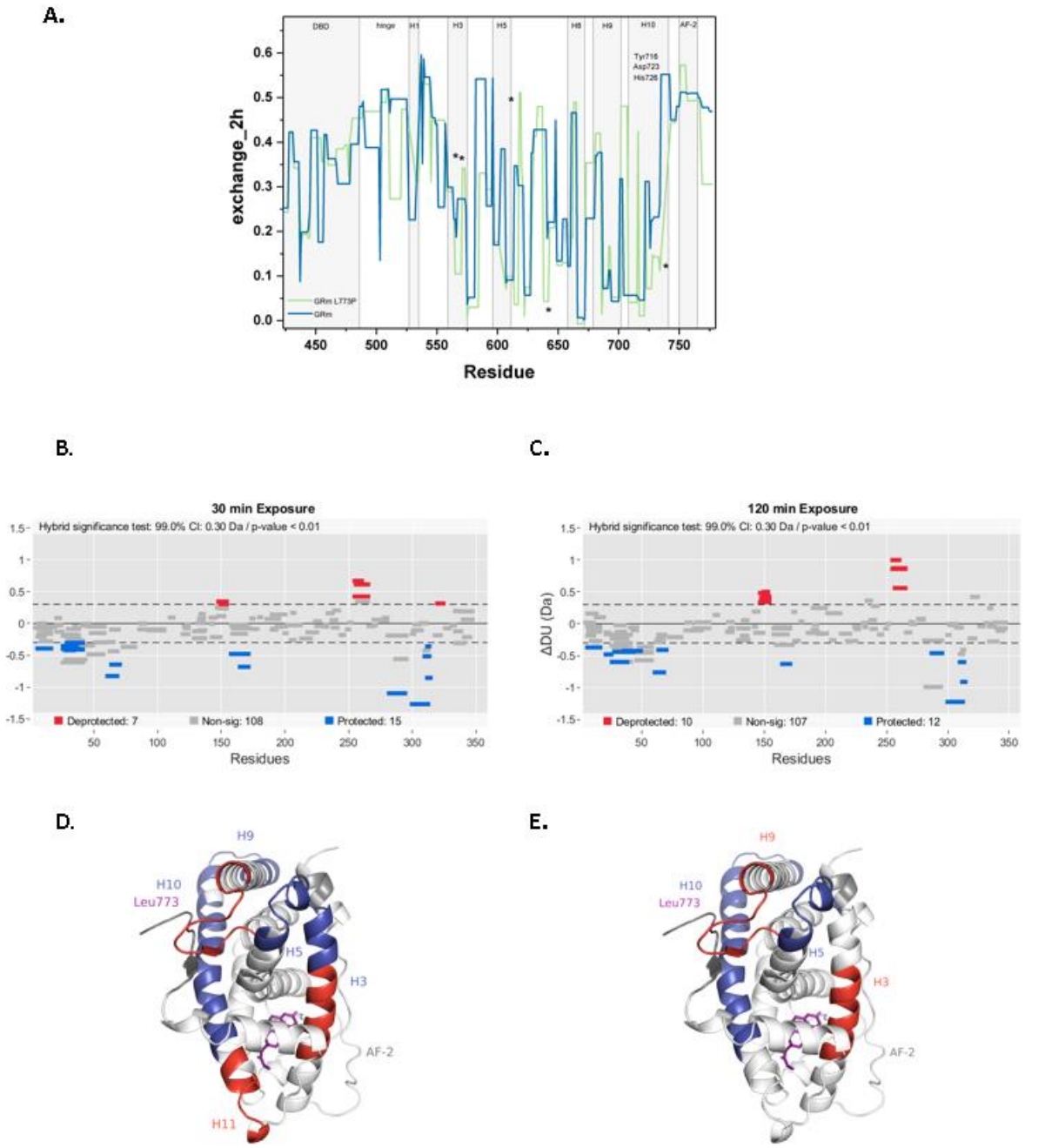

Figure 4.34. Comparison of GRm and GRm L773P in the presence of dexamethasone by hydrogen-deuterium exchange coupled to MS. A. The hydrogen-deuterium exchange is plotted for GRm and GRmL773P. Hormone binding residues are indicated with asterisks and characteristic GRLBD elements are highlighted on the plot. Both proteins are highly flexible and differences in their exchange rate can be observed for the various GR elements. B-D. Wood's plots based on two experiments, constructed with the Deuteros software for time points of 30 and 120 min and using hybrid statistics (p-value <0.01). Significant differential

signals concern the DBD/hinge, H3, H4/5, H9, H10 and β-sheet 2 of GR. E. The most significant relative changes in fractional uptake are mapped on the GR LBD structure for 30 min (D) and 2h (E) of exchange and are color coded in blue (low exchange) to red (high exchange).

Hsp90 interaction with GRm followed by HDX-MS

This analysis was then repeated in the presence of human Hsp0β and ATP (Figure 4.35). This experiment reveals the conformational consequences of Hsp90 interaction with GRm while comparison to GRm L773P in the presence of Hsp90β and ATP can point to the elements that follow different dynamics.

Wood's plots, constructed for different time points with the Deuteros software and using the hybrid significance test (p-value< 0.01), indicate the GR elements that are significantly affected by the chaperone interaction. This data is mapped on the GRLBD structure and helps visualize that β-sheet 2, is significantly protected when GR is in complex with Hsp90β. H9, H10 andH4/5 experience a mutual deprotection upon interaction with the chaperone while elements in H7, H5 and H3 exhibit lower fractional uptake (protection) around the ligand binding pocket.

Mapping this data on the model constructed for GRLBD in complex with nematode HSP-90 shows that these regions overlap with the receptor·chaperone interface and the significant deprotection in the upper part of the receptor and around the protected β-sheet 2, may refelect the way the chaperone facilitates the access of ligand to the binding pocket.

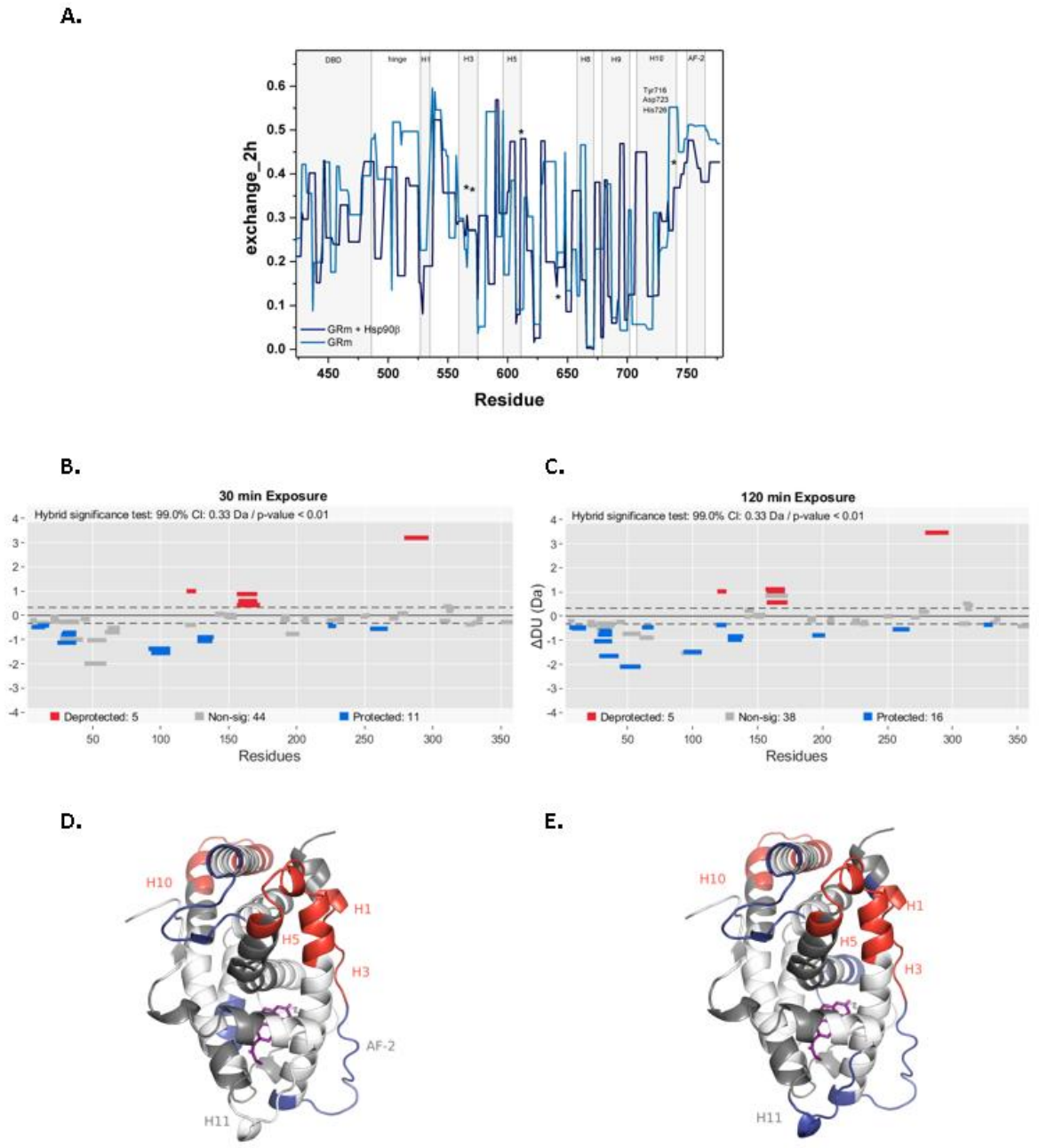

Figure 4.35. **Comparison of GRm in the absence and in the presence of Hsp90β and ATP by hydrogen-deuterium exchange coupled to MS reveals the conformational consequences of chaperone binding to GRm.** A) Fractional uptake plots of GRm in the absence (blue) and presence (navy) of Hsp90β and ATP. Hormone binding residues are indicated with asterisks and characteristic GRLBD elements are highlighted on the plot. B,C) Wood's plots based on two experiments, constructed with the Deuteros software for time points of 30 and 120 min and using hybrid statistics (p-value< 0.01) show the significantly affected GR elements due to chaperone interaction. D,E) Significant changes in fractional uptake are mapped on the GR

LBD structure for 30 minutes (D) and 2h (E) and are color coded in blue (low exchange) to red (high exchange).

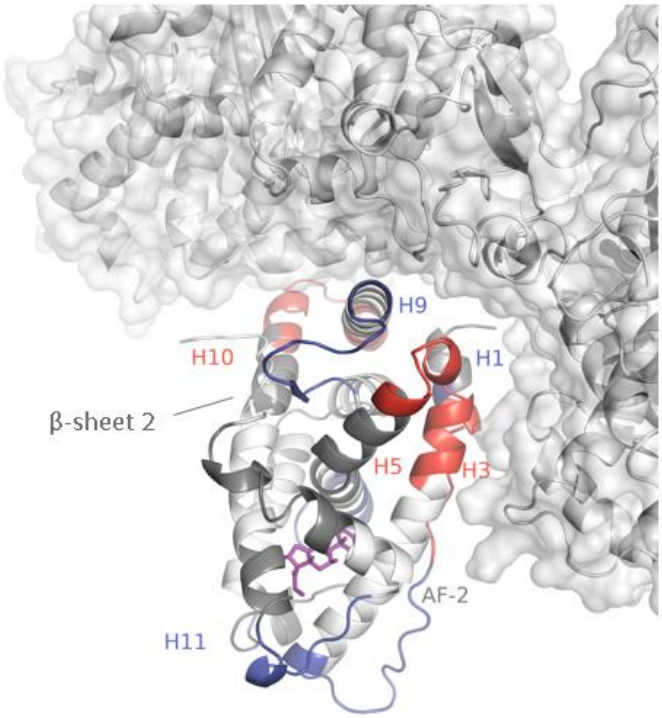

Figure 4.36. Shown is the differential HD/X data (from Figure 34E) for GRm in the presence of Hsp90β and ATP after 2h of exchange projected onto the GR·HSP-90 structure generated by crosslink-guided molecular docking.

Hsp90β interaction with GRm L773P followed by H/DX-MS

The same analysis was performed with GRm L773P in the absence and presence of Hsp90β and ATP. This analysis shows the effect that Hsp90β has on the mutant receptor, which displays an overall deprotection of the ligand binding pocket.

In contrast to GRm, the β-sheet 2, consisting of the strand located between H8 and H9 and the C-terminal strand following AF-2, is significantly deprotected upon interaction with Hsp90 β (compared to the GRm analysis in Figure 4.35 that was protected). The AF-2 interface and C-terminal peptide of GR harboring the mutation, show significant deprotection while no significantly protected peptides were observed around the ligand binding pocket. On the contrary, the elements from H7 and H11 that get protected upon interaction with Hsp90 β in the case of GRm, here show a relative deprotection. The DBD and hinge regions of the mutant receptor also experience a deprotection that was not observed in the GRm analysis (Figure 4. 37).

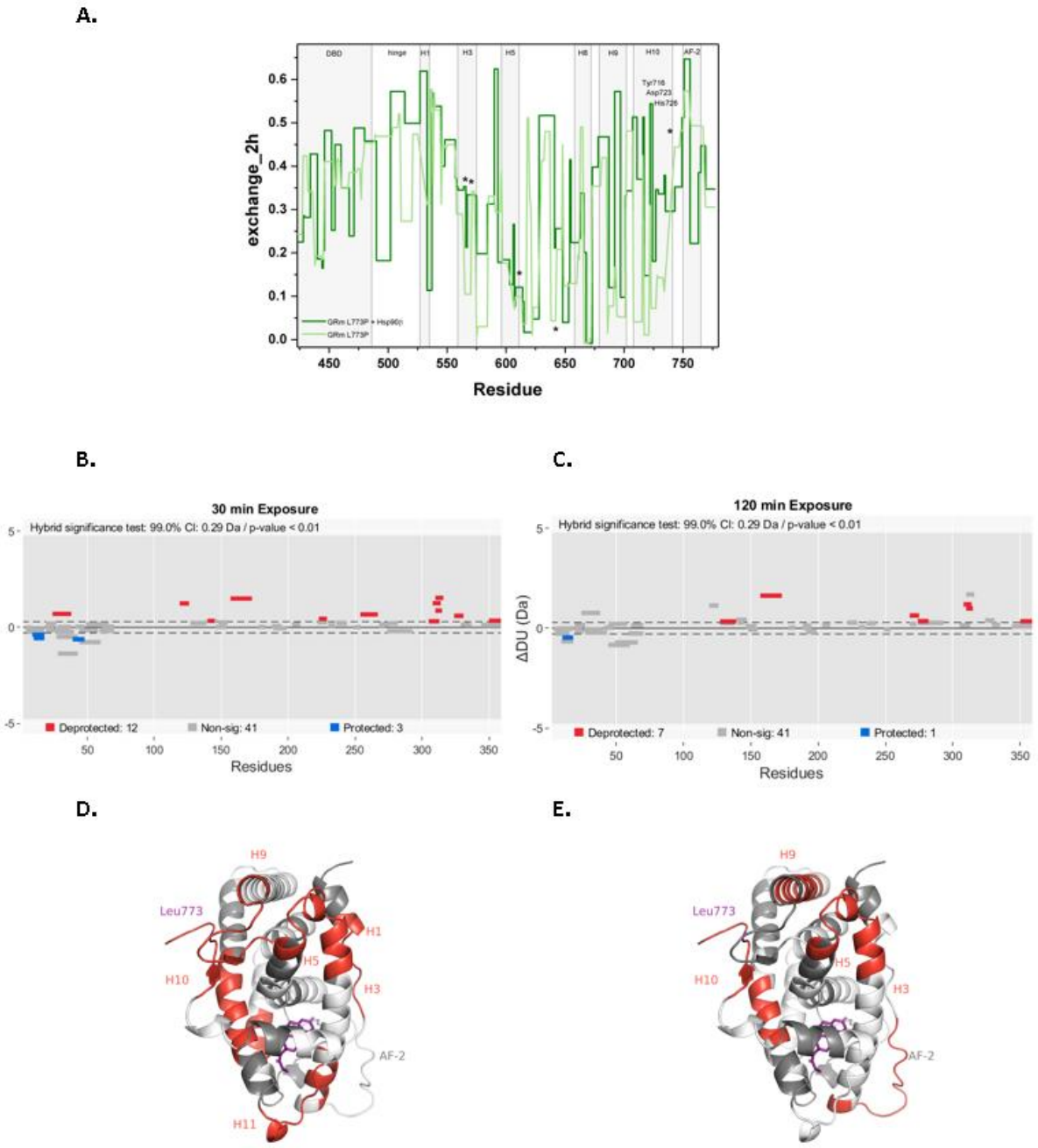

Figure 4.37. **Comparison of GRm L773P in the absence and in the presence of Hsp90β and ATP by hydrogen-deuterium exchange coupled to MS reveals the conformational consequences of chaperone binding to GRm L773P glucocorticoid resistant mutant.** A) Fractional uptake plots of GRm L773P in the absence and presence of Hsp90β and ATP. Hormone binding residues are indicated with asterisks and characteristic GRLBD elements are highlighted on the plot. B,C) Wood's plots based on two experiments, constructed with the Deuteros software for time points of 30 and 120 min and using hybrid statistics (p-value< 0.01)

show the significantly affected GR elements due to chaperone interaction. D,E) Significant changes in fractional uptake are mapped on the GR LBD structure for 30 minutes (D) and 2h (E) and are color coded in blue (low exchange) to red (high exchange).

Upon comparison of GRm and GRL773P by H/DX-MS and in line with the other biophysical experiments, the DBD and hinge regions of the receptor exhibit altered properties (Figure 4.34) i.e GRm L773P's DBD exhibits significantly lower fractional uptake (protection) in the absence of chaperone The differential HD/X data for the two constructs in the presence of Hsp90β and ATP was, therefore, projected onto the structure of dimeric GR DBD in complex with an *fkbp5*-derived GRE (PDB ID 3G6R)to visualize the differences in the presence of chaperone for this domain (228). It can here be observed that the DNA reading helix in GRm L773P experiences a deprotection instead of the protection observed for GRm when Hsp90β is present. After 2h of exchange GRmL773P exhibits only minimal changes in this domain compared to GRm, which seems strongly protected.

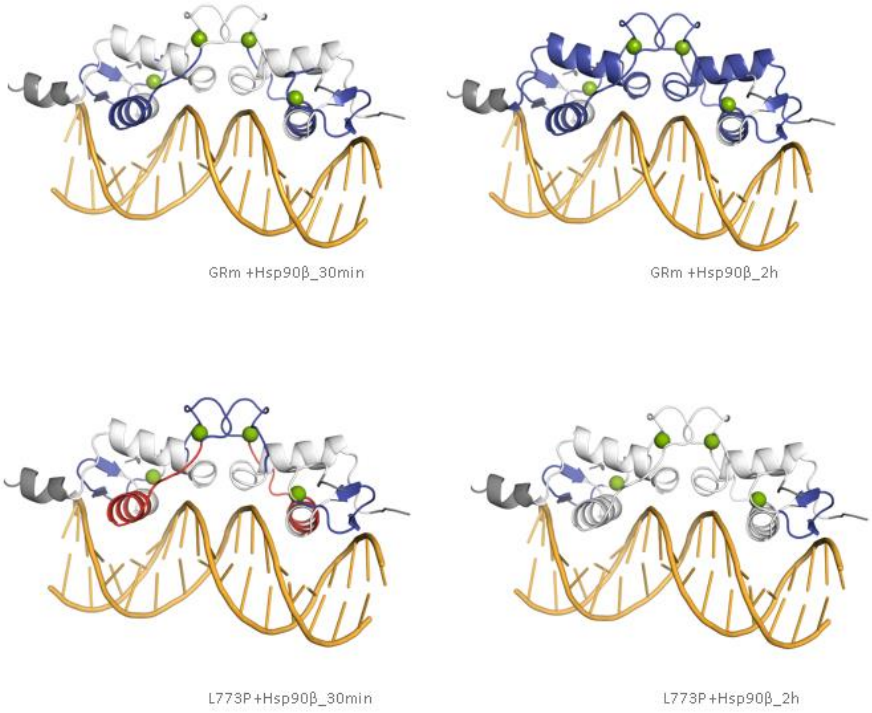

Figure 4.38. Significant changes in the conformational dynamics of GR DBD can be observed in the presence of Hsp90β and ATP. Projection of the differential H/DX data for GRm and GRmL773P onto the crystal structure of the GR DBD in complex with an *fkbp5*-derived GRE. Significant changes in H/DX for GRm or GRm L773P, as indicated in the plot, in the presence of Hsp90β and ATP are color coded in blue (low exchange) to red (high exchange).

Interestingly, plotting the fractional uptake for the GR DNA reading helix in the presence and absence of chaperone helps visualize that this element undergoes opposite exchange dynamics in GRm and GRm L773P (as observed in the Wood's plots in Figures 4.35 and 4.36 and visualized in figure 4.38) in the presence of chaperone, ultimately adopts the same exchange status with GRm upon interaction with the chaperone (Figure 4.39).

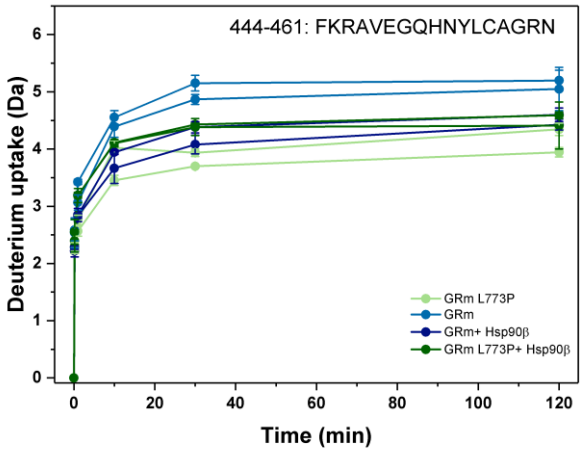

Figure 4.39. Uptake plots for GR residues 444-461 that consist the DNA reading helix.

The comparison of both variants in the presence of the Hsp90β machinery and ATP can help summarize the persistent differences in their interaction with the chaperone, the perturbations that chaperone binding cannot buffer (Figure 4.40). This figure shows that changes originating from elements proximal to the mutation site and the β-sheet 2 of GR, over 2h of exchange in the presence of Hsp90β and ATP concern H1, H3, H4/5 and H7. The changes observed in β-sheet 2 and the DBD of the receptor can not be observed in this Wood's plot since apparently the chaperone is able to restore their dynamics.

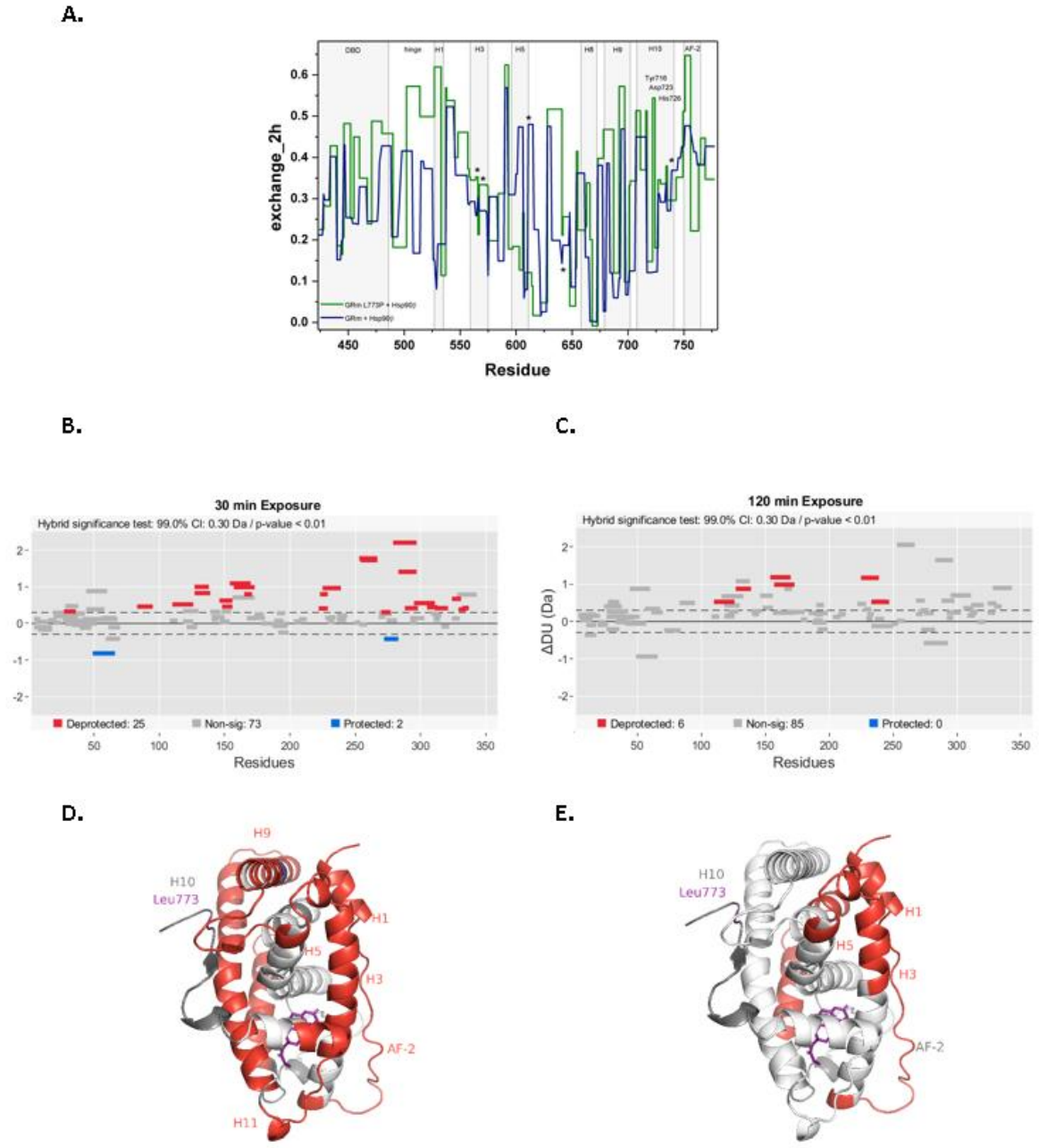

Figure 4.40. Comparison of GRm and GRm L773P in the presence of Hsp90β and ATP by hydrogen-deuterium exchange coupled to MS. A) The hydrogen-deuterium exchange is plotted for GRm +Hsp90β/ATP (navy) and GRmL773P +Hsp90β/ATP (olive). Hormone binding residues are indicated with asterisks and characteristic GRLBD elements are highlighted on the plot. F. Persistent after 2h altered dynamics mapped on our previously described model of GRLBD with *C.elegans* Hsp90, showing how these signals overlap with the binding interface. B, C) Wood's plots based on two experiments, constructed with the Deuteros software for time points of 30 and 120 min and using hybrid statistics (p-value< 0.02). Significant differential signals are here suppressed over time and persisting differences concern the H1,

H3, H4/5 and H7. D. The most significant relative changes in fractional uptake are mapped on the GR LBD structure for 30 minutes (E) and 2h (F) exchange and are color coded in blue (low exchange) to red (high exchange).

In silico insight into L773P point mutation conformational consequences

To further understand the conformational consequences of the single-point mutation L773P, the two GR variants were examined in silico by Molecular Dynamics (MD) simulations in the presence of dexamethasone. Leucine 773 was mutated to proline in the FoldX force field, employing the crystal structure solved for GRLBD by Hemmerilng et al (PDB 5NFP) and by coloring the protein surface for amino acid hydrophobicity according to the Kyte-Doolittle scale, it is apparent that there is a very hydrophobic spot around the mutation site that is discontinued once leucine 773 is mutated to proline (Figure 4.41 A) (209).

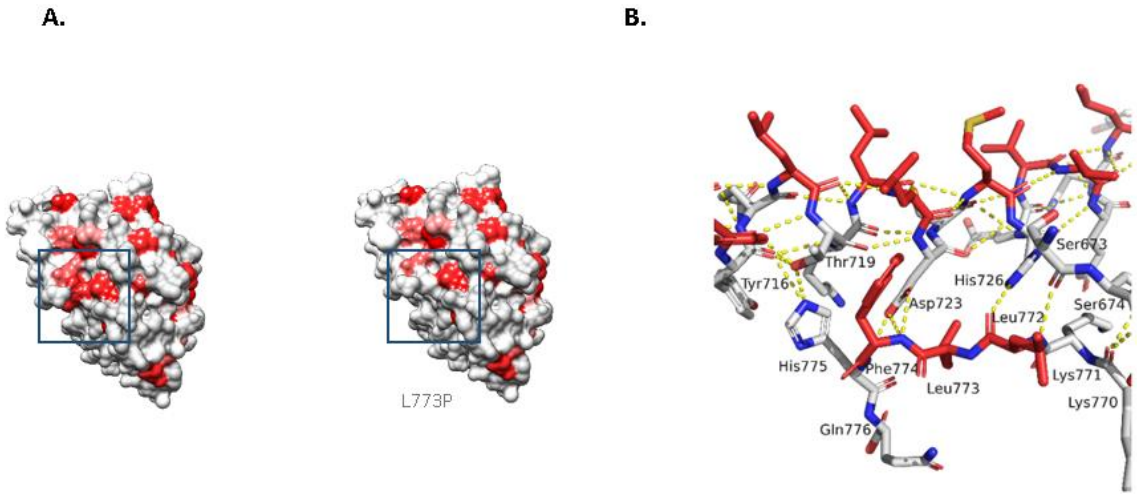

Figure 4.41. A) GRLBD surface colored for aminoacid hydrophobicity according to the Kyte-Doolittle scale. The hydrophobic residue network around the leucine 773 (left structure), as indicated with the frame is discontinued once leucine is mutated to proline (right structure). B) The hydrogen bonding network in the hydrophobic residue network around leucine 773. Hydrophobic aminoacids are colored red.

With a closer look at the hydrogen bonding network within this hydrophobic spot, it is apparent that the C-terminal residues around the mutation are involved in hydrogen bonds with H10 residues His726, Asp723 and Tyr 716 (Figure4.41 B). These residues also show an

intense change in deuterium uptake in the HDX analysis. MD simulations were performed with the GROMACS software in the CHARMM36 force field to examine hydrogen bonding between the respective pairs. The leucine variant displays an average distance of approximately 3 Å between the hydrogen bond donors and acceptors in the MD simulations, a distance consistent with the existence of an H-bond. In contrast, the mutated construct exhibits considerably larger distances between these pairs, which implies that the point mutation affects the positioning of the C-terminal peptide towards H10 and β-sheet 2 (Figure 4.36).

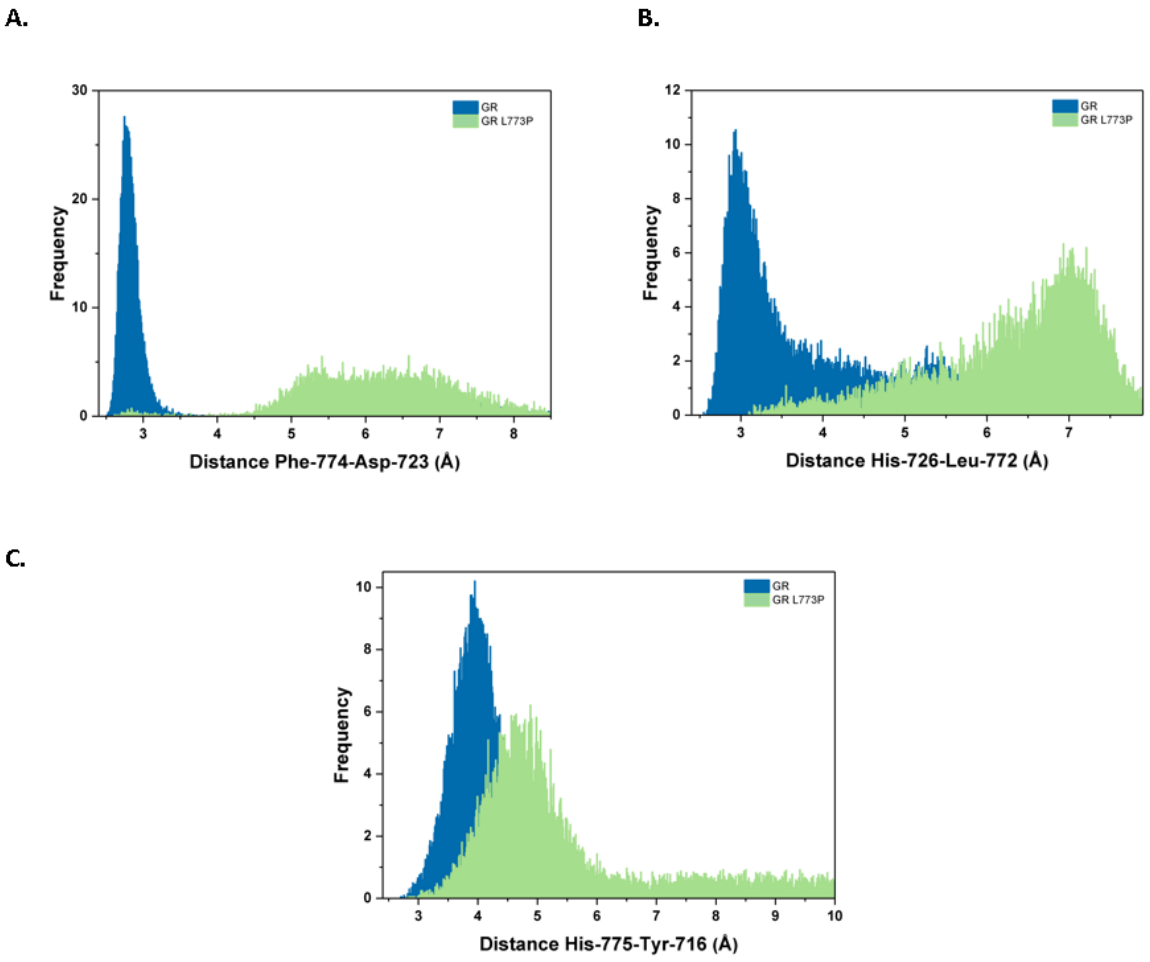

Figure 4.42. Mutation of leucine 773 to proline leads to a disrupted hydrogen-bonding network at GR's terminus. Hydrogen bond pairs as indicated in the plots between GR's C-terminus and H10 residues exhibit higher distances in GRLBD L773P MD simulations (n=2, t=100ns).

Once hydrophobic interactions are visualized, it is clear that the neighboring to the mutation residues His 775, Phe774 and Leu772 participate in complex hydrophobic interactions, highlighting the importance of proper positioning of GR's C-terminus. The neighboring to the mutation site Phe774 and Leu772 seem to be in the epicenter of hydrophobic interactions with H10 (Tyr 716, His 725, Asp723), β-sheet 2 (Pro676, Val675, Lys770) and also H9 (Leu680, Phe 686, Arg690) and H8 (Leu672) residues that stabilize the other β-strand of β-sheet 2. As other distances, like Leu770-Val675 and His775- Thr719, are not significantly affected in this approach, a local relaxation of the structure, which destabilizes β-sheet 2, is likely the reason for the increased dynamics observed via H/DX in this region (Figure 4.44).

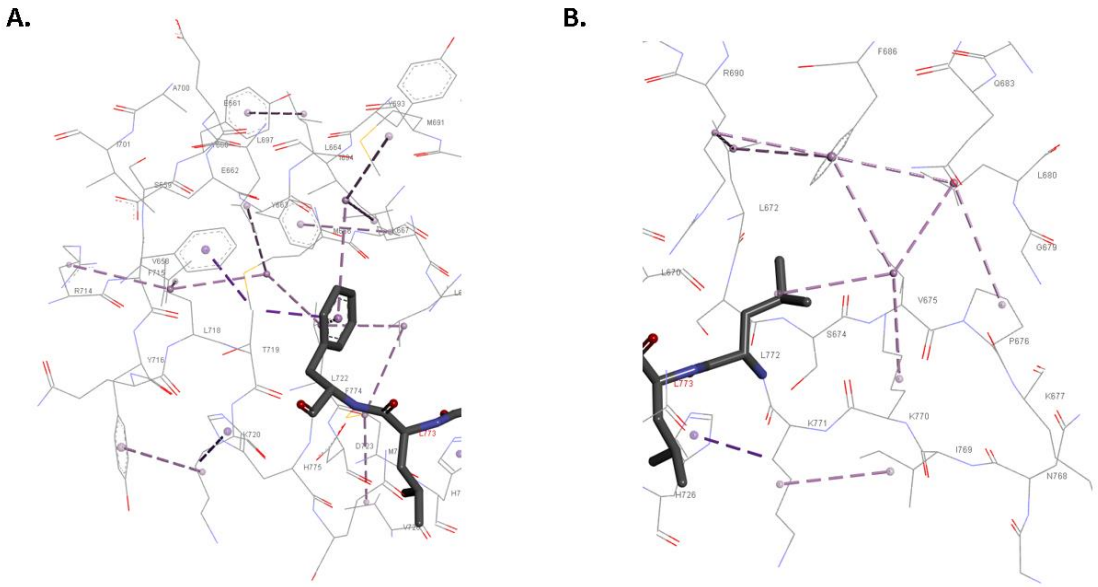

Figure 4.43. Hydrophobic interaction network around the mutation site shows how the neighboring to the mutation residues, Phe774 and Leu772 are in the middle of extensive hydrophobic interactions with GR elements in H10, β-sheet 2, H9 and H8. Figure was created with BIOVIA discovery studio.

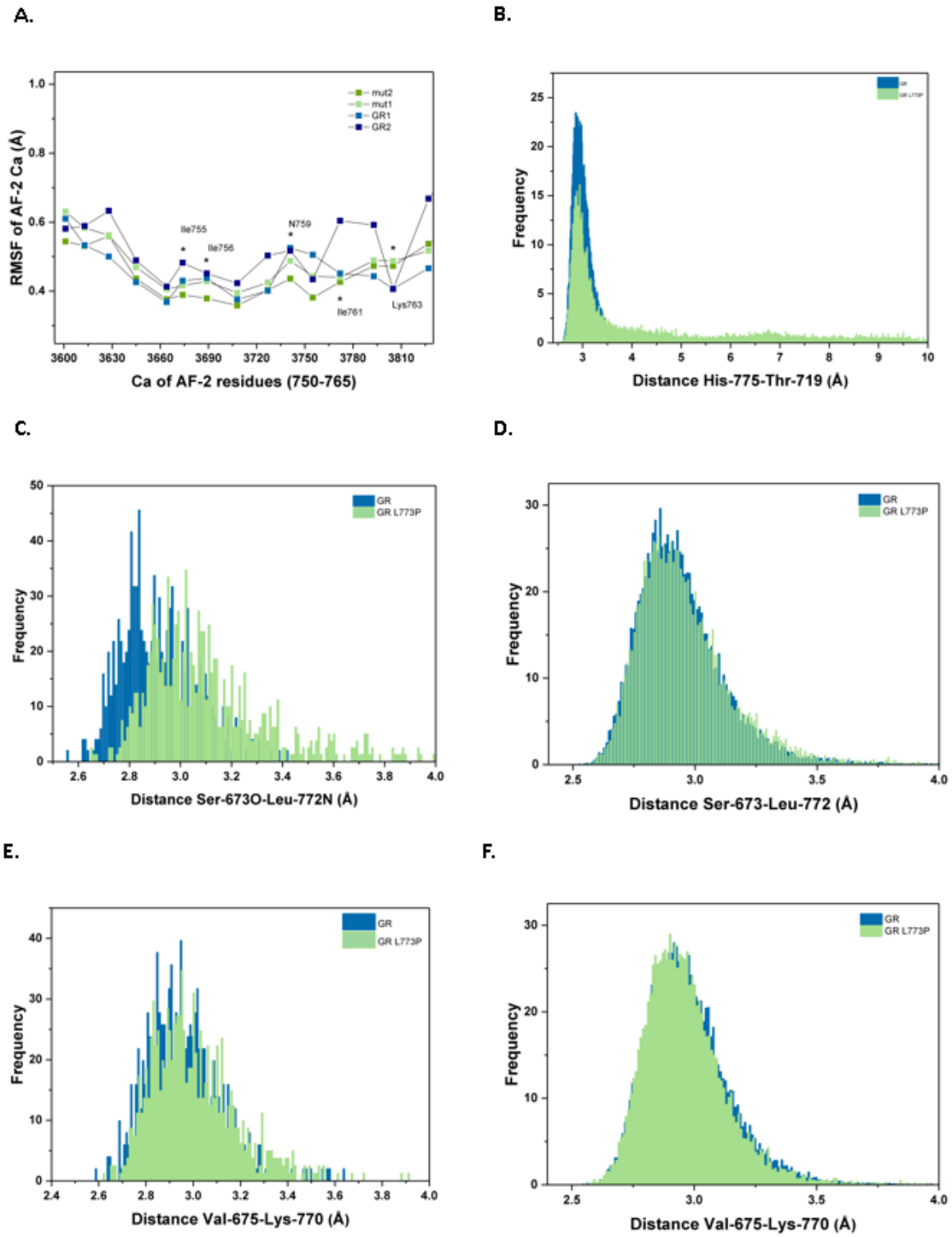

Figure 4.44 Other pair distances, proximal to the mutation site and relevant to β-sheet 2 seem to follow comparable dynamics in both constructs. A) RMSF of AF-2 Ca shows slightly increased flexibility for GRLBD but both variants seem to behave similarly in this approach.

B,D,F) Distance calculation of the indicated pairs based on MD simulations (n=2, t=100ns). C, E) Distance calculation of the indicated pairs based on MD simulations (n=7, t=1ns).

4.6 AHR

Stable expression of an aryl-hydrocarbon receptor construct

The AHR protein sequence is predicted to yield a very unstable protein, so the design of a stable construct of AHR LBD that should contain the LBD and Hsp90 binding regions of the receptor was attempted. Three constructs with variable termini were cloned and recombinantly expressed in *E.coli*, using autoinduction media ZYM5052. After small scale test expression in the presence and absence of dexamethasone that could also be stabilizing the AHR in a similar manner to GR, showed substantial expression only for the shorter construct, AHR3 (Figure 4.45 A). The presence and absence of DEX showed a similar protein expression yield, so the ligand was not utilized for protein purification. The purification consisted of Ni-NTA and two SEC steps. The isolated AHR is folded, as CD spectroscopy shows high α-helical content, common in the nuclear receptor family (Figure 4.45 B). This AHR construct, as determined by both CD thermal transitions and Thermal Shift Assays with the Cypro Orange dye, is stable up to approximately 40 °C and then starts to unfold in a cooperative transition, with a melting temperature Tm= 51.4°C and 50 °C by each method respectively (Figure 4.45 C, D).

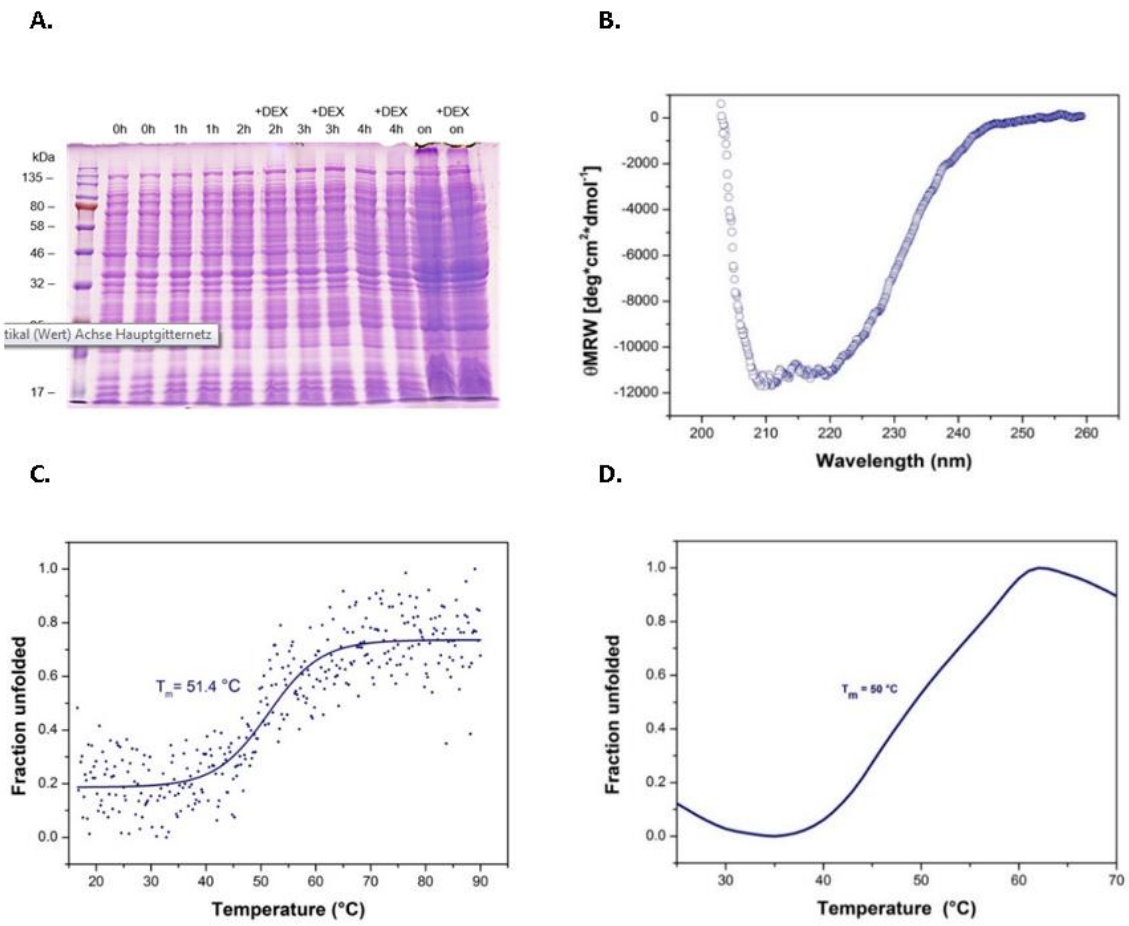

Figure 4.45. AHR construct is a folded and thermally stable protein. A) Small scale test expression, showing AHR expression overnight at the expected size of 40kDa. Biophysical characterization of AHR by C) CD spectroscopy C) CD thermal transition D) thermal shift assay.

The AHRr construct was then fluorescently labeled with ATTO-488 and was subjected to analytical centrifugation coupled to fluorescence detection. AHR sedimented with 2 S and bound to Hsp90β. The same was observed with sedimentation velocity AUC coupled to absorbance optics (data not shown). An interaction with the aryl-hydrocarbon interacting protein, AIP, could not be detected within this set-up (data not shown).

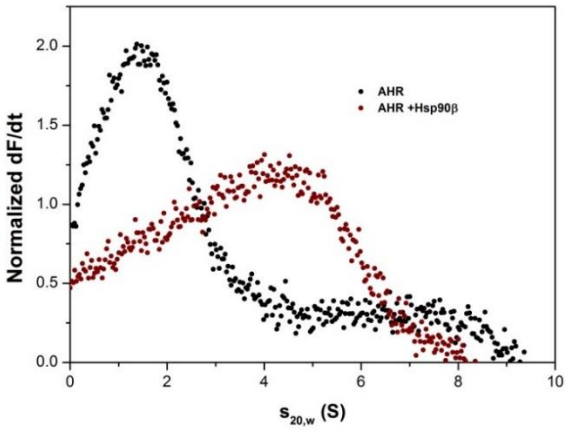

4.46. Sedimentation velocity AUC of fluorescently labelled AHR in the absence and presence of Hsp90β.

4.7 Whole-genome level responses of HEK293 cells to Hsp90β-selective inhibitor KUNB31 and dexamethasone

Microarray experiments were employed to analyze the transcriptional responses of human HEK293 cells to dexamethasone and KUNB31, a recently developed Hsp90β-selective inhibitor, to construct and then determine, which coexpression cliques are up- or down-regulated under such conditions and map the chaperone·SHR-specific genetic interactions (144). KUNB31 exhibited antiproliferative activity against various cancer cell lines, overcoming the induction of the heat shock response, observed with Hsp90 pan-inhibitors (144). The study describing the development of this molecule, reports a ~50-fold selectivity over Hsp90α and Grp94 *in vitro*, IC_{50} values in the lower micromolar range against cancer cell lines while no antiproliferative activity was observed with HEK293 cells treated with up to 100 μM KUNB31. *In vitro*, 1-30 μM KUNB31 concentrations were used to assess degradation of client proteins and chaperones 24h post to treatment, and an Hsp70 and Akt-1 depletion can be observed at 1 μM KUNB31.

To determine an inhibitor and hormone concentration and ensure cells are not only viable but also not in an apoptotic program before microarray analysis, HEK293 cells were treated with DMSO, DEX and/or KUNB31 and early apoptosis was monitored with the RealTime-Glo™ Annexin V Apoptosis assay. This assay employs Annexin V fusion proteins containing complementary subunits of the NanoBit ® luciferase (Annexin V-LgBiT and Annexin V-SmBiT) that form a functional luciferase once they bind the phosphatidylserine on the outer leaflet of cell membranes that gets exposed during apoptosis. A common dexamethasone treatment in the GEO database was 100 nM of DEX for 6 h so this treatment was selected and since Hsp70 and Akt-1 depletion can be observed at 1 μM KUNB31, the Annexin V assay was employed to see whether and at which time point, cells treated with 100nM DEX and/or 1μM KUNB31 exhibit signs of early-apoptosis. For this assay, cells were grown in CO2-independent media and were seeded in a 96-well plate 24h prior to treatment. Upon treatment (at approximately 60-70% confluency) with DMSO, DEX and/or KUNB31, luminescence was recorded with a plate reader. Under these conditions and up to 55 hours after treatment no significant increase in the luminescence signal was observed (Figure 4.47).

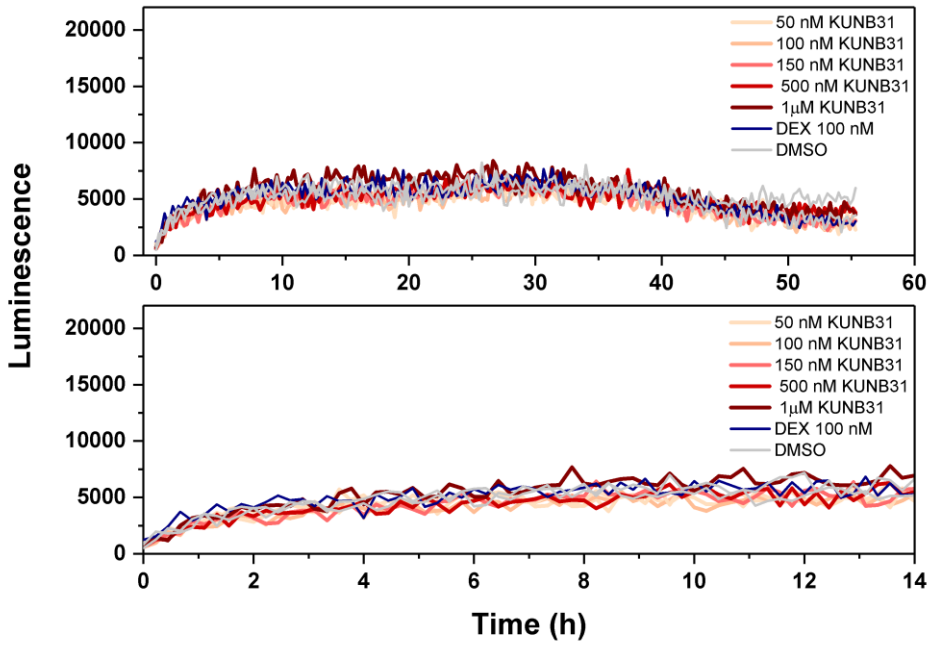

Figure 4.47. Annexin V assays show no significant exposure of phosphatidylserine upon treatment of HEK293 with KUNB31, as indicated in the plot, up to 55 hours post treatment.

At this point, Radicicol was employed as a positive apoptosis control to assess the magnitude of early apoptosis compared to the hormone and KUNB31 treatments. A Radicicol concentration of 25 μM that caused a sharp increase in the apoptosis signal was considered as a maximal response while concentrations up to 500 nM showed a signal comparable to the DMSO control samples throughout time (Figure 4.48).

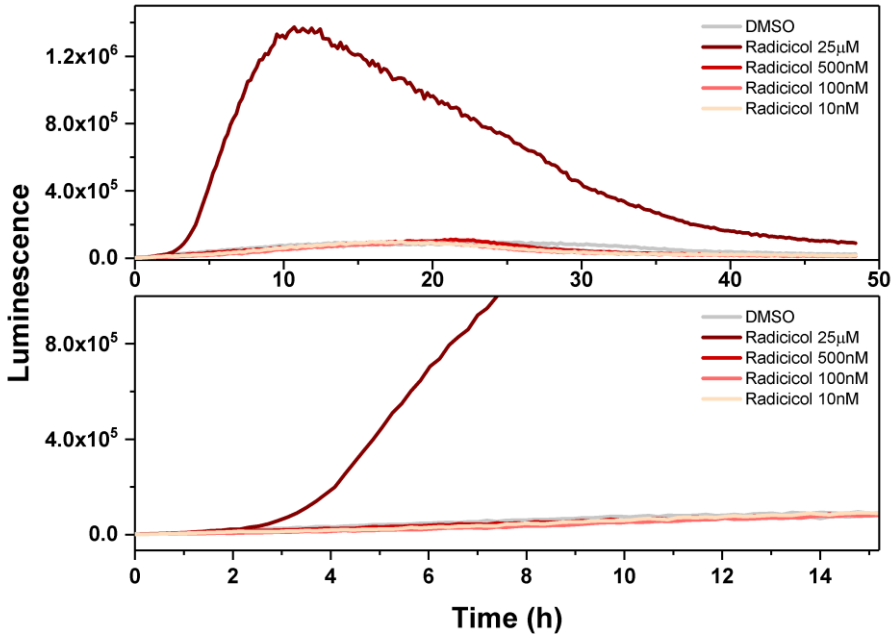

Figure 4.48. Annexin V luminescence upon treatment of HEK293 cells with Radicicol, as indicated in the plot.

Cells were also tested at a confluency of approximately 80%, the background signal is here slightly elevated, but the DEX and KUNB31 treatments give a luminescence signal comparable to control over time and therefore, a treatment with 1µM KUNB31 for 3h and 100nM DEX (where appropriate) for 6 further hours was considered a condition where the cells are not only viable but also do not show any signs of early apoptosis. Cells treated with DMSO, 1µM KUNB31 and/or 100nM DEX were spun down and the cell pellet was shock-frozen. RNA extraction and microarray analysis was carried out at KFB in University of Regensburg as a fee-for-service.

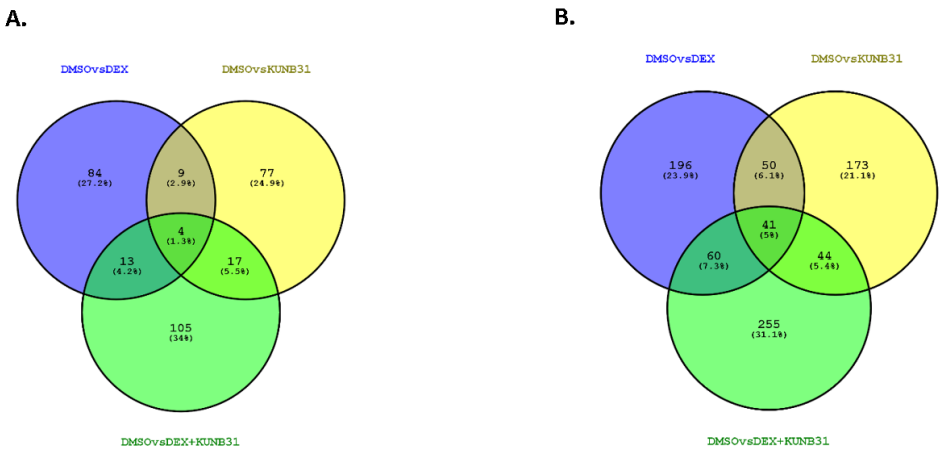

Figure 4.49. Venn diagrams of the significantly up or downregulated genes after the indicated treatments with a 1.5 fold-change and p-value <0.05 (A) and 1.15 fold change and p-value <0.01. (B).

Each treatment yielded a fraction of significantly up- or down- regulated genes that were not significantly affected in the other treatments while in all cases, no significant induction of heat shock proteins, like HSF-1 and the chaperones Hsp90 and Hsp70, was observed (Figure 4.49 and data not shown). This study was designed with the aim to construct and visualize the up- or down-regulated co-expression cliques with the ClusterEx algorithm (Klaus Richter, www.clusterex.de) that previously performed well in generating predefined cliques from publicly available data for the yeast and *C.elegans* genomes (229-231). However, and since this is a more demanding calculation, the human clusters could not be satisfactorily separated and the gene lists were, for the time being, filtered with the TAC software for significance and fold change to extract some indications of modified pathways.

Transcriptional response of HEK293 cells to Dexamethasone treatment

Table4.6.: A summary of the most up- or down-regulated genes that were unique to DEX treatment under the tested conditions and could also readily be assigned to Gene Symbols (DMSO vs DEX, fold change<>1.5, p-value <0.05).

ID	DEX Avg (log2)	DMSO Avg (log2)	Fold Change	P-val	Gene Symbol	Description
16929631	5.97	4.82	-2.23	0.043	**APOL1**	apolipoprotein L1
16922036	5.91	5.05	-1.81	0.0083	**BACH1**	BTB and CNC homology 1, basic leucine zipper transcription factor 1
17114470	6.55	5.96	-1.5	0.0444	**CT45A10; CT45A6; CT45A5**	cancer/testis antigen family 45, member A10,6,5
16834154	6.98	6.34	-1.56	0.012	**KRTAP9-4**	keratin associated protein 9-4
17114400	5.5	4.87	-1.54	0.0262	**LINC00633**	long intergenic non-protein coding RNA 633
16813419	4.87	4.09	-1.71	0.0329	**LINC00930**	long intergenic non-protein coding RNA 930
17073137	5.82	5.19	-1.55	0.0038	**LINC01300**	long intergenic non-protein coding RNA 1300
16852174	4.24	3.57	-1.59	0.0159	**LOC284263**	uncharacterized LOC284263
16838238	5.61	4.3	-2.47	0.0248	**LOC100996273**	uncharacterized LOC100996273
16957947	3.37	2.72	-1.57	0.0112	**LOC105374069**	uncharacterized LOC105374069
17070341	4.16	3.52	-1.56	0.0062	**LOC105375928**	uncharacterized LOC105375928
17094076	5.42	4.79	-1.55	0.0417	**LOC105376039**	uncharacterized LOC105376039
16956554	5.58	4.99	-1.51	0.0249	**LOC105377198**	uncharacterized LOC105377198
16679961	6.31	5.56	-1.69	0.0003	**LOC105379689**	F-box only protein 25-like
17104941	2.45	3.46	2	0.0133	**MIR374C**	microRNA 374c
16660734	5.48	4.83	-1.57	0.0405	**MIR378F**	microRNA 378f
17114680	5.26	4.53	-1.66	0.0201	**MIR505**	microRNA 505
16865072	5.06	4.18	-1.84	0.0098	**MIR516B2**	microRNA 516b-2
16865066	4.33	4.94	1.53	0.0348	**MIR520D**	microRNA 520d
16971046	3.07	3.68	1.53	0.0094	**MIR3139**	microRNA 3139
16741491	3.46	4.34	1.84	0.0095	**MIR3664**	microRNA 3664
16742775	5.15	5.81	1.58	0.0367	**MIR4300**	microRNA 4300
16975417	2.56	3.19	1.55	0.0472	**MIR4802**	microRNA 4802
16735317	3.09	2.44	-1.57	0.0178	**OR5P2**	olfactory receptor, family 5, subfamily P, member 2
16712766	4.92	4.31	-1.53	0.008	**PTCHD3**	patched domain containing 3
16774158	5.08	4.32	-1.7	0.0028	**RNU6-56P**	RNA, U6 small nuclear 56, pseudogene
16734927	3.85	3.24	-1.52	0.04	**TRIM5; HBG2**	tripartite motif containing 5; hemoglobin, gamma G

Less pronounced differences , as depicted in Figure 4.50, with a lower fold change but at a higher level of significance were also taken into consideration (fold change < or > 1.15 and p-value< 0.02, Figure 4.50). A summary of the genes that could be assigned to a gene symbol and a GO-category, grouped together for high-level GO-category with ShinyGO can be seen in Table 4.7. A fraction of the genes up- or down-regulated upon treatment could not get assigned to a Gene symbol and is not represented presented in the set.

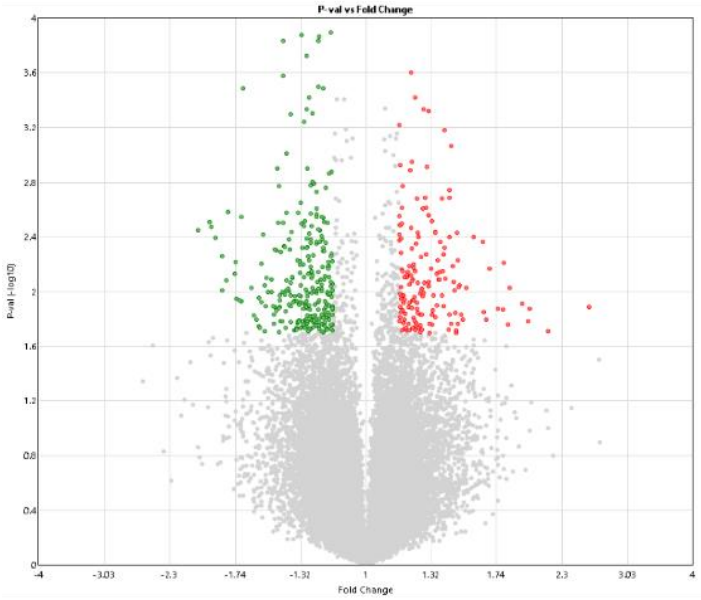

Figure 4.50. Volcano plot summarizing the greater than 1.15-fold up- or down-regulated genes upon treatment with dexamethasone (p-value<0.02).

Table 4.7. Summary of the genes that are unique to DEX treatment within 1.15 fold-change and a p value<0.02, and could also readily be assigned to a gene symbol and a GO-category, grouped together for high-level GO-category.

N	High level GO category	Genes
19	Regulation of signaling	LRP5L IL23A IFI6 EDA2R SHISA7 SHISA8 RAPGEF2 AIDA APBA2 GLI2 CA2 PPARGC1A DMRT1 PLEKHG4B SLC30A8 ARAP1 KLF14 RCN3 RAD9B
19	Regulation of response to stimulus	LRP5L IL23A IFI6 EDA2R MBL2 SCARA3 SHISA7 SHISA8 RAPGEF2 AIDA GLI2 PPARGC1A DMRT1 PLEKHG4B KLF14 RCN3 SH2D1B RAD9B ARAP1
18	Response to stress	EDA2R RAD9B MBL2 SCARA3 MT1M IL23A BACH1 RNASE6 PARP10 AIDA CA2 PPARGC1A ITGB6 IFI6 RCN3 DCD SLC30A8 SH2D1B
17	Regulation of biological quality	LRP5L IFI6 ENPP6 SUN3 SLC30A8 SHISA7 MT1M SHISA8 MORC3 APBA2 NAALAD2 CA2 PPARGC1A RCN3 RAB38 ARAP1 RAPGEF2
14	Anatomical structure morphogenesis	LRP5L PGM5 MBL2 SCARA3 RAPGEF2 GLI2 CA2 PPARGC1A FEZF1 DMRT1 HOXB2 SERPINB5 ARAP1 MGP
13	Regulation of molecular function	PPARGC1A IL23A IFI6 SHISA7 SERPINB5 SHISA8 RAPGEF2 EDA2R AIDA ARAP1 LPA RCN3 PARP10
11	Immune system process	LRP5L IL23A MBL2 SCARA3 RNASE6 CA2 IFI6 SLC30A8 SH2D1B GLI2 DCD
11	Regulation of localization	LRP5L SLC30A8 SHISA7 SHISA8 CA2 APBA2 PPARGC1A IL23A MBL2 ARAP1 RAPGEF2
11	Macromolecule localization	LRP5L RAB38 SUN3 SLC30A8 MORC3 APBA2 ITGB6 RCN3 SHISA7 LPA RAPGEF2
11	Regulation of developmental process	IL23A RAPGEF2 GLI2 NMRK2 CA2 PPARGC1A MGP FEZF1 DMRT1 MAMSTR ARAP1
10	System process	TAS2R5 OR5P2 PPARGC1A OR13J1 OR2B11 SHISA7 OR6K2 OR10Z1 HOXB2 LPA
10	Cell proliferation	IL23A DMRT1 BTG3 GLI2 RAPGEF2 MORC3 PARP10 PPARGC1A FEZF1 SERPINB5
10	Regulation of multicellular organismal process	IL23A RAPGEF2 ITGB6 GLI2 CA2 PPARGC1A MGP FEZF1 DMRT1 SHISA7
10	Multi-organism process	DMRT1 IL23A MBL2 RNASE6 PPARGC1A ITGB6 IFI6 MORC3 DCD PARP10
9	Response to external stimulus	IL23A MBL2 RNASE6 GLI2 PPARGC1A IFI6 FEZF1 DCD RAB38
8	Immune response	IL23A MBL2 SCARA3 RNASE6 IFI6 SLC30A8 SH2D1B DCD
7	Locomotion	ITGB6 GLI2 PPARGC1A IL23A FEZF1 DMRT1 RAPGEF2
7	Cellular component biogenesis	PGM5 RAB38 CLYBL PARP10 RAPGEF2 ARAP1 PPARGC1A
7	Cellular localization	LRP5L RAB38 SUN3 MORC3 APBA2 SHISA7 RAPGEF2
6	Immune effector process	IL23A MBL2 SCARA3 RNASE6 IFI6 SH2D1B
6	Regulation of immune system process	IL23A MBL2 SCARA3 CA2 GLI2 SH2D1B
6	Response to biotic stimulus	IL23A MBL2 RNASE6 PPARGC1A IFI6 DCD
6	Cell motility	ITGB6 PPARGC1A IL23A FEZF1 DMRT1 RAPGEF2
6	Detection of stimulus	TAS2R5 OR13J1 OR2B11 OR5P2 OR6K2 OR10Z1
6	Localization of cell	ITGB6 PPARGC1A IL23A FEZF1 DMRT1 RAPGEF2

6	Response to other organism	IL23A MBL2 RNASE6 PPARGC1A IFI6 DCD
5	Catabolic process	NAALAD2 PPARGC1A RCN3 ENPP6 RNASE6
5	Response to abiotic stimulus	RAD9B BACH1 CA2 PPARGC1A SCARA3
5	Growth	MBL2 SCARA3 APBA2 GLI2 MT1M
5	Interspecies interaction between organisms	MBL2 ITGB6 MORC3 DCD PARP10
4	Immune system development	LRP5L IL23A CA2 GLI2
4	Cell adhesion	IL23A ITGB6 PGM5 GLI2
4	Behavior	APBA2 SHISA7 NMS TAS2R5
4	Cell cycle process	DMRT1 RAD9B BACH1 ARAP1
4	Biological adhesion	IL23A ITGB6 PGM5 GLI2
4	Developmental growth	MBL2 SCARA3 APBA2 GLI2
3	Reproduction	DMRT1 GLI2 SERPINB5
3	Cell killing	IL23A DCD MBL2
3	Developmental process involved in reproduction	DMRT1 GLI2 SERPINB5
3	Response to endogenous stimulus	CA2 RAPGEF2 PPARGC1A
3	Reproductive process	DMRT1 GLI2 SERPINB5
3	Regulation of locomotion	PPARGC1A IL23A RAPGEF2
3	Taxis	GLI2 IL23A FEZF1
3	Regulation of multi-organism process	IL23A MBL2 PARP10
3	Regulation of cellular component biogenesis	PARP10 RAPGEF2 ARAP1
3	Leukocyte activation	IL23A GLI2 SH2D1B
3	Maintenance of location	SUN3 SLC30A8 MORC3
2	Activation of immune response	MBL2 SCARA3
2	Circadian rhythm	PPARGC1A NMS
2	Locomotory behavior	APBA2 NMS
2	Regulation of cell adhesion	IL23A GLI2
2	Killing of cells of other organism	DCD MBL2
2	Modification of morphology or physiology of other organism	DCD MBL2
2	Regulation of growth	MBL2 MT1M
2	Rhythmic process	PPARGC1A NMS
2	Anatomical structure formation involved in morphogenesis	PGM5 GLI2
2	Protein activation cascade	MBL2 SCARA3

The GeneMANIA algorithm uses a large database of functional interaction networks from multiple organisms to identify the most related genes to a query gene set, using a guilt-by-association approach while each related gene is traceable to the source network used to make the prediction (232). The network constructed for the dexamethasone treatment shows the genes that were significantly up- or down-regulated, connected for coexpression, genetic interactions and shared protein domains (Figure 4.52).

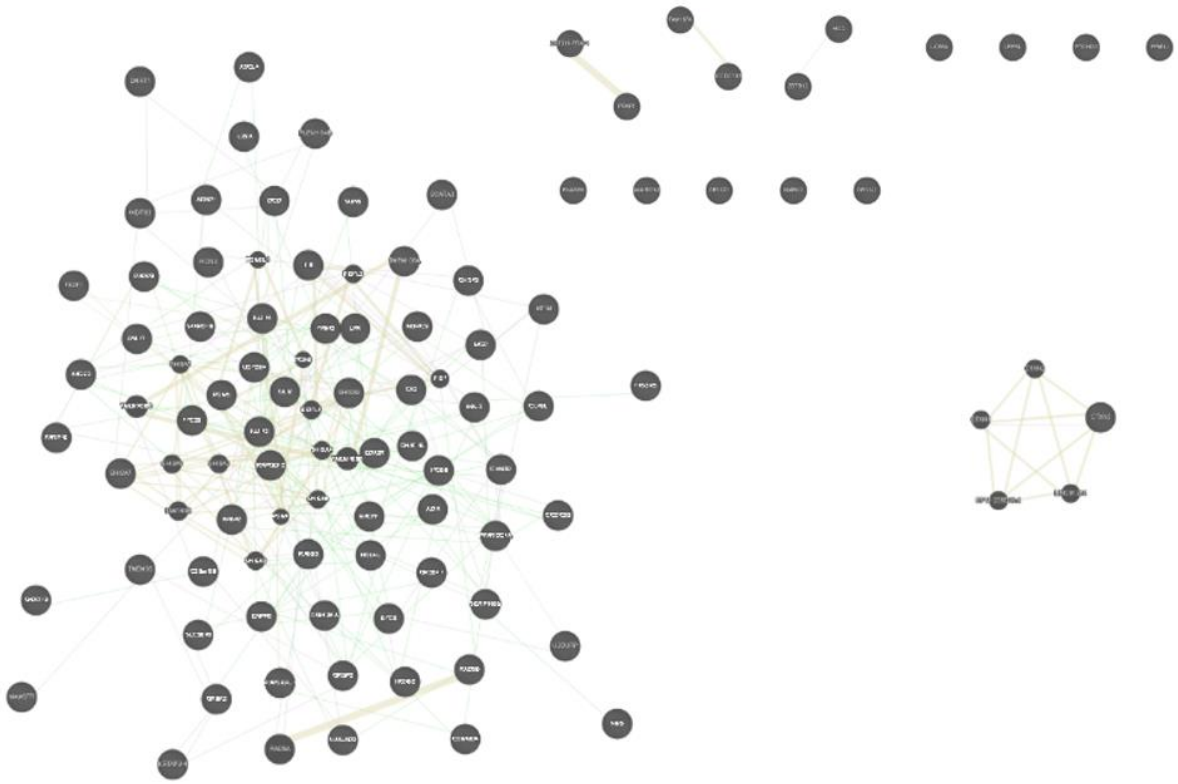

Figure 4.52. Network representation of the significantly up- or down-regulated genes upon dexamethasone treatment of HEK293 cells, constructed with the GeneMANIA algorithm and connecting genes for coexpression (pink), genetic interactions(29) and shared protein domains (ochre).

Transcriptional response off HEK293 cells to KUNB31 treatment

In the same type of analysis as with the dexamethasone treatment, the most significantly up- or down-regulated genes after treatment with KUNB31 were identified (Table.4.8, 4.9).

Table 4.8: A summary of the most significantly up- or down-regulated genes that are unique to KUNB31 treatment and could also readily be assigned to Gene Symbols (DMSO vs DEX, fold change>1.5, p-value<0.05).

ID	DMSO Avg (log2)	KUNB31 Avg (log2)	Fold Change	p-value	Gene Symbol	Description
16748498	4.81	5.47	-1.57	0.0022	**MIR613**	microRNA 613
16737019	5.23	4.64	1.51	0.0031	**DCDC1**	doublecortin domain containing 1
16949503	3.38	4.2	-1.76	0.0062	**MIR28**	microRNA 28
16701608	4.42	2.85	2.97	0.008	**OR2M7**	olfactory receptor, family 2, subfamily M, member 7
16711795	3.6	2.44	2.23	0.0082	**MIR548AK**	microRNA 548ak
16834162	2.63	3.39	-1.7	0.0083	**KRTAP9-6**	keratin associated protein 9-6
16817210	2.29	2.92	-1.55	0.009	**MIR548W**	microRNA 548w
16833706	4.93	4.17	1.7	0.0102	**MIR4727**	microRNA 4727
16732846	4.61	3.84	1.7	0.0119	**OR8A1**	olfactory receptor, family 8, subfamily A, member 1
17065935	5.31	4.7	1.53	0.0122	**LOC101930149**	uncharacterized LOC101930149
16931864	6.57	5.93	1.56	0.0123	**POTEH, POTEG**	POTE ankyrin domain family, member H; POTE ankyrin domain family, member G
16952379			-1.82	0.0124	**LOC105377643**	uncharacterized LOC105377643
16786454	5.02	5.78	-1.7	0.0149	**VRTN**	vertebrae development associated
17115998	5.38	4.46	1.9	0.017	**TSPY2**	testis specific protein, Y-linked 2
16983540	5.95	5.03	1.89	0.0183	**PMCHL1**	pro-melanin-concentrating hormone-like 1, pseudogene
16659944	5.55	4.74	1.76	0.0186	**LOC101927806; LOC440570**	uncharacterized LOC101927806; uncharacterized LOC440570
16820655	6.9	6.21	1.62	0.0187	**CLEC18A; CLEC18C**	C-type lectin domain family 18, member A; C-type lectin domain family 18, member C
17047247	5.34	5.95	-1.53	0.0224	**PMS2P5**	PMS1 homolog 2, mismatch repair system component pseudogene 5
17004536	4.95	5.55	-1.52	0.0233	**LOC101928047**	uncharacterized LOC101928047
16983843	6.1	5.4	1.62	0.0242	**LOC646652**	integral membrane glycoprotein-like
16797531	3.39	2.72	1.59	0.025	**IGHV4-39**	immunoglobulin heavy variable 4-39

17104893	5.41	4.74	1.59	0.0264	**PABPC1L2B**	poly(A) binding protein, cytoplasmic 1-like 2B
16909693	4.07	4.98	-1.88	0.0274	**DNAJB3**	DnaJ (Hsp40) homolog, subfamily B, member 3
17117655	5.48	4.9	1.5	0.0278	**LOC100507079**	Uncharacterized LOC100507079
16966169	2.79	3.74	-1.93	0.0282	**LOC105374419**	Uncharacterized OC105374419
16663284	3.77	4.36	-1.5	0.0305	**CCDC30**	coiled-coil domain containing 30
16788745	1.89	2.64	-1.68	0.0346	**MIR376A1**	MIR376A1
16965041	4.68	3.65	2.05	0.0393	**DEFB131**	defensin, beta 131
17114687	6.32	5.58	1.66	0.0417	**LOC105373343**	uncharacterized LOC105373343
16876428	3.62	4.8	-2.25	0.0432	**LOC101927468**	uncharacterized LOC101927468
16679876	3.47	4.39	-1.89	0.0463	**LOC728323**	uncharacterized LOC728323
16833224	4.15	4.96	-1.76	0.0472	**CCL8**	chemokine (C-C motif) ligand 8
16882736	2.97	2.32	1.57	0.0475	**IGKV2D-29**	immunoglobulin kappa variable 2D-29
16780174	4.94	5.58	-1.56	0.0485	**LINC00410**	long intergenic non-protein coding RNA 410

The less pronounced differences with a lower fold change but at a higher level of significance (Figure 4.53) that are depicted in Figure 4.53, were also taken into consideration (fold change < or> 1.15 and p-value< 0.02). The genes that could be assigned to a gene symbol and a GO-category were grouped together according to high-level GO-category with ShinyGO (Table 4.9).

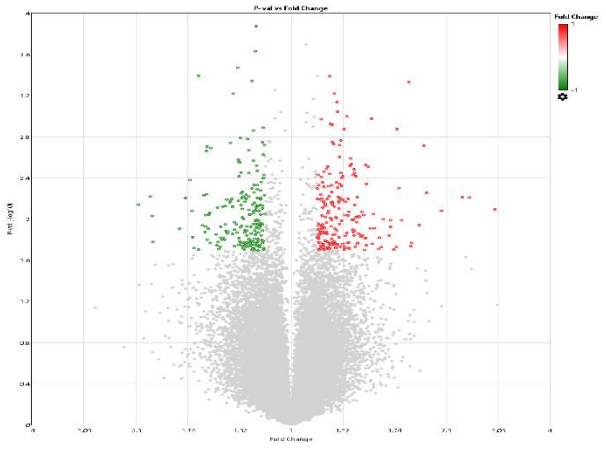

Figure 4.53. Volcano plot summarizing the greater than 1.15-fold up- (red) or down-(29) regulated genes upon treatment with KUNB31 (p-value<0.02).

Table 4.9. Summary of the up-or downregulated upon KUNB31 treatment genes that could be assigned to a gene symbol and a GO-category, grouped together for high-level GO-category.

N	High level GO category	Genes
11	Cell proliferation	GPLD1 TMIGD2 DYNAP UNCX HMX2 DCHS2 LGALS3 NACC1 LTBP3 NAB2 SLC29A2
11	Anatomical structure morphogenesis	CCM2 AP1AR UNCX NAB2 CNP HMX2 LAMB3 GPLD1 TMIGD2 SYNPO2L ZNF22
10	Regulation of response to stimulus	ULBP1 CCL18 GPR143 GPLD1 LGALS3 SH2D6 ENHO SYNPO2L CD3G ARHGAP30
9	Cell adhesion	CDHR4 TMIGD2 COL19A1 CRISP2 AP1AR LAMB3 DCHS2 LGALS3 HAS1
9	Biological adhesion	CDHR4 TMIGD2 COL19A1 CRISP2 AP1AR LAMB3 DCHS2 LGALS3 HAS1
9	Regulation of signaling	CCL18 GPR143 LGALS3 SH2D6 ENHO AP1AR GPLD1 SYNPO2L ARHGAP30
9	Cellular component biogenesis	HAS1 SYNPO2L CEP295NL NACC1 TUBB1 AP1AR LRRN1 CD3G LAMB3
9	Regulation of molecular function	CCL18 LGALS3 DYNAP MLLT1 NAB2 ENHO CEP295NL ARHGAP30 GPLD1
8	Regulation of developmental process	AP1AR KRT84 UNCX NAB2 LRRN1 TMIGD2 LTBP3 LGALS3
7	Regulation of biological quality	SLC29A2 DND1 AP1AR ENHO CNP LRRN1 GPLD1
6	Immune system process	ULBP1 CD3G TMIGD2 CCL18 GPLD1 LGALS3
6	Immune response	ULBP1 TMIGD2 CCL18 GPLD1 LGALS3 CD3G
6	Catabolic process	MMP27 ANKZF1 DND1 GPLD1 CNP COL19A1
6	Cellular localization	SLC29A2 AP1AR TRAPPC3L GPR143 LGALS3 GPLD1
5	Regulation of immune system process	ULBP1 GPLD1 LGALS3 TMIGD2 CD3G
5	System process	OR8A1 OR5L2 CIC OR2M7 GPR143
5	Response to stress	ULBP1 ANKZF1 CCL18 LGALS3 CCM2
5	Regulation of localization	LGALS3 GPR143 AP1AR HAS1 GPLD1
5	Macromolecule localization	LGALS3 AP1AR ENHO CD3G GPLD1
5	Locomotion	CCL18 LGALS3 AP1AR HAS1 GPLD1
5	Cell motility	CCL18 LGALS3 AP1AR HAS1 GPLD1
5	Regulation of multicellular organismal process	TMIGD2 KRT84 LRRN1 GPLD1 LGALS3
5	Localization of cell	CCL18 LGALS3 AP1AR HAS1 GPLD1
5	Multi-organism process	PRM2 CIC ULBP1 CNP DND1
4	Regulation of locomotion	LGALS3 AP1AR HAS1 GPLD1
4	Regulation of cellular component biogenesis	SYNPO2L CEP295NL AP1AR LRRN1
4	Leukocyte activation	ULBP1 CD3G TMIGD2 LGALS3
4	Anatomical structure formation involved in morphogenesis	LAMB3 GPLD1 TMIGD2 SYNPO2L
3	Reproduction	PRM2 HAS1 DND1
3	Immune effector process	ULBP1 LGALS3 CD3G
3	Activation of immune response	GPLD1 LGALS3 CD3G
3	Response to external stimulus	CCL18 LGALS3 CNP
3	Response to endogenous stimulus	HAS1 GPLD1 ENHO
3	Cell cycle process	CEP295NL TUBB1 DCDC1
3	Reproductive process	PRM2 HAS1 DND1
3	Regulation of cell adhesion	TMIGD2 AP1AR LGALS3
3	Multicellular organism reproduction	PRM2 HAS1 DND1
3	Multicellular organismal reproductive process	PRM2 HAS1 DND1
3	Detection of stimulus	OR2M7 OR8A1 OR5L2

2	Immune system development	CD3G LGALS3
2	Developmental process involved in reproduction	PRM2 DND1
2	Behavior	CIC CNP
2	Sexual reproduction	PRM2 DND1
2	Taxis	CCL18 LGALS3
2	Multi-organism reproductive process	PRM2 DND1
2	Leukocyte migration	CCL18 LGALS3

The up- or down- regulated gene list was subjected to the Hsp90 interactome database (www.picard.ch) provided by Echeverria and coworkers (38). This search returned LGALS3BP, the gene that encodes Galectin-3-binding protein, a member of the lectin family, as an identified HSP90AB1 (Heat Shock Protein 90 Alpha Family Class B Member 1) interactor but no further Hsp90-relevant interactions were identified upon this treatment. LGALS3BP interacts with LGALS3 that was found significantly downregulated (-1.17 fold change, p-value= 0.0018) after KUNB31 treatment(233).

The network constructed with GeneMANIA for the KUNB31 treatment shows the genes that were significantly up- or down-regulated, connected for coexpression and shared protein domains (Figure 4.54).

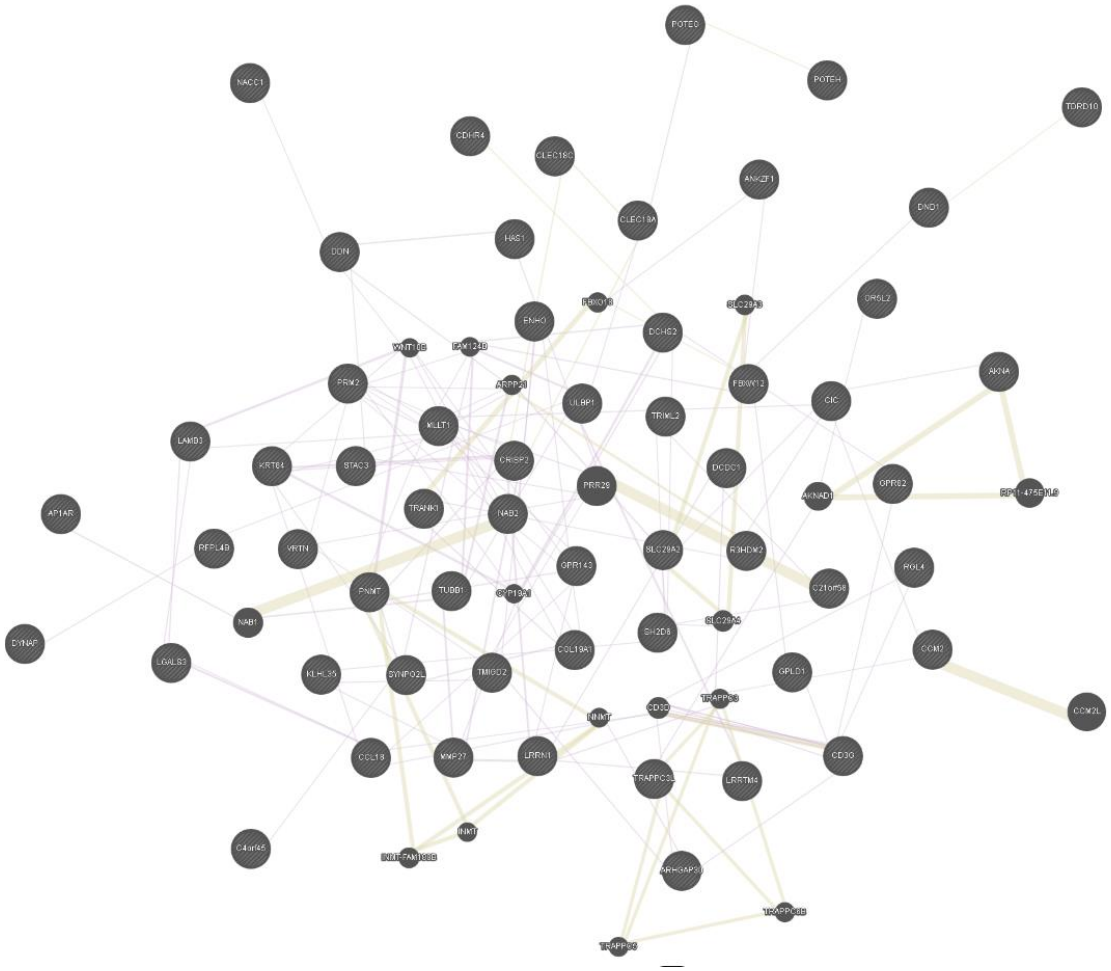

Figure 4.54. Network representation of the significantly up- or down-regulated genes upon KUNB31 treatment of HEK293 cells, constructed with the GeneMANIA algorithm and connecting genes for coexpression (pink) and shared protein domains (ochre).

Transcriptional responses of HEK293 cells to a combination of DEX and KUNB31 treatment

A combination of dexamethasone and KUNB31 treatment gave a distinct transcriptional response, which may reveal SHR-Hsp90-specific relationships on the genome level. The most significantly up- or down-regulated genes after treatment with the combination of KUNB31 and dexamethasone were identified (Table.4.10, 4.11).

Table 4.10. A summary of the most significantly up- or down-regulated genes that are unique to KUNB31+DEX treatment and could also readily be assigned to Gene Symbols (DMSO vs KUNB31+DEX, fold change>1.5, p-value<0.05).

ID	Gene Symbol	DMSO Avg (log2)	KUNB31 +DEX Avg (log2)	Fold Change	p-value	Description
16679136	**LOC105373218**	4.61	5.29	1.6	0.0133	uncharacterized LOC105373218
16691016	**LINC01356**	7.24	6.59	-1.58	0.0445	long intergenic non-protein coding RNA 1356
16708511	**MIR3158-1**	3.24	3.86	1.54	0.0118	microRNA 3158-1
16710666	**TCERG1L-AS1**	2.01	2.67	1.58	0.0387	TCERG1L antisense RNA 1
16724783	**OR8K3**	5.14	4.36	-1.72	0.0099	olfactory receptor, family 8, subfamily K, member 3 (gene/pseudogene)
16738333	**TRIM51HP**	3.73	4.35	1.54	0.0246	tripartite motif-containing 51H, pseudogene
16755600	**MIR1827**	3.31	2.7	-1.53	0.0390	microRNA 1827
16760790	**CD163L1**	3.37	4.35	1.96	0.0185	CD163 molecule-like 1
16767886	**LOC105369860**	3.19	2.51	-1.6	0.0229	uncharacterized LOC105369860
16788655	**SNORD114-10**	4.47	4.03	-1.35	0.0027	small nucleolar RNA, C/D box 114-10
16801691	**LOC101928907**	5.6	4.99	-1.53	0.0259	uncharacterized LOC101928907
16830235	**ALOX12P2**	5.59	4.95	-1.55	0.0028	arachidonate 12-lipoxygenase pseudogene 2
16859213	**OR10H4**	4.86	5.53	1.58	0.0136	olfactory receptor, family 10, subfamily H, member 4
16894398	**MIR4261**	4.99	4.12	-1.83	0.0435	microRNA 4261
16928329	**BCRP3**	3.44	4.07	1.55	0.0133	breakpoint cluster region pseudogene 3
16931912	**XKR3**	4.68	4.06	-1.53	0.0439	X-linked Kx blood group related 3
16932716	**P2RX6P**	5.67	5.06	-1.52	0.0166	purinergic receptor P2X, ligand gated ion channel, 6 pseudogene
16976533	**UGT2B15**	1.97	2.65	1.6	0.0036	UDP glucuronosyltransferase 2 family, polypeptide B15
16976583	**UGT2A2; UGT2A1**	3.77	4.55	1.72	0.0002	UDP glucuronosyltransferase 2 family, polypeptide A2; UDP glucuronosyltransferase 2 family, polypeptide A1, complex locus
16979892	**LOC10192741, LOC105377444**	3.44	2.86	-1.5	0.0197	uncharacterized LOC101927414; uncharacterized LOC105377444
16980254	**GYPB**	3.59	4.54	1.93	0.0173	glycophorin B (MNS blood group)

16990542	**LOC105378210**	4.72	4.07	-1.57	0.0463	uncharacterized LOC105378210
17006605	**HCP5**	5.09	4.45	-1.56	0.0167	HLA complex P5 (non-protein coding)
17056827	**TRGV11**	3.68	4.32	1.56	0.0128	T cell receptor gamma variable 11 (non-functional)
17086337	**LOC101927552**	4.55	3.94	-1.52	0.0218	uncharacterized LOC101927552
17094372	**LOC105376050 LOC105379263 LOC105379816**	4.41	5.41	2	0.0193	uncharacterized LOC105376050; uncharacterized LOC105379263; uncharacterized LOC105379816
17095633	**MIR4290HG**	6.44	5.79	-1.57	0.0106	MIR4290 host gene
17107640	**LOC101927685**	6.08	6.7	1.54	0.0422	heat shock transcription factor, X-linked-like
17114768	**MIR892A**	3.07	3.79	1.65	0.0121	microRNA 892a
17117431	**LOC645010**	5.37	5.96	1.51	0.0082	uncharacterized LOC645010

The less pronounced differences with a lower fold change but at a higher level of significance depicted in Figure 4.55, were also taken into consideration (fold change < or> 1.15 and p-value < 0.02, Figure). The genes that could be assigned to a gene symbol and a GO-category were grouped together according to high-level GO-category with ShinyGO (Table 4.10).

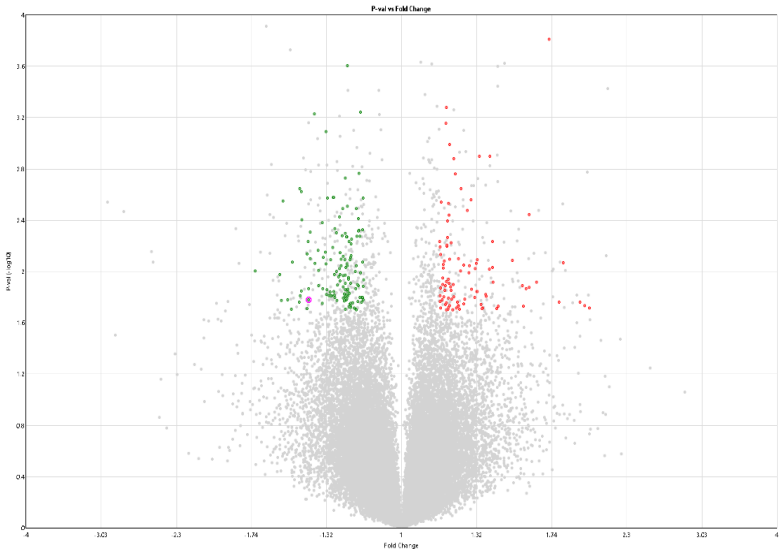

Figure 4.55. Volcano plot summarizing the greater than 1.15-fold up- (red) or down-(29) regulated genes upon treatment with KUNB31 (p-value<0.02).

Table 4.11: Up- and down-regulated genes (fold change < or> 1.15 and p-value < 0.02) upon DEX+ KUNB31 treatment are grouped by functional categories defined by high-level GO terms with the ShinyGO tool.

N	High level GO category	Genes
37	Regulation of biological quality	WNT5A NEDD4 NOS1 HTR2A SNX16 ATP4A TRPV4 SLC9A2 ARHGAP40 BRWD3 XRN1 TACR1 STXBP4 WNT10B DDIT3 PLEKHN1 TXNDC16 PTN CPT1A TNNC1 LRP4 RNASEL FBN2 TMEM108 NPHS1 GRIK2 GALR2 NF1 GJA5 DNMBP TBX3 TMIGD1 NGFR FGD2 ACSM3 DNAJC5 GRM4
36	Regulation of response to stimulus	ARHGAP40 FRZB TRABD2B DDIT3 HTR2A WNT5A COLEC11 GRM4 LRP4 FAIM2 PTPN13 STXBP4 NEDD4 NOS1 IL27RA PTN DNMBP TRPV4 TNNC1 FGFBP1 FBN2 TMEM108 FGD2 IL24 GRIK2 WNT10B GPC5 C10ORF99 CXCL17 NF1 HES5 BIRC6 EPG5 ARHGAP12 USP17L2 RNASEL
35	Regulation of signaling	ARHGAP40 GRM4 FRZB GRIK2 TRABD2B DDIT3 HTR2A WNT5A LRP4 FAIM2 PTPN13 STXBP4 NEDD4 NOS1 PTN DNMBP CPT1A TRPV4 TACR1 FGFBP1 FBN2 TMEM108 FGD2 IL24 WNT10B GPC5 C10ORF99 NF1 HES5 GJA5 BIRC6 ARHGAP12 CXCL17 USP17L2 RNASEL
32	Regulation of localization	NEDD4 HTR2A SNX16 TACR1 NGFR FGFBP1 STXBP4 TMIGD1 C10ORF99 NOS1 DNAJC5 IL27RA CFAP69 PTN B9D1 CPT1A TRPV4 WNT5A TNNC1 LRP4 RNASEL NPHS1 IL24 TMEM37 DDIT3 CXCL17 NF1 CPTP GJA5 TTBK2 GALR2 USP17L2
32	Macromolecule localization	NEDD4 PRELID3A C12ORF50 ZDHHC20 CPTP NGFR PTN WNT5A PNPLA8 STXBP4 PITPNM2 HTR2A SNX16 IL27RA B9D1 CPT1A TRPV4 SLC9A2 KIF17 LRP4 FBN2 LYST GRIK2 NBEA DDIT3 NPIPA1 NF1 AP5B1 GJA5 NPHS1 TTBK2 USP17L2
30	Anatomical structure morphogenesis	NEDD4 BRWD3 EPHA10 HES5 TBX3 FGFBP1 PTN B9D1 MAN2A1 WNT5A LRP4 FAIM2 FBN2 TMEM108 NPHS1 FRZB WNT10B ATOH1 PROP1 CXCL17 NF1 GJA5 NGFR DNMBP TRPV4 TNNC1 ARHGAP12 DICER1 FGD2 NOS1
28	Regulation of multicellular organismal process	NEDD4 TNNC1 HES5 PTN FGFBP1 DDIT3 GJA5 NOS1 HTR2A IL27RA TRPV4 MAN2A1 WNT5A TACR1 LRP4 TBX3 FBN2 TMEM108 NPHS1 FRZB WNT10B ATOH1 NF1 CPTP NGFR DICER1 CXCL17 USP17L2
27	Response to stress	TRPV4 DDIT3 ZNF771 NOS1 WNT5A TBX3 RNASEL STXBP4 PLEKHN1 C10ORF99 IL27RA PTN TACR1 COLEC11 FAIM2 FGD2 NPHS1 IL24 GRIK2 WNT10B NF1 NEDD4 LYST EPG5 ZBTB38 CXCL17 USP17L2
27	Cellular component biogenesis	TRAPPC6A ARHGAP40 TTBK2 SRPK3 TUBGCP5 DICER1 DDIT3 GJA5 TRABD2B H2AFB3 B9D1 CPT1A TRPV4 WNT5A TACR1 LRP4 RNASEL NPHS1 TDRD5 PTPN13 WNT10B HES5 USP17L2 CPTP FGD2 KIF17 KRT5
27	Cellular localization	TRAPPC6A NEDD4 HTR2A KIF17 C12ORF50 ZDHHC20 AP5B1 NGFR PTN WNT5A STXBP4 NOS1 DNAJC5 TNNC1 LRP4 TMEM108 EPG5 GRIK2 DDIT3 NF1 SNX16 TTBK2 LYST USP17L2 B9D1 CPT1A GRM4
24	Regulation of molecular function	NEDD4 NOS1 SNX16 ARHGAP12 SERPINB11 HTR2A WNT5A GRM4 TTBK2 DDIT3 NF1 USP17L2 TRAPPC6A PTN TNNC1 BIRC6 ARHGAP40 FGD2 IL24 WNT10B GALR2 C10ORF99 NGFR CXCL17
23	Catabolic process	NEDD4 NOS1 DICER1 LPIN2 BIRC6 EPG5 TET3 PNPLA8 DDIT3 PLEKHN1 HTR2A CPT1A XRN1 RNASEL WNT10B CYP4F3 GK2 TECPR2 USP17L2 WNT5A LRP4 CPTP GPC5
23	Regulation of developmental process	NEDD4 BRWD3 HES5 PTN TBX3 FGFBP1 FRZB WNT10B DDIT3 NOS1 HTR2A IL27RA TRPV4 MAN2A1 WNT5A LRP4 FBN2 ATOH1 NF1 NGFR DNMBP DICER1 FGD2
22	System process	NOS1 TNNC1 MYH4 HTR2A CFAP69 PTN TRPV4 TACR1 TMEM108 NPHS1 GRIK2 WNT10B UGT2A1 OR10H4 NF1 OR10D3 OR10G2 GJA5 TBX3 DICER1 ACSM3 GALR2

20	Locomotion	TACR1 EPHA10 FGFBP1 TMIGD1 C10ORF99 IL27RA CFAP69 PTN TRPV4 WNT5A IL24 ATOH1 PROP1 CXCL17 NF1 TTBK2 NEDD4 USP17L2 LYST GYPB
19	Immune system process	WNT5A COLEC11 RNASEL WNT10B C10ORF99 NEDD4 IL27RA PTN TRPV4 TACR1 STXBP4 CXCL17 NF1 HES5 LYST EPG5 USP17L2 DNAJC5 GYPB
18	Cell proliferation	PTN WNT5A TBX3 FGFBP1 FRZB WNT10B TMIGD1 HTR2A TACR1 BIRC6 IL24 NF1 HES5 NGFR KLF9 STXBP4 USP17L2 DICER1
18	Response to endogenous stimulus	NOS1 LPIN2 SCGB2A2 NGFR NEDD4 KLF9 PTN TRPV4 XRN1 WNT5A TACR1 LRP4 FGFBP1 FBN2 TMEM108 STXBP4 WNT10B HES5
18	Cell motility	TACR1 FGFBP1 TMIGD1 C10ORF99 IL27RA CFAP69 PTN TRPV4 WNT5A IL24 ATOH1 PROP1 CXCL17 NF1 TTBK2 USP17L2 LYST GYPB
18	Localization of cell	TACR1 FGFBP1 TMIGD1 C10ORF99 IL27RA CFAP69 PTN TRPV4 WNT5A IL24 ATOH1 PROP1 CXCL17 NF1 TTBK2 USP17L2 LYST GYPB
17	Response to external stimulus	NOS1 EPHA10 COLEC11 RNASEL C10ORF99 HTR2A IL27RA PTN TRPV4 WNT5A TACR1 IL24 ATOH1 DDIT3 CXCL17 USP17L2 LYST
17	Multi-organism process	NOS1 COLEC11 RNASEL C10ORF99 NEDD4 HTR2A IL27RA CFAP69 PTN WNT5A TACR1 DPEP3 HERC4 TDRD5 IL24 USP17L2 LYST
15	Anatomical structure formation involved in morphogenesis	HES5 FGFBP1 PTN WNT5A TBX3 FAIM2 FBN2 NPHS1 WNT10B CXCL17 NF1 GJA5 NGFR DICER1 NOS1
14	Regulation of locomotion	TACR1 FGFBP1 TMIGD1 C10ORF99 IL27RA CFAP69 PTN TRPV4 WNT5A IL24 CXCL17 NF1 TTBK2 USP17L2
13	Regulation of immune system process	WNT5A COLEC11 C10ORF99 IL27RA PTN TRPV4 TACR1 CXCL17 NF1 HES5 EPG5 USP17L2 RNASEL
10	Reproduction	TUBGCP5 CFAP69 PTN WNT5A TACR1 BIRC6 DPEP3 HERC4 TDRD5 TBX3
10	Immune response	WNT5A COLEC11 NEDD4 IL27RA STXBP4 LYST EPG5 USP17L2 DNAJC5 RNASEL
10	Response to biotic stimulus	NOS1 COLEC11 RNASEL C10ORF99 IL27RA WNT5A IL24 DDIT3 USP17L2 LYST
10	Cell cycle process	TUBGCP5 DDIT3 C10ORF99 KLLN WNT5A BIRC6 DPEP3 WNT10B STXBP4 USP17L2
10	Reproductive process	TUBGCP5 CFAP69 PTN WNT5A TACR1 BIRC6 DPEP3 HERC4 TDRD5 TBX3
9	Response to other organism	NOS1 COLEC11 RNASEL C10ORF99 IL27RA WNT5A IL24 USP17L2 LYST
8	Behavior	HTR2A CFAP69 PTN CPT1A TACR1 GRIK2 NF1 GALR2
8	Response to abiotic stimulus	TRPV4 NOS1 PLEKHN1 HTR2A PTN TACR1 NF1 NEDD4
8	Regulation of cellular component biogenesis	ARHGAP40 TRABD2B WNT5A TACR1 NPHS1 WNT10B USP17L2 CPTP
8	Leukocyte migration	C10ORF99 IL27RA TRPV4 TACR1 CXCL17 WNT5A LYST GYPB
7	Immune effector process	COLEC11 RNASEL IL27RA WNT5A LYST USP17L2 DNAJC5
7	Taxis	EPHA10 C10ORF99 TRPV4 WNT5A ATOH1 CXCL17 LYST
6	Immune system development	WNT5A WNT10B IL27RA PTN NF1 HES5
6	Cell adhesion	PTN WNT5A NPHS1 NF1 HES5 TRPV4
6	Sexual reproduction	CFAP69 PTN TACR1 DPEP3 HERC4 TDRD5
6	Biological adhesion	PTN WNT5A NPHS1 NF1 HES5 TRPV4
6	Multicellular organism reproduction	CFAP69 PTN TACR1 DPEP3 HERC4 TDRD5
6	Multi-organism reproductive process	CFAP69 PTN TACR1 DPEP3 HERC4 TDRD5
6	Multicellular organismal reproductive process	CFAP69 PTN TACR1 DPEP3 HERC4 TDRD5
6	Detection of stimulus	HTR2A OR10H4 OR10D3 OR10G2 TACR1 UGT2A1
5	Developmental process involved in reproduction	PTN WNT5A BIRC6 TDRD5 TBX3
5	Autophagy	EPG5 TECPR2 CPTP DDIT3 NEDD4
5	Growth	FRZB WNT5A LRP4 TMEM108 WNT10B

5	Leukocyte activation	NEDD4 IL27RA TACR1 WNT5A DNAJC5
5	Rhythmic process	PASD1 NGFR PTN KLF9 CPT1A
4	Neurotransmitter secretion	HTR2A NF1 DNAJC5 GRM4
4	Circadian rhythm	PASD1 KLF9 NGFR CPT1A
4	Regulation of cell adhesion	PTN WNT5A NF1 TRPV4
4	Developmental growth	WNT5A LRP4 TMEM108 WNT10B
4	Maintenance of location	HTR2A FBN2 DDIT3 NOS1
4	Maintenance of cell number	PTN TBX3 VPS72 HES5
3	Activation of immune response	COLEC11 EPG5 USP17L2
3	Feeding behavior	CPT1A TACR1 GALR2
3	Cell growth	FRZB WNT5A TMEM108
3	Pigmentation	TRAPPC6A NF1 LYST
3	Regulation of multi-organism process	RNASEL CFAP69 USP17L2
3	Interspecies interaction between organisms	RNASEL NEDD4 HTR2A
2	Production of molecular mediator of immune response	IL27RA WNT5A
2	Synaptic vesicle exocytosis	HTR2A DNAJC5
2	Methylation	TDRD5 TET3
2	Regulation of growth	FRZB WNT5A
2	Multi-multicellular organism process	PTN TACR1
2	Biological phase	WNT5A WNT10B
2	Hair cycle phase	WNT5A WNT10B
2	Regulation of action potential	TACR1 GJA5
2	Meiotic cell cycle process	WNT5A DPEP3
2	Regulation of reproductive process	CFAP69 WNT5A

The network constructed with GeneMANIA for the KUNB31+DEX treatment shows the genes that were significantly up- or down-regulated, connected for coexpression, biological pathway and predicted interactions (Figure 4.56).

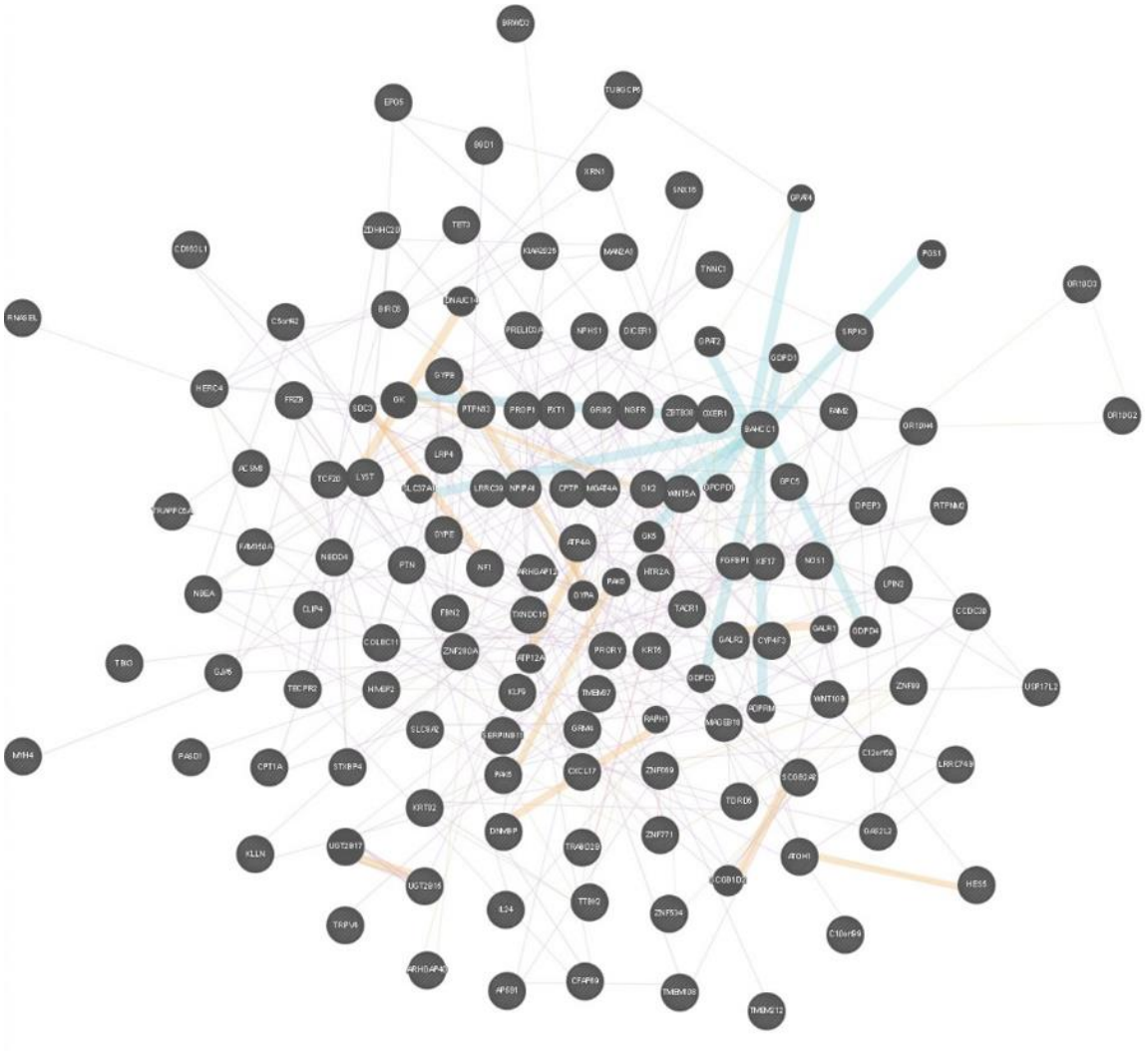

Figure 4.56. Network representation of the significantly up- or down-regulated genes upon KUNB31+DEX treatment of HEK293 cells, constructed with the GeneMANIA algorithm and connecting the genes for coexpression (pink), biological pathway (29) and predicted interactions (orange).

The same gene list was submitted in the Hsp90 interactor database (https://www.picard.ch/Hsp90Int/) and Hsp90-relevant regulators that may be affected upon treatment with DEX+KUNB31 were reported.

Table: Summary of Hsp90 relevant protein-protein interactions that may be affected (at least one of the interactors) upon treatment of HEK293 cells with DEX+ KUNB31.

Interactor_A	Interactor_B	Experimental_system	Source_database	pubmed_ID
DNAJC7	NF1	in vivo	HRPD_human	8836031
DYNLL1	NOS1	in vitro in vivo yeast 2-hybrid	HRPD_human	-
EPHA10	CDC37	LUMIER Assay	www.picard.ch (literature curation)	22939624
GNAQ	HTR2A	in vivo	HRPD_human	11916537
GRIN1	NF1	in vivo	HRPD_human	10862698
GRIN2D	NF1	in vivo	HRPD_human	10862698
HERC4	HSP90AB1	LUMIER Assay	www.picard.ch (literature curation)	22939624
HRAS	NF1	in vitro	HRPD_human	8628317
HSP90AA1	NLRP4	-	www.picard.ch (literature curation)	17435760
HSP90AA1	NOS1	in vitro in vivo	HRPD_human	-
HTR2A	GLUL	yeast 2-hybrid	HRPD_human	16537434
HTR2A	JAK2	in vivo	HRPD_human	9169451
HTR2A	PPP5C	yeast 2-hybrid	HRPD_human	16537434
NF1	APP	in vivo	HRPD_human	16374483
PAK7	CDC37	LUMIER Assay	www.picard.ch (literature curation)	22939624
PRKACA	NOS1	in vitro	HRPD_human	-
PRKCA	NOS1	in vitro	HRPD_human	-
RNF10	HSP90AB1	LUMIER Assay	www.picard.ch (literature curation)	22939624
RNF111	HSP90AB1	LUMIER Assay	www.picard.ch (literature curation)	22939624
RNF19B	HSP90AB1	LUMIER Assay	www.picard.ch (literature curation)	22939624
SGK2	CDC37	LUMIER Assay	www.picard.ch (literature curation)	22939624
SGK2	HSP90AB1	LUMIER Assay	www.picard.ch (literature curation)	22939624
SGK223	CDC37	LUMIER Assay	www.picard.ch (literature curation)	22939624
SGK223	HSP90AB1	LUMIER Assay	www.picard.ch (literature curation)	22939624
SRPK3	HSP90AB1	LUMIER Assay	www.picard.ch (literature curation)	22939624
SYN1	NOS1	Reconstituted Complex	BioGrid_human	11867766

Supplementary Figures.

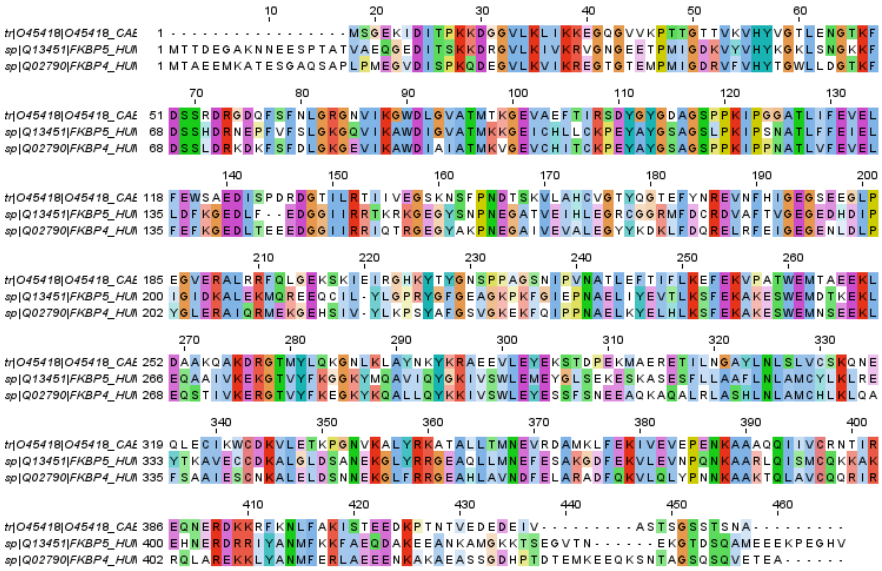

Figure S1. Sequence alignment of FKB-6. FKBP51, FKBP52 generated by ClustalOmega.

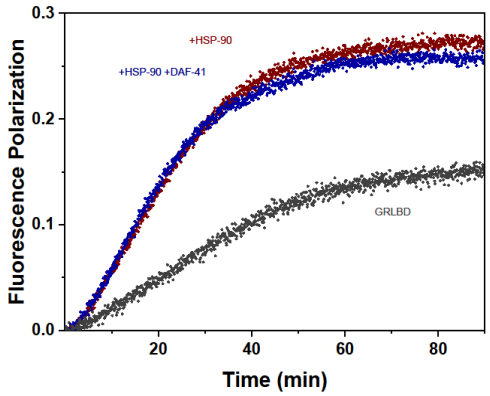

Figure S2. Fluorescence polarization following binding of GRLBD to HSP-90/ATP in the presence and absence of CE p23/DAF-41.

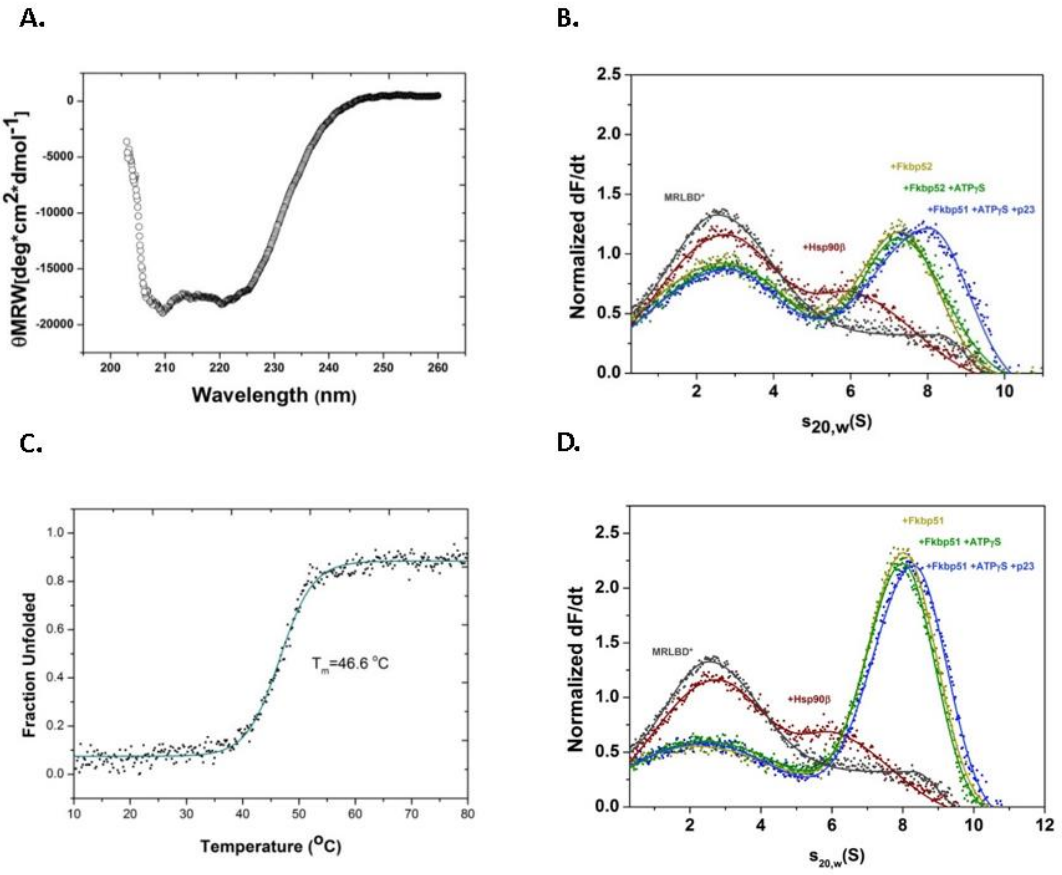

Figure S3. MR complex formation shows a similar cooperativity with Hsp90β and immunophilins Fkbp51 and Fkbp52 to GR while the same requirement for cofactor p23 for Hsp90β to adopt a more compact conformation is observed. A) CD spectrum shows a high α-helical content, common in the SHR family. B, D) Sedimentation velocity AUC analysis of *MRLBD in the presence of Hsp90β and Fkbp51 or Fkbp52 as indicated in the plot. C) CD thermal transition for MRLBD shows a Tm of 46.6 °C.

5. Discussion

5.1 Discussion on C.elegans and human Hsp90 chaperone assemblies

GR·Hsp90 complexes have been studied extensively since the 1980s in cellular lysates of reticulocytes and wheat germ, leading to the identification of Hsp90 as a chaperone bound to GR and also to the description of assemblies involving several Hsp90 co-chaperones (98,234-236).Much of our current structural understanding of GR complexes *in vitro* originates from yeast Hsp90 and its cofactors and only recently, structural data on higher eukaryotic species became available(44,61,66,68,105). The extent and timing of movements performed by Hsp90 and the biochemical contribution of the cochaperones are still rather unclear, but the recent purification of client proteins makes in vitro studies possible (44,81,237). We here focus on the nematode and human Hsp90 chaperone systems to clarify which conserved principles are observable between the different eukaryotic species. The nematode system contains only one homolog of all major cofactors and a highly conserved Hsp90 protein, which has cellular contact to client proteins of all known Hsp90 client classes. There are at least 200 nuclear receptors in nematodes, but which of them are clients of the Hsp90 machinery is currently unknown. In this study, we used a stabilized GRLBDm mutant of the ligand binding domain of the human GR to model the wild-type protein, which is unstable (227). The LBD domain of the human GR shows homology to the *C. elegans* nuclear hormone receptors NHR-25, NHR-47 and, FAX-1 that bind so far unknown ligands and to some extent, to the receptor for dafachronic acid, DAF-12. Based on our results, *C. elegans* HSP-90 appears to perform its closing reaction with an efficiency in-between yeast and human. Even under conditions where the nucleotide ATPγS is present, formation of the closed, twisted state does not proceed for the isolated HSP-90 or Hsp90β. This contrasts with the homologous yeast Hsp82 protein. Instead, the nematode or human Hsp90s remain in an open-like conformation and also the presence of a client protein does not induce the closing reaction. The TPR cofactor STI-1 and the ATPase activator AHSA-1 could hardly be detected in GRLBDm·HSP-90 complexes. This is in agreement with experiments performed in yeast (44). The human homologue of STI-1, Hop, is known to deliver the GRLBD bound to the chaperone Hsp70 to Hsp90 and ATP hydrolysis by Hsp90 is thought to induce the release of Hsp70 and Hop (105). Thus, STI-1 alone may not be detected as a component of GRLBDm·HSP-90 complexes in the absence of the HSP-70

chaperone. Further, we see that the binary GRLBDm·HSP-90 complex is disrupted once excess STI-1 is added, hinting at a competition for a binding site on HSP-90. Technically, the STI-1·HSP-90 complex cannot be observed by fluorescence AUC with labeled GRLBDm, it is, however, noticeable, since GRLBDm is exclusively observed in the unbound fraction. STI-1 interacts primarily with the C-terminal MEEVD-peptide of Hsp90, but also the M domain, which is likely the binding site that STI-1 and GRLBDm compete for (51,110,226). For AHSA-1, we also observe competitive binding with GRLBDm, which could be due to the different conformational requirements or overlapping binding sites on the Hsp90 chaperone (65,66). In particular, the binding site in the middle domain of the chaperone may be used by both proteins and therefore such ternary complexes may not form efficiently. Only in trimeric complexes with the cofactors PPH-5 or FKB-6 does HSP-90 perform nucleotide-induced conformational rearrangements and reach a compacted state. These cofactors also strongly facilitate the binding of GRLBDm to the chaperone. Thus, the nematode HSP-90 cycle seems to be based on cooperative events between TPR-proteins, nucleotide and client protein (Figure 5.1).The cofactor p23 has been thought to stabilize Hsp90-client interactions, which is supported in our experiments with the human chaperone system (81,219). A recent study, however, shows that p23 stimulates GRLBD dissociation from the chaperone with ATP but not with the non-hydrolysable nucleotides and that it thus, can function as a substrate release factor for Hsp90 (238). For AUC analysis, we utilize the non-hydrolysable nucleotide ATPγS in an attempt to stabilize the closed states of the client·Hsp90 and client·Hsp90·TPR cofactor complexes in the presence and absence of p23. In this set-up the affinity for Cep23/DAF-41 is rather low. In complexes consisting of the nematode proteins, 0.22 ± 0.05 of the GRLBDm fraction is bound to the chaperone in the presence of ATPγS while 0.28 ± 0.03 is bound when Cep23/DAF-41 is added. In contrast, 0.49 ± 0.05 of GRLBDm is bound to the chaperone in the absence of ATPγS. We therefore, can say with conviction that ATPγS reduces the affinity of HSP-90 to GR, but the further integration of Cep23/DAF-41 may not change the affinity significantly ($p = 0.1493$). Given that the nematode protein responds much stronger to the binding of ATPγS, it can be assumed that the observed differences between nematode HSP-90 and human Hsp90β relate to the different flexibility and response of the protein to the nucleotide. Based on mass spectrometry data, we investigated whether the observed cooperativity in complex formation may originate from contacts between the cofactor and client proteins on the chaperone scaffold. Our structural interpretation for GRLBDm·HSP-90 is

in good agreement with the structural model proposed previously for yeast Hsp90 in complex with GRLBDm (44). Electron microscopy structural studies also report GRLBD being bound to the MD and CTD domains of human Hsp90, as part of a complex with Hsp70, Hop and Hsp90 (105). This binding site is also in line with the client-binding region of E. coli Hsp90 described by Genest et al (42). Our results on the GRLBDm·HSP-90·FKB-6 topology are consistent with recent findings regarding the human Fkbp51 (239). This study also postulates a stepwise interaction with Hsp90, with affinities decreasing in the order TPR > FK2 > FK1. In the case of PPH-5, the arrangement of the cofactor in GRLBDm·HSP-90·PPH-5 complexes is similar to the previous study on the binary HSP-90·PPH-5 complex (188). To illustrate these topologies, we used the identified crosslinked peptides in docking calculations with HADDOCK and obtained structural models for the dimeric GRLBDm·HSP-90 complex as well as the trimeric complexes with the two TPR cofactors (222,223). These calculations bring both cofactors' catalytic domain in close proximity to the client, which may be setting the basis for the observed cooperativity. The client may then be accessible to undergo transformations towards dephosphorylation and receptor maturation. The cooperative complex formation and hormone binding patterns seem similar in the nematode and human Hsp90 systems, albeit the persistence of the "open" state is stronger for the human Hsp90β protein. Here, Fkbp-containing and Pp5-containing complexes appear unable to perform the closing reaction induced by ATPγS and only with the support of p23 are these rearrangements possible and lead to the progression of the Hsp90 cycle. This data highlights that, despite the conserved features of the cofactors, the different degree of flexibility within the Hsp90 protein from the two organisms influences the principles during chaperone·cofactor·client complex formation.

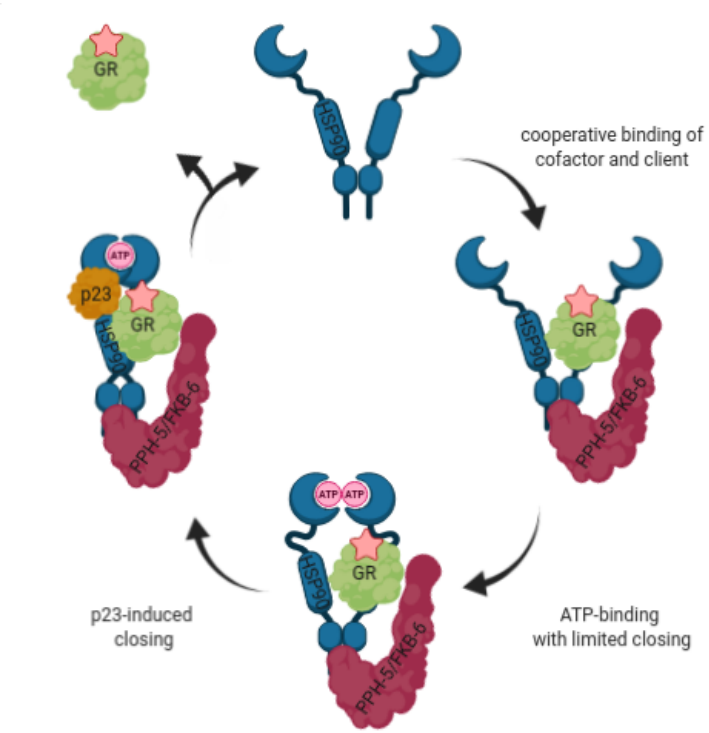

Figure 5.1 Hypothetical cycle of the *C. elegans* HSP-90 interaction with nematode cofactors and the glucocorticoid receptor LBD. In the case of direct binding of GR to the HSP-90 machinery, cooperative client and cofactor (PPH-5 or FKB-6) binding occurs favoring the indicated stoichiometry. Binding of nucleotide then leads to progression of the cycle towards a more compact state of HSP-90 and to more efficient hormone binding. Upon p23 inclusion in the HSP-90 assemblies, the closed state is stabilized. ATP hydrolysis may then trigger GR and cofactor release. The figure was created with BioRender.com.

5.2 Discussion on glucocorticoid resistance conferring mutation L773P

Glucocorticoid receptor is a remarkable molecule, whose exact properties, despite the extensive research, are not yet clarified. We here attempted to gain some insight into the conformational requirements for GR to bind ligand, coactivator and Hsp90β by observing the behavior of a glucocorticoid resistant mutant.

Normally, upon agonist binding, a repositioned AF-2 forms a pocket with H3 and H5, forming the lid of the ligand binding pocket (126). The extended strand following AF-2, where the hGR L773P point mutation addressed in this study resides, seems to be crucial for hormone binding, as truncation of it leads to an inactive receptor (139). Charmandari et al report that the mutant receptor demonstrates decreased transcriptional activity but preserves its ability to bind DNA, decreased affinity for ligand, delayed nuclear translocation, altered interaction, only through the AF-1, with the NCOA-2 coactivator and exerts a dominant negative effect on wild-type hGRα *in vivo* (132). This behavior is in agreement with the presented *in vitro* investigations: the L→P mutation at position 773 does not seem to have overt effects on the protein, but GRm L773P exhibited a 2.4-fold rate decrease in dexamethasone binding and an altered *in vitro* interaction of the AF-2 with a NCOA2-derived peptide and also the Hsp90β chaperone. Moreover, the mutant receptor was found to be competent in DNA binding but with altered dimerization properties.

Transcriptional coactivators develop multiple hydrophobic interactions via their LxxLL helical motifs with AF-2 while this element is directly involved in ligand binding, in the case of dexamethasone, through L753 (140). The H3-H5 interaction has previously been reported to act as a switch, conserved among steroid receptors and crucial to receptor sensitivity for ligand.(240) This study introduces a leucine at position 604 of GR's H5, which may develop a vdW interaction with G567 of H3 and leads to a receptor able to get activated by 10 times lower steroid concentrations. H3 is also affected as a result of the partial unfolding of GR by the chaperone Hsp70, which at the same time causes ligand release (105).In the previous section, peptides from H3 were identified in crosslinked products with *C.elegans* Hsp90 (59). Importantly, ligand binding residues N564 and Q570 that form three out of six hydrogen bonds between GR and DEX. H8 has also been reported as an important switch for GR function and the L687-690A mutation examined in the respective study, led to decreased transcriptional

activity and association of GR with Hsp*90 in vivo*, without overt effects on receptor protein stability (241).

H/DX analysis shows an overall more dynamic GRm L773P, both in the absence and presence of Hsp90β. Significant changes concern H3, H5, H8, H9, β-sheet 2, H10, AF-2 and in addition H1 in the presence of Hsp90β. These regions overlap well with the Hsp90β binding site while hormone binding residues follow intensely altered dynamics. Taken together, this data demonstrates the disruption of the hydrophobic network in GRs C-terminus that further translates to an overall perturbation of the extensive conformational changes GR performs upon ligand binding and besides AF-2, also affects GR elements distant to the mutation site. Importantly, dimerization properties of the receptor are altered, even though the dimer interface is on the opposite site of the molecule (Figure 5.2). Judging from Charmandari and coworkers' results and the altered dimerization properites and H/DX behavior of the DBD and hinge regions of GR, it can be expected that the mutant receptor can not meet the conformational requirements for proper domain communication and could therefore, serve as a model to understand the domain interaction of this complex molecule.

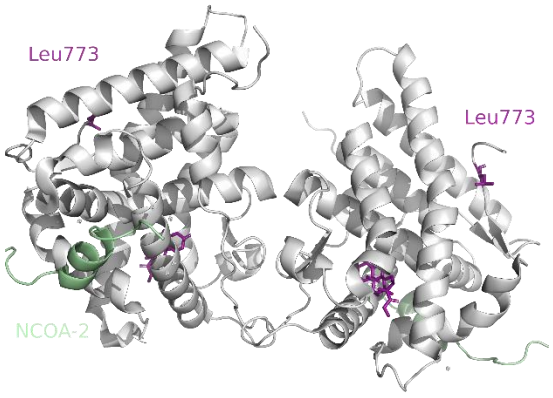

Figure 5.2. Structure of dimeric GR LBD in complex with NCOA-2 peptide and DEX based on PDB ID 1M2Z.

Hsp90β is thought to maintain the ligand binding pocket in an open state and judging from the extensive deprotection observed by H/DX, it seems probable that the point mutation leads to an overall more exposed pocket. This would also explain the increased polarization rate of F-DEX while binding to GRm L773P in the presence of Hsp90β: since the two species have the same size, increased polarization should reflect the increased tumbling rate of F-DEX in the deprotected pocket.

Hsp90β, however, does restore hormone binding to GRm L773P that coincides with the suppression of H/DX changes observed in the absence of the chaperone. This may be reflecting the buffering effect of Hsp90β on a mutated client protein. There are, however, pronounced differences, in elements overlapping with the GR·Hsp90β interface, that chaperone binding cannot overcome. Especially in the H9- β-sheet 2- H8 and H3-H5 interfaces, perturbations persist. Comparing the non-mutated GR construct with GRm L773P supported that proper contacts within the hydrophobic network of residues in GR's C-terminus are important for allosteric communications in this complex molecule.

5.3 Discussion on transcriptional responses to dexamethasone and selective Hsp90β inhibition

Microarray experiments and construction of gene co-expression cliques can help reveal transcriptomic changes on unprecedented detail and may contain diagnostic value in identifying modified biological pathways. This method was employed to compare the responses of human HEK293 cells to dexamethasone and KUNB31, an Hsp90β-selective inhibitor reported recently, and see whether we can, by selectively reducing Hsp90β activity and bypassing the toxic effects of Hsp90 pan-inhibition, observe the changes in the transcriptome. The ClusterEx algorithm (Klaus Richter, www.clusterex.de) could previously perform well in elucidating the networks of the up- or down-regulated genes in response to the expression of toxic polyglutamine proteins in yeast, based on co-regulatory relationships obtained from the SPELL database and additionally predict further differentially expressed genes. (230). The approach was also used to identify the differentially expressed gene clusters after Hsp90-depletion in *C. elegans* and in both systems co-regulation clusters could be well separated (229-231). Comparing the KUNB31 response to dexamethasone treatment and a combination of dexamethasone and KUNB31 treatment, may help reveal chaperone·SHR-specific genetic interactions and the results of selective Hsp90β inhibition on whole-genome level. In principle, these responses should have co-expression cliques in common, as Hsp90 is responsible for the transformation of steroid receptors to their hormone-binding competent state (91).

Extracting the higher density patches as individual cliques from a genome-wide co-expression database, based on publicly available microarray data, is a more challenging calculation for the human compared to the yeast and *C.elegans* genome. ClusterEx would need further optimization in order to yield a lower signal to noise ratio and construct human cliques as well. The gene lists were, for the time being, filtered with the TAC software for significance and fold change to extract some indications of modified pathways. Gene networks, based on these gene lists and constructed with the GeneMANIA algorithm, show an individual response upon each treatment (232). Even though it may be appropriate to also complement these analyses with experiments performed in other time points or with higher KUNB31 concentrations, these results already suggest pathways that may be affected and the enriched GO terms provide a summary of the potentially modified biological functions. Scanning the network

constructed for the Hsp90 interactome by Echeverria and coworkers for the hits identified in the present study, already links a few protein-protein interactions to KUNB31 treatment but is only a “test” approach for reading this data set, compared to hit-to-hit relationships visualized in transcriptional cluster detail (38).

This search returned HTR2A, a G protein-coupled receptor of the serotonin receptor family, NOS1, nitric oxide synthase, and NF1, Neurofibromin 1, hits that were not pronounced with as strong fold change as other genes in this analysis, but were, nevertheless, significantly affected and are involved in PPIs with Hsp90 cochaperones PP5, AHSA1 and DNAJC7 (Figure 5.3A, B). AHSA1 activates the ATPase activity of Hsp90 while the PP5 phosphatase dephosphorylates a myriad of signaling proteins, like kinases and nuclear receptors that link this cochaperone to a wide spectrum of cellular processes (65,221). DNAJC7, better known as Tpr2, is a TPR domain-containing type III J protein, implicated in SHR chaperoning (87,242). Tpr2, like the adaptor protein Hop, can bind to Hsp90 and Hsp70 simultaneously. Unlike Hop, Tpr2 binding to Hsp70 in the presence of Hsp90 is ATP-dependent while Tpr2 cannot replace Hop in Hsp90 chaperoning *in vitro* or *in vivo*.(87,242). *In vivo*, a change in Tpr2 expression reduces GR activation, suggesting that Tpr2 is required at a narrowly defined expression level and it was proposed that it acts as a recycling chaperone, mediating the return of substrates from Hsp90 to Hsp70, so to earlier stages of chaperoning if further folding is required (87,242) Tpr2 enhances p53 stability and activity through blocking the complex formation between p53 and MDM2 and more recently it was identified as a novel gene implicated in the development of amyotrophic lateral sclerosis (243,244). The J domain of Tpr2 regulates its interaction with the proapoptotic and cell-cycle checkpoint protein, Rad9, which was significantly down-regulated (-1.2 fold change, p-value=0.0199) in the dexamethasone treatment but not in the treatments containing KUNB31 (245).

A.

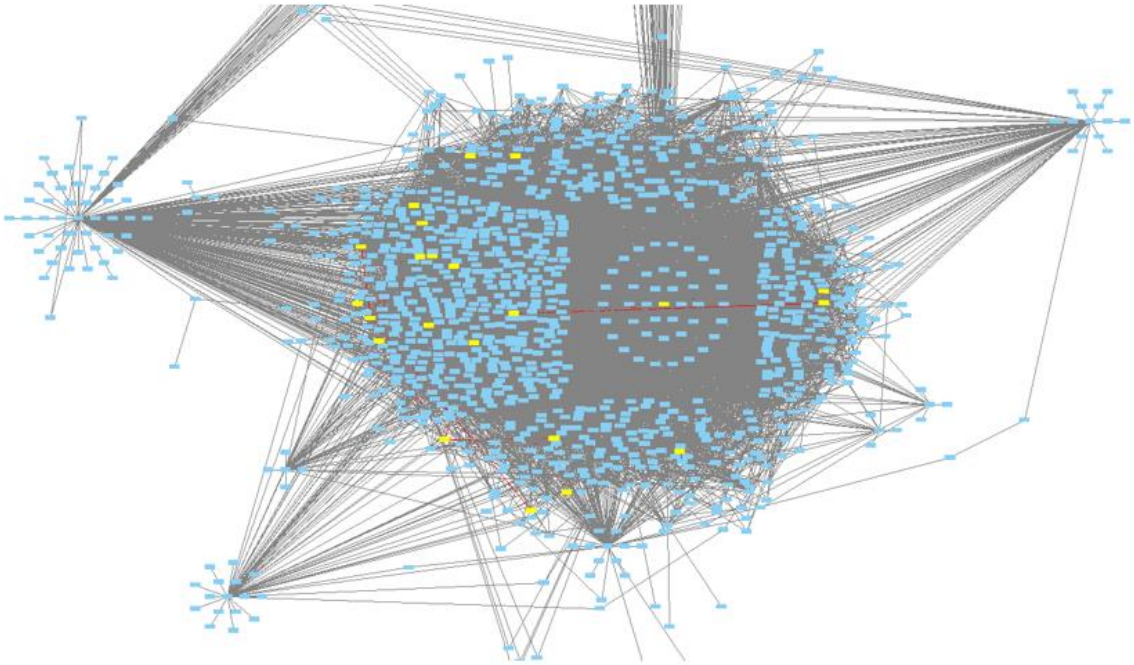

B.

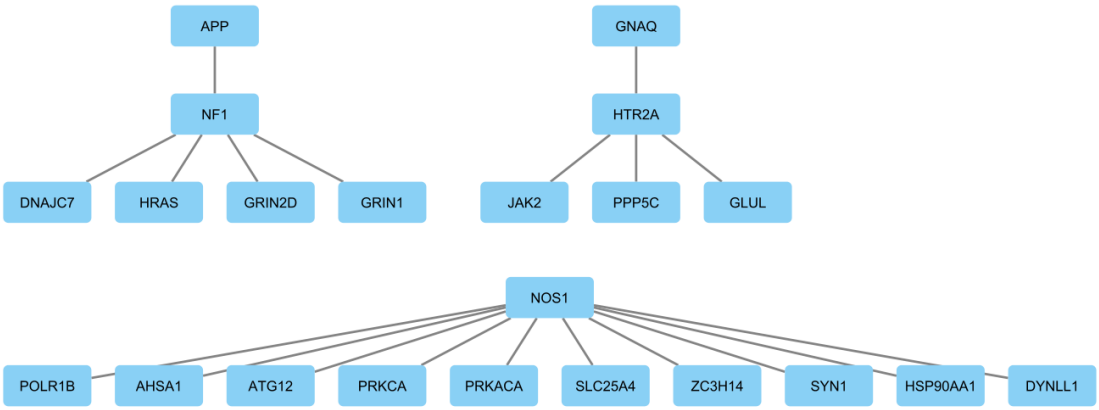

Figure 5.3. A) The identified interactors (NF1, HTR2A and NOS1) upon treatment with KUNB31+DEX and their first neighbors are visualized (yellow) on the Hsp90 interactome network constructed by Echeverria and coworkers (38). B) NF1, HTR2A, NOS1 and their first neighbor interactors as extracted from the Hsp90 interactome network.

Another member of the Hsp40 family, DNAJB3 was one of the most down-regulated genes in the KUNB31 (-1.88 fold-change, p value=0.0274) but not in the DEX+KUNB31 treatment. This protein was recently found to attenuate ER stress and to improve glucose uptake (246). Upon DEX+KUNB31 treatment, but not treatment with DEX or KUNB31, DNAJC5 was downregulated (-1.22 fold-change, p-value =0.0115). DNAJC5 encodes cysteine string protein α (CSPα) that is abundant in presynaptic vesicles to assure correct folding of synaptic proteins through interaction with Hsc70 (247).

The C-type lectins CLEC18A and CLEC18C were significantly upregulated (1.62 fold up-regulation, p-value= 0.0187) in the KUNB31 treatment but not the KUNB31+DEX treatment. C-type lectins also emerged as hits upon down-regulation of Hsp90 in *C.elegans* (229). C-type lectins are attractive therapeutic targets, better known for their involvement in innate and adaptive antimicrobial immune responses and are increasingly being recognized as key regulators of autoimmune diseases and many other aspects of multicellular existence (248,249). Another member of the lectin family, galectin-3 was downregulated upon KUNB31 treatment (-1.17 fold change, p-value= 0.0018). This protein, LGALS3, interacts with LGALS3-binding protein, LGALS3BP an Hsp90β client (38,233). It is an increasingly used diagnostic marker for different cancers while galectins cooperate with TRIMs to direct autophagy (250,251). TRIM51HP was 1.54 fold upregulated in the DEX+KUNB31 (p-value= 0.0246) while TRIM5; HBG2 was 1.5 fold downregulated (p-value= 0.04) upon dexamethasone treatment. Several TRIM proteins are confirmed Hsp90 clients (38). Thorough visualization and linking of the hits, that include many other interesting factors may help reveal the relevance of the above observations.

TPR proteins should be able to compete for binding to the Hsp90 dimer and it has been suggested that their impact depends on the relative abundance and mode of action of the other TPR proteins present in the same cell (53,119). DNAJ proteins are responsible for much of the functional diversity of Hsp70 proteins (252). Construction of up- or down- regulated gene clusters reflecting treatments like SHR activation and/or Hsp90 inhibition, followed by experimental verification of the observations, may help to better understand the context-specific or client-specific roles of cochaperones and direct further *in vitro* investigations while it may be possible to assign transcription factors to certain coexpression cliques.

6 References

1. Torday, J. S. (2015) Homeostasis as the Mechanism of Evolution. *Biology (Basel)* **4**, 573-590
2. Wingfield, J. C. (2003) Control of behavioural strategies for capricious environments. *Animal Behaviour* **66**, 807-816
3. Halfon, N., and Hochstein, M. (2002) Life Course Health Development: An Integrated Framework for Developing Health, Policy, and Research. *The Milbank Quarterly* **80**, 433-479
4. Jahn, T. R., and Radford, S. E. (2005) The Yin and Yang of protein folding. *The FEBS Journal* **272**, 5962-5970
5. Chiti, F., and Dobson, C. M. (2017) Protein Misfolding, Amyloid Formation, and Human Disease: A Summary of Progress Over the Last Decade. *Annu Rev Biochem* **86**, 27-68
6. Taipale, M., Jarosz, D. F., and Lindquist, S. (2010) HSP90 at the hub of protein homeostasis: emerging mechanistic insights. *Nat Rev Mol Cell Biol* **11**, 515-528
7. Hartl, F. U., Bracher, A., and Hayer-Hartl, M. (2011) Molecular chaperones in protein folding and proteostasis. *Nature* **475**, 324-332
8. Dunker, A. K., Silman, I., Uversky, V. N., and Sussman, J. L. (2008) Function and structure of inherently disordered proteins. *Curr Opin Struct Biol* **18**, 756-764
9. Dunker, A. K., Oldfield, C. J., Meng, J., Romero, P., Yang, J. Y., Chen, J. W., Vacic, V., Obradovic, Z., and Uversky, V. N. (2008) The unfoldomics decade: an update on intrinsically disordered proteins. *BMC Genomics* **9 Suppl 2**, S1
10. Hartl, F. U. (1996) Molecular chaperones in cellular protein folding. *Nature* **381**, 571-579
11. Dahiya, V., and Buchner, J. (2019) Chapter One - Functional principles and regulation of molecular chaperones. in *Advances in Protein Chemistry and Structural Biology* (Donev, R. ed.), Academic Press. pp 1-60
12. Schopf, F. H., Biebl, M. M., and Buchner, J. (2017) The HSP90 chaperone machinery. *Nat Rev Mol Cell Biol* **18**, 345-360
13. Zimmerman, S. B., and Trach, S. O. (1991) Estimation of macromolecule concentrations and excluded volume effects for the cytoplasm of Escherichia coli. *J Mol Biol* **222**, 599-620
14. Hartl, F. U., and Hayer-Hartl, M. (2009) Converging concepts of protein folding in vitro and in vivo. *Nature Structural & Molecular Biology* **16**, 574-581
15. Anfinsen, C. B., Haber, E., Sela, M., and White, F. H. (1961) THE KINETICS OF FORMATION OF NATIVE RIBONUCLEASE DURING OXIDATION OF THE REDUCED POLYPEPTIDE CHAIN. *Proceedings of the National Academy of Sciences* **47**, 1309-1314
16. Anfinsen, C. B. (1973) Principles that Govern the Folding of Protein Chains. *Science* **181**, 223
17. Zwanzig, R., Szabo, A., and Bagchi, B. (1992) Levinthal's paradox. *Proceedings of the National Academy of Sciences of the United States of America* **89**, 20-22
18. Baldwin, R. L. (2017) Clash between energy landscape theory and foldon-dependent protein folding. *Proceedings of the National Academy of Sciences of the United States of America* **114**, 8442-8443
19. Marston, F. A. (1986) The purification of eukaryotic polypeptides synthesized in Escherichia coli. *The Biochemical journal* **240**, 1-12

20. Zettlmeissl, G., Rudolph, R., and Jaenicke, R. (1979) Reconstitution of lactic dehydrogenase. Noncovalent aggregation vs. reactivation. 1. Physical properties and kinetics of aggregation. *Biochemistry* **18**, 5567-5571
21. Bryngelson, J. D., Onuchic, J. N., Socci, N. D., and Wolynes, P. G. (1995) Funnels, pathways, and the energy landscape of protein folding: a synthesis. *Proteins* **21**, 167-195
22. Englander, S. W., and Mayne, L. (2017) The case for defined protein folding pathways. *Proc Natl Acad Sci U S A* **114**, 8253-8258
23. Privalov, P. L. (1996) Intermediate states in protein folding. *J Mol Biol* **258**, 707-725
24. Krivov, S. V., and Karplus, M. (2004) Hidden complexity of free energy surfaces for peptide (protein) folding. *Proc Natl Acad Sci U S A* **101**, 14766-14770
25. Honeycutt, J. D., and Thirumalai, D. (1990) Metastability of the folded states of globular proteins. *Proc Natl Acad Sci U S A* **87**, 3526-3529
26. Lattman, E. E., and Rose, G. D. (1993) Protein Folding-What's the Question? *Proceedings of the National Academy of Sciences of the United States of America* **90**, 439-441
27. Callaway, E. (2020) 'It will change everything': DeepMind's AI makes gigantic leap in solving protein structures. *Nature* **588**, 203-204
28. (2005) So Much More to Know &#133. *Science* **309**, 78
29. Senior, A. W., Evans, R., Jumper, J., Kirkpatrick, J., Sifre, L., Green, T., Qin, C., Žídek, A., Nelson, A. W. R., Bridgland, A., Penedones, H., Petersen, S., Simonyan, K., Crossan, S., Kohli, P., Jones, D. T., Silver, D., Kavukcuoglu, K., and Hassabis, D. (2020) Improved protein structure prediction using potentials from deep learning. *Nature* **577**, 706-710
30. AlQuraishi, M. (2020) A watershed moment for protein structure prediction. *Nature* **577**, 627-628
31. Dill, K. A., Ozkan, S. B., Shell, M. S., and Weikl, T. R. (2008) The protein folding problem. *Annu Rev Biophys* **37**, 289-316
32. Zuehlke, A., and Johnson, J. L. (2010) Hsp90 and co-chaperones twist the functions of diverse client proteins. *Biopolymers* **93**, 211-217
33. Klaips, C. L., Jayaraj, G. G., and Hartl, F. U. (2017) Pathways of cellular proteostasis in aging and disease. *Journal of Cell Biology* **217**, 51-63
34. Hipp, M. S., Kasturi, P., and Hartl, F. U. (2019) The proteostasis network and its decline in ageing. *Nature Reviews Molecular Cell Biology* **20**, 421-435
35. Prodromou, C. (2012) The 'active life' of Hsp90 complexes. *Biochim Biophys Acta* **1823**, 614-623
36. Rutherford, S. L., and Lindquist, S. (1998) Hsp90 as a capacitor for morphological evolution. *Nature* **396**, 336-342
37. Echtenkamp, F. J., Gvozdenov, Z., Adkins, N. L., Zhang, Y., Lynch-Day, M., Watanabe, S., Peterson, C. L., and Freeman, B. C. (2016) Hsp90 and p23 Molecular Chaperones Control Chromatin Architecture by Maintaining the Functional Pool of the RSC Chromatin Remodeler. *Mol Cell* **64**, 888-899
38. Echeverría, P. C., Bernthaler, A., Dupuis, P., Mayer, B., and Picard, D. (2011) An Interaction Network Predicted from Public Data as a Discovery Tool: Application to the Hsp90 Molecular Chaperone Machine. *PLOS ONE* **6**, e26044
39. Taipale, M., Krykbaeva, I., Koeva, M., Kayatekin, C., Westover, K. D., Karras, G. I., and Lindquist, S. (2012) Quantitative analysis of HSP90-client interactions reveals principles of substrate recognition. *Cell* **150**, 987-1001

40. Felts, S. J., Owen, B. A., Nguyen, P., Trepel, J., Donner, D. B., and Toft, D. O. (2000) The hsp90-related protein TRAP1 is a mitochondrial protein with distinct functional properties. *J Biol Chem* **275**, 3305-3312
41. Jakob, U., Lilie, H., Meyer, I., and Buchner, J. (1995) Transient interaction of Hsp90 with early unfolding intermediates of citrate synthase. Implications for heat shock in vivo. *J Biol Chem* **270**, 7288-7294
42. Genest, O., Reidy, M., Street, T. O., Hoskins, J. R., Camberg, J. L., Agard, D. A., Masison, D. C., and Wickner, S. (2013) Uncovering a region of heat shock protein 90 important for client binding in E. coli and chaperone function in yeast. *Mol Cell* **49**, 464-473
43. Karagöz, G. E., Duarte, A. M., Akoury, E., Ippel, H., Biernat, J., Morán Luengo, T., Radli, M., Didenko, T., Nordhues, B. A., Veprintsev, D. B., Dickey, C. A., Mandelkow, E., Zweckstetter, M., Boelens, R., Madl, T., and Rüdiger, S. G. (2014) Hsp90-Tau complex reveals molecular basis for specificity in chaperone action. *Cell* **156**, 963-974
44. Lorenz, O. R., Freiburger, L., Rutz, D. A., Krause, M., Zierer, B. K., Alvira, S., Cuellar, J., Valpuesta, J. M., Madl, T., Sattler, M., and Buchner, J. (2014) Modulation of the Hsp90 chaperone cycle by a stringent client protein. *Mol Cell* **53**, 941-953
45. Mayer, Matthias P., and Le Breton, L. (2015) Hsp90: Breaking the Symmetry. *Molecular Cell* **58**, 8-20
46. Prodromou, C., Siligardi, G., O'Brien, R., Woolfson, D. N., Regan, L., Panaretou, B., Ladbury, J. E., Piper, P. W., and Pearl, L. H. (1999) Regulation of Hsp90 ATPase activity by tetratricopeptide repeat (TPR)-domain co-chaperones. *Embo j* **18**, 754-762
47. Hainzl, O., Lapina, M. C., Buchner, J., and Richter, K. (2009) The charged linker region is an important regulator of Hsp90 function. *J Biol Chem* **284**, 22559-22567
48. Jahn, M., Rehn, A., Pelz, B., Hellenkamp, B., Richter, K., Rief, M., Buchner, J., and Hugel, T. (2014) The charged linker of the molecular chaperone Hsp90 modulates domain contacts and biological function. *Proc Natl Acad Sci U S A* **111**, 17881-17886
49. Tsutsumi, S., Mollapour, M., Prodromou, C., Lee, C. T., Panaretou, B., Yoshida, S., Mayer, M. P., and Neckers, L. M. (2012) Charged linker sequence modulates eukaryotic heat shock protein 90 (Hsp90) chaperone activity. *Proc Natl Acad Sci U S A* **109**, 2937-2942
50. Zuehlke, A. D., and Johnson, J. L. (2012) Chaperoning the chaperone: a role for the co-chaperone Cpr7 in modulating Hsp90 function in Saccharomyces cerevisiae. *Genetics* **191**, 805-814
51. Röhl, A., Wengler, D., Madl, T., Lagleder, S., Tippel, F., Herrmann, M., Hendrix, J., Richter, K., Hack, G., Schmid, A. B., Kessler, H., Lamb, D. C., and Buchner, J. (2015) Hsp90 regulates the dynamics of its cochaperone Sti1 and the transfer of Hsp70 between modules. *Nat Commun* **6**, 6655
52. Scheufler, C., Brinker, A., Bourenkov, G., Pegoraro, S., Moroder, L., Bartunik, H., Hartl, F. U., and Moarefi, I. (2000) Structure of TPR domain-peptide complexes: critical elements in the assembly of the Hsp70-Hsp90 multichaperone machine. *Cell* **101**, 199-210
53. Schülke, J.-P., Wochnik, G. M., Lang-Rollin, I., Gassen, N. C., Knapp, R. T., Berning, B., Yassouridis, A., and Rein, T. (2010) Differential Impact of Tetratricopeptide Repeat Proteins on the Steroid Hormone Receptors. *PLOS ONE* **5**, e11717
54. Smith, D. F. (2004) Tetratricopeptide repeat cochaperones in steroid receptor complexes. *Cell Stress Chaperones* **9**, 109-121
55. Southworth, D. R., and Agard, D. A. (2008) Species-dependent ensembles of conserved conformational states define the Hsp90 chaperone ATPase cycle. *Molecular cell* **32**, 631-640

56. Dollins, D. E., Warren, J. J., Immormino, R. M., and Gewirth, D. T. (2007) Structures of GRP94-nucleotide complexes reveal mechanistic differences between the hsp90 chaperones. *Mol Cell* **28**, 41-56
57. Richter, K., and Buchner, J. (2006) hsp90: Twist and Fold. *Cell* **127**, 251-253
58. Shiau, A. K., Harris, S. F., Southworth, D. R., and Agard, D. A. (2006) Structural Analysis of E. coli hsp90 reveals dramatic nucleotide-dependent conformational rearrangements. *Cell* **127**, 329-340
59. Kaziales, A., Barkovits, K., Marcus, K., and Richter, K. (2020) Glucocorticoid receptor complexes form cooperatively with the Hsp90 co-chaperones Pp5 and FKBPs. *Scientific Reports* **10**, 10733
60. Richter, K., Muschler, P., Hainzl, O., and Buchner, J. (2001) Coordinated ATP hydrolysis by the Hsp90 dimer. *J Biol Chem* **276**, 33689-33696
61. Ali, M. M., Roe, S. M., Vaughan, C. K., Meyer, P., Panaretou, B., Piper, P. W., Prodromou, C., and Pearl, L. H. (2006) Crystal structure of an Hsp90-nucleotide-p23/Sba1 closed chaperone complex. *Nature* **440**, 1013-1017
62. Hessling, M., Richter, K., and Buchner, J. (2009) Dissection of the ATP-induced conformational cycle of the molecular chaperone Hsp90. *Nat Struct Mol Biol* **16**, 287-293
63. Astl, L., Stetz, G., and Verkhivker, G. M. (2020) Allosteric Mechanism of the Hsp90 Chaperone Interactions with Cochaperones and Client Proteins by Modulating Communication Spines of Coupled Regulatory Switches: Integrative Atomistic Modeling of Hsp90 Signaling in Dynamic Interaction Networks. *J Chem Inf Model* **60**, 3616-3631
64. Harst, A., Lin, H., and Obermann, W. M. (2005) Aha1 competes with Hop, p50 and p23 for binding to the molecular chaperone Hsp90 and contributes to kinase and hormone receptor activation. *Biochem J* **387**, 789-796
65. Lotz, G. P., Lin, H., Harst, A., and Obermann, W. M. (2003) Aha1 binds to the middle domain of Hsp90, contributes to client protein activation, and stimulates the ATPase activity of the molecular chaperone. *J Biol Chem* **278**, 17228-17235
66. Meyer, P., Prodromou, C., Liao, C., Hu, B., Roe, S. M., Vaughan, C. K., Vlasic, I., Panaretou, B., Piper, P. W., and Pearl, L. H. (2004) Structural basis for recruitment of the ATPase activator Aha1 to the Hsp90 chaperone machinery. *Embo j* **23**, 1402-1410
67. Panaretou, B., Siligardi, G., Meyer, P., Maloney, A., Sullivan, J. K., Singh, S., Millson, S. H., Clarke, P. A., Naaby-Hansen, S., Stein, R., Cramer, R., Mollapour, M., Workman, P., Piper, P. W., Pearl, L. H., and Prodromou, C. (2002) Activation of the ATPase Activity of Hsp90 by the Stress-Regulated Cochaperone Aha1. *Molecular Cell* **10**, 1307-1318
68. Siligardi, G., Hu, B., Panaretou, B., Piper, P. W., Pearl, L. H., and Prodromou, C. (2004) Co-chaperone regulation of conformational switching in the Hsp90 ATPase cycle. *J Biol Chem* **279**, 51989-51998
69. McLaughlin, S. H., Smith, H. W., and Jackson, S. E. (2002) Stimulation of the weak ATPase activity of human hsp90 by a client protein. *J Mol Biol* **315**, 787-798
70. Rehn, A., Moroni, E., Zierer, B. K., Tippel, F., Morra, G., John, C., Richter, K., Colombo, G., and Buchner, J. (2016) Allosteric Regulation Points Control the Conformational Dynamics of the Molecular Chaperone Hsp90. *J Mol Biol* **428**, 4559-4571
71. Lee, C. T., Graf, C., Mayer, F. J., Richter, S. M., and Mayer, M. P. (2012) Dynamics of the regulation of Hsp90 by the co-chaperone Sti1. *Embo j* **31**, 1518-1528
72. Rutz, D. A., Luo, Q., Freiburger, L., Madl, T., Kaila, V. R. I., Sattler, M., and Buchner, J. (2018) A switch point in the molecular chaperone Hsp90 responding to client interaction. *Nature Communications* **9**, 1472

73. Rehn, A., Lawatscheck, J., Jokisch, M.-L., Mader, S. L., Luo, Q., Tippel, F., Blank, B., Richter, K., Lang, K., Kaila, V. R. I., and Buchner, J. (2020) A methylated lysine is a switch point for conformational communication in the chaperone Hsp90. *Nature Communications* **11**, 1219
74. Mollapour, M., Bourboulia, D., Beebe, K., Woodford, M. R., Polier, S., Hoang, A., Chelluri, R., Li, Y., Guo, A., Lee, M. J., Fotooh-Abadi, E., Khan, S., Prince, T., Miyajima, N., Yoshida, S., Tsutsumi, S., Xu, W., Panaretou, B., Stetler-Stevenson, W. G., Bratslavsky, G., Trepel, J. B., Prodromou, C., and Neckers, L. (2014) Asymmetric Hsp90 N domain SUMOylation recruits Aha1 and ATP-competitive inhibitors. *Mol Cell* **53**, 317-329
75. Mollapour, M., Tsutsumi, S., and Neckers, L. (2010) Hsp90 phosphorylation, Wee1 and the cell cycle. *Cell Cycle* **9**, 2310-2316
76. Bachman, A. B., Keramisanou, D., Xu, W., Beebe, K., Moses, M. A., Vasantha Kumar, M. V., Gray, G., Noor, R. E., van der Vaart, A., Neckers, L., and Gelis, I. (2018) Phosphorylation induced cochaperone unfolding promotes kinase recruitment and client class-specific Hsp90 phosphorylation. *Nat Commun* **9**, 265
77. Xu, W., Beebe, K., Chavez, J. D., Boysen, M., Lu, Y., Zuehlke, A. D., Keramisanou, D., Trepel, J. B., Prodromou, C., Mayer, M. P., Bruce, J. E., Gelis, I., and Neckers, L. (2019) Hsp90 middle domain phosphorylation initiates a complex conformational program to recruit the ATPase-stimulating cochaperone Aha1. *Nat Commun* **10**, 2574
78. Blacklock, K., and Verkhivker, G. M. (2014) Allosteric regulation of the Hsp90 dynamics and stability by client recruiter cochaperones: protein structure network modeling. *PLoS One* **9**, e86547
79. Miyata, Y., Nakamoto, H., and Neckers, L. (2013) The therapeutic target Hsp90 and cancer hallmarks. *Curr Pharm Des* **19**, 347-365
80. Ratzke, C., Nguyen, M. N., Mayer, M. P., and Hugel, T. (2012) From a ratchet mechanism to random fluctuations evolution of Hsp90's mechanochemical cycle. *J Mol Biol* **423**, 462-471
81. Sahasrabudhe, P., Rohrberg, J., Biebl, M. M., Rutz, D. A., and Buchner, J. (2017) The Plasticity of the Hsp90 Co-chaperone System. *Mol Cell* **67**, 947-961.e945
82. Röhl, A., Rohrberg, J., and Buchner, J. (2013) The chaperone Hsp90: changing partners for demanding clients. *Trends in Biochemical Sciences* **38**, 253-262
83. Biebl, M. M., Lopez, A., Rehn, A., Freiburger, L., Lawatscheck, J., Blank, B., Sattler, M., and Buchner, J. (2021) Structural elements in the flexible tail of the co-chaperone p23 coordinate client binding and progression of the Hsp90 chaperone cycle. *Nature Communications* **12**, 828
84. Verba, K. A., Wang, R. Y.-R., Arakawa, A., Liu, Y., Shirouzu, M., Yokoyama, S., and Agard, D. A. (2016) Atomic structure of Hsp90-Cdc37-Cdk4 reveals that Hsp90 traps and stabilizes an unfolded kinase. *Science (New York, N.Y.)* **352**, 1542-1547
85. Wu, H., Hyun, J., Martinez-Yamout, M. A., Park, S. J., and Dyson, H. J. (2018) Characterization of an Hsp90-Independent Interaction between Co-Chaperone p23 and Transcription Factor p53. *Biochemistry* **57**, 935-944
86. Keramisanou, D., Aboalroub, A., Zhang, Z., Liu, W., Marshall, D., Diviney, A., Larsen, R. W., Landgraf, R., and Gelis, I. (2016) Molecular Mechanism of Protein Kinase Recognition and Sorting by the Hsp90 Kinome-Specific Cochaperone Cdc37. *Molecular cell* **62**, 260-271
87. Brychzy, A., Rein, T., Winklhofer, K. F., Hartl, F. U., Young, J. C., and Obermann, W. M. (2003) Cofactor Tpr2 combines two TPR domains and a J domain to regulate the Hsp70/Hsp90 chaperone system. *Embo j* **22**, 3613-3623

88. Smith, D. F., and Toft, D. O. (2008) Minireview: The Intersection of Steroid Receptors with Molecular Chaperones: Observations and Questions. *Molecular Endocrinology* **22**, 2229-2240
89. Grad, I., and Picard, D. (2007) The glucocorticoid responses are shaped by molecular chaperones. *Molecular and Cellular Endocrinology* **275**, 2-12
90. Dittmar, K. D., Hutchison, K. A., Owens-Grillo, J. K., and Pratt, W. B. (1996) Reconstitution of the Steroid Receptor·hsp90 Heterocomplex Assembly System of Rabbit Reticulocyte Lysate*. *Journal of Biological Chemistry* **271**, 12833-12839
91. Hutchison, K. A., Dittmar, K. D., and Pratt, W. B. (1994) All of the factors required for assembly of the glucocorticoid receptor into a functional heterocomplex with heat shock protein 90 are preassociated in a self-sufficient protein folding structure, a "foldosome". *J Biol Chem* **269**, 27894-27899
92. Bodwell, J. E., Hu, L.-M., Hu, J.-M., Ortí, E., and Munck, A. (1993) Glucocorticoid receptors: ATP-dependent cycling and hormone-dependent hyperphosphorylation. *The Journal of Steroid Biochemistry and Molecular Biology* **47**, 31-38
93. Howard, K. J., and Distelhorst, C. W. (1988) Effect of the 90 kDa heat shock protein, HSP90, on glucocorticoid receptor binding to DNA-cellulose. *Biochemical and Biophysical Research Communications* **151**, 1226-1232
94. Ziemiecki, A., Catelli, M.-G., Joab, I., and Moncharmont, B. (1986) Association of the heat shock protein HSP90 with steroid hormone receptors and tyrosine kinase oncogene products. *Biochemical and Biophysical Research Communications* **138**, 1298-1307
95. Catelli, M. G., Binart, N., Jung-Testas, I., Renoir, J. M., Baulieu, E. E., Feramisco, J. R., and Welch, W. J. (1985) The common 90-kd protein component of non-transformed '8S' steroid receptors is a heat-shock protein. *Embo j* **4**, 3131-3135
96. Joab, I., Radanyi, C., Renoir, M., Buchou, T., Catelli, M. G., Binart, N., Mester, J., and Baulieu, E. E. (1984) Common non-hormone binding component in non-transformed chick oviduct receptors of four steroid hormones. *Nature* **308**, 850-853
97. Nair, S. C., Toran, E. J., Rimerman, R. A., Hjermstad, S., Smithgall, T. E., and Smith, D. F. (1996) A pathway of multi-chaperone interactions common to diverse regulatory proteins: estrogen receptor, Fes tyrosine kinase, heat shock transcription factor Hsf1, and the aryl hydrocarbon receptor. *Cell Stress Chaperones* **1**, 237-250
98. Cheung, J., and Smith, D. F. (2000) Molecular chaperone interactions with steroid receptors: an update. *Mol Endocrinol* **14**, 939-946
99. Smith, D. F., Baggenstoss, B. A., Marion, T. N., and Rimerman, R. A. (1993) Two FKBP-related proteins are associated with progesterone receptor complexes. *J Biol Chem* **268**, 18365-18371
100. Smith, D. F., Stensgard, B. A., Welch, W. J., and Toft, D. O. (1992) Assembly of progesterone receptor with heat shock proteins and receptor activation are ATP mediated events. *J Biol Chem* **267**, 1350-1356
101. Smith, D. F., Sullivan, W. P., Marion, T. N., Zaitsu, K., Madden, B., McCormick, D. J., and Toft, D. O. (1993) Identification of a 60-kilodalton stress-related protein, p60, which interacts with hsp90 and hsp70. *Molecular and Cellular Biology* **13**, 869-876
102. Chen, M.-S., Silverstein, A. M., Pratt, W. B., and Chinkers, M. (1996) The Tetratricopeptide Repeat Domain of Protein Phosphatase 5 Mediates Binding to Glucocorticoid Receptor Heterocomplexes and Acts as a Dominant Negative Mutant *. *Journal of Biological Chemistry* **271**, 32315-32320

103. Johnson, J. L., and Toft, D. O. (1994) A novel chaperone complex for steroid receptors involving heat shock proteins, immunophilins, and p23. *J Biol Chem* **269**, 24989-24993
104. Pratt, W. B., and Toft, D. O. (1997) Steroid receptor interactions with heat shock protein and immunophilin chaperones. *Endocr Rev* **18**, 306-360
105. Kirschke, E., Goswami, D., Southworth, D., Griffin, P. R., and Agard, D. A. (2014) Glucocorticoid receptor function regulated by coordinated action of the Hsp90 and Hsp70 chaperone cycles. *Cell* **157**, 1685-1697
106. Pratt, W. B., Morishima, Y., Murphy, M., and Harrell, M. (2006) Chaperoning of Glucocorticoid Receptors. in *Molecular Chaperones in Health and Disease* (Starke, K., and Gaestel, M. eds.), Springer Berlin Heidelberg, Berlin, Heidelberg. pp 111-138
107. Tsuboyama, K., Tadakuma, H., and Tomari, Y. (2018) Conformational Activation of Argonaute by Distinct yet Coordinated Actions of the Hsp70 and Hsp90 Chaperone Systems. *Mol Cell* **70**, 722-729.e724
108. Pratt, W. B., and Welsh, M. J. (1994) Chaperone functions of the heat shock proteins associated with steroid receptors. *Seminars in Cell Biology* **5**, 83-93
109. Bose, S., Weikl, T., Bügl, H., and Buchner, J. (1996) Chaperone function of Hsp90-associated proteins. *Science* **274**, 1715-1717
110. Schmid, A. B., Lagleder, S., Gräwert, M. A., Röhl, A., Hagn, F., Wandinger, S. K., Cox, M. B., Demmer, O., Richter, K., Groll, M., Kessler, H., and Buchner, J. (2012) The architecture of functional modules in the Hsp90 co-chaperone Sti1/Hop. *Embo j* **31**, 1506-1517
111. Barent, R. L., Nair, S. C., Carr, D. C., Ruan, Y., Rimerman, R. A., Fulton, J., Zhang, Y., and Smith, D. F. (1998) Analysis of FKBP51/FKBP52 chimeras and mutants for Hsp90 binding and association with progesterone receptor complexes. *Mol Endocrinol* **12**, 342-354
112. Wochnik, G. M., Rüegg, J., Abel, G. A., Schmidt, U., Holsboer, F., and Rein, T. (2005) FK506-binding proteins 51 and 52 differentially regulate dynein interaction and nuclear translocation of the glucocorticoid receptor in mammalian cells. *J Biol Chem* **280**, 4609-4616
113. Riggs, D. L., Cox, M. B., Tardif, H. L., Hessling, M., Buchner, J., and Smith, D. F. (2007) Noncatalytic role of the FKBP52 peptidyl-prolyl isomerase domain in the regulation of steroid hormone signaling. *Molecular and Cellular Biology* **27**, 8658-8669
114. Davies, T. H., Ning, Y. M., and Sánchez, E. R. (2002) A new first step in activation of steroid receptors: hormone-induced switching of FKBP51 and FKBP52 immunophilins. *J Biol Chem* **277**, 4597-4600
115. Ni, L., Yang, C. S., Gioeli, D., Frierson, H., Toft, D. O., and Paschal, B. M. (2010) FKBP51 promotes assembly of the Hsp90 chaperone complex and regulates androgen receptor signaling in prostate cancer cells. *Mol Cell Biol* **30**, 1243-1253
116. Febbo, P. G., Lowenberg, M., Thorner, A. R., Brown, M., Loda, M., and Golub, T. R. (2005) Androgen mediated regulation and functional implications of fkbp51 expression in prostate cancer. *J Urol* **173**, 1772-1777
117. Stechschulte, L. A., and Sanchez, E. R. (2011) FKBP51-a selective modulator of glucocorticoid and androgen sensitivity. *Curr Opin Pharmacol* **11**, 332-337
118. Galigniana, M. D., Radanyi, C., Renoir, J. M., Housley, P. R., and Pratt, W. B. (2001) Evidence that the peptidylprolyl isomerase domain of the hsp90-binding immunophilin FKBP52 is involved in both dynein interaction and glucocorticoid receptor movement to the nucleus. *J Biol Chem* **276**, 14884-14889
119. Silverstein, A. M., Galigniana, M. D., Kanelakis, K. C., Radanyi, C., Renoir, J. M., and Pratt, W. B. (1999) Different regions of the immunophilin FKBP52 determine its association with

the glucocorticoid receptor, hsp90, and cytoplasmic dynein. *J Biol Chem* **274**, 36980-36986
120. Silverstein, A. M., Galigniana, M. D., Chen, M. S., Owens-Grillo, J. K., Chinkers, M., and Pratt, W. B. (1997) Protein phosphatase 5 is a major component of glucocorticoid receptor.hsp90 complexes with properties of an FK506-binding immunophilin. *J Biol Chem* **272**, 16224-16230
121. Golden, T., Swingle, M., and Honkanen, R. E. (2008) The role of serine/threonine protein phosphatase type 5 (PP5) in the regulation of stress-induced signaling networks and cancer. *Cancer Metastasis Rev* **27**, 169-178
122. Davies, T. H., Ning, Y. M., and Sánchez, E. R. (2005) Differential control of glucocorticoid receptor hormone-binding function by tetratricopeptide repeat (TPR) proteins and the immunosuppressive ligand FK506. *Biochemistry* **44**, 2030-2038
123. Rousseau, G. G. (1984) Control of gene expression by glucocorticoid hormones. *The Biochemical journal* **224**, 1-12
124. Chrousos, G. P. (2004) The glucocorticoid receptor gene, longevity, and the complex disorders of Western societies. *The American Journal of Medicine* **117**, 204-207
125. Chrousos, G. P., and Kino, T. (2009) Glucocorticoid signaling in the cell. Expanding clinical implications to complex human behavioral and somatic disorders. *Ann N Y Acad Sci* **1179**, 153-166
126. Bledsoe, R. K., Stewart, E. L., and Pearce, K. H. (2004) Structure and function of the glucocorticoid receptor ligand binding domain. *Vitam Horm* **68**, 49-91
127. Kauppi, B., Jakob, C., Färnegårdh, M., Yang, J., Ahola, H., Alarcon, M., Calles, K., Engström, O., Harlan, J., Muchmore, S., Ramqvist, A. K., Thorell, S., Ohman, L., Greer, J., Gustafsson, J. A., Carlstedt-Duke, J., and Carlquist, M. (2003) The three-dimensional structures of antagonistic and agonistic forms of the glucocorticoid receptor ligand-binding domain: RU-486 induces a transconformation that leads to active antagonism. *J Biol Chem* **278**, 22748-22754
128. Darimont, B. D., Wagner, R. L., Apriletti, J. W., Stallcup, M. R., Kushner, P. J., Baxter, J. D., Fletterick, R. J., and Yamamoto, K. R. (1998) Structure and specificity of nuclear receptor-coactivator interactions. *Genes Dev* **12**, 3343-3356
129. Samarasinghe, R. A., Witchell, S. F., and DeFranco, D. B. (2012) Cooperativity and complementarity: synergies in non-classical and classical glucocorticoid signaling. *Cell Cycle* **11**, 2819-2827
130. Nicolaides, N. C., and Charmandari, E. (2019) Glucocorticoid Resistance. in *Genetics of Endocrine Diseases and Syndromes* (Igaz, P., and Patócs, A. eds.), Springer International Publishing, Cham. pp 85-102
131. Nicolaides, N. C., and Charmandari, E. (2019) Glucocorticoid Resistance. *Exp Suppl* **111**, 85-102
132. Charmandari, E., Raji, A., Kino, T., Ichijo, T., Tiulpakov, A., Zachman, K., and Chrousos, G. P. (2005) A novel point mutation in the ligand-binding domain (LBD) of the human glucocorticoid receptor (hGR) causing generalized glucocorticoid resistance: the importance of the C terminus of hGR LBD in conferring transactivational activity. *J Clin Endocrinol Metab* **90**, 3696-3705
133. Chrousos, G. P., Vingerhoeds, A., Brandon, D., Eil, C., Pugeat, M., DeVroede, M., Loriaux, D. L., and Lipsett, M. B. (1982) Primary cortisol resistance in man. A glucocorticoid receptor-mediated disease. *J Clin Invest* **69**, 1261-1269

134. Al Argan, R., Saskin, A., Yang, J. W., D'Agostino, M. D., and Rivera, J. (2018) Glucocorticoid resistance syndrome caused by a novel NR3C1 point mutation. *Endocr J* **65**, 1139-1146
135. Nicolaides, N. C., Roberts, M. L., Kino, T., Braatvedt, G., Hurt, D. E., Katsantoni, E., Sertedaki, A., Chrousos, G. P., and Charmandari, E. (2014) A novel point mutation of the human glucocorticoid receptor gene causes primary generalized glucocorticoid resistance through impaired interaction with the LXXLL motif of the p160 coactivators: dissociation of the transactivating and transreppressive activities. *J Clin Endocrinol Metab* **99**, E902-907
136. Nicolaides, N. C., Skyrla, E., Vlachakis, D., Psarra, A. M., Moutsatsou, P., Sertedaki, A., Kossida, S., and Charmandari, E. (2016) Functional characterization of the hGRαT556I causing Chrousos syndrome. *Eur J Clin Invest* **46**, 42-49
137. Roberts, M. L., Kino, T., Nicolaides, N. C., Hurt, D. E., Katsantoni, E., Sertedaki, A., Komianou, F., Kassiou, K., Chrousos, G. P., and Charmandari, E. (2013) A novel point mutation in the DNA-binding domain (DBD) of the human glucocorticoid receptor causes primary generalized glucocorticoid resistance by disrupting the hydrophobic structure of its DBD. *J Clin Endocrinol Metab* **98**, E790-795
138. Briassoulis, G., Horvath, A., Christoforou, P., Lodish, M., Xekouki, P., Quezado, M., Patronas, N., Keil, M. F., and Stratakis, C. A. (2012) Lack of mutations in the gene coding for the hGR (NR3C1) in a pediatric patient with ACTH-secreting pituitary adenoma, absence of stigmata of Cushing's syndrome and unusual histologic features. *J Pediatr Endocrinol Metab* **25**, 213-219
139. Zhang, S., Liang, X., and Danielsen, M. (1996) Role of the C terminus of the glucocorticoid receptor in hormone binding and agonist/antagonist discrimination. *Mol Endocrinol* **10**, 24-34
140. Bledsoe, R. K., Montana, V. G., Stanley, T. B., Delves, C. J., Apolito, C. J., McKee, D. D., Consler, T. G., Parks, D. J., Stewart, E. L., Willson, T. M., Lambert, M. H., Moore, J. T., Pearce, K. H., and Xu, H. E. (2002) Crystal structure of the glucocorticoid receptor ligand binding domain reveals a novel mode of receptor dimerization and coactivator recognition. *Cell* **110**, 93-105
141. Whitesell, L., Mimnaugh, E. G., De Costa, B., Myers, C. E., and Neckers, L. M. (1994) Inhibition of heat shock protein HSP90-pp60v-src heteroprotein complex formation by benzoquinone ansamycins: essential role for stress proteins in oncogenic transformation. *Proc Natl Acad Sci U S A* **91**, 8324-8328
142. Flandrin, P., Guyotat, D., Duval, A., Cornillon, J., Tavernier, E., Nadal, N., and Campos, L. (2008) Significance of heat-shock protein (HSP) 90 expression in acute myeloid leukemia cells. *Cell Stress Chaperones* **13**, 357-364
143. Neckers, L., and Workman, P. (2012) Hsp90 molecular chaperone inhibitors: are we there yet? *Clin Cancer Res* **18**, 64-76
144. Khandelwal, A., Kent, C. N., Balch, M., Peng, S., Mishra, S. J., Deng, J., Day, V. W., Liu, W., Subramanian, C., Cohen, M., Holzbeierlein, J. M., Matts, R., and Blagg, B. S. J. (2018) Structure-guided design of an Hsp90β N-terminal isoform-selective inhibitor. *Nature communications* **9**, 425-425
145. Rodina, A., Wang, T., Yan, P., Gomes, E. D., Dunphy, M. P., Pillarsetty, N., Koren, J., Gerecitano, J. F., Taldone, T., Zong, H., Caldas-Lopes, E., Alpaugh, M., Corben, A., Riolo, M., Beattie, B., Pressl, C., Peter, R. I., Xu, C., Trondl, R., Patel, H. J., Shimizu, F., Bolaender, A., Yang, C., Panchal, P., Farooq, M. F., Kishinevsky, S., Modi, S., Lin, O., Chu, F., Patil, S., Erdjument-Bromage, H., Zanzonico, P., Hudis, C., Studer, L., Roboz, G. J., Cesarman, E.,

Cerchietti, L., Levine, R., Melnick, A., Larson, S. M., Lewis, J. S., Guzman, M. L., and Chiosis, G. (2016) The epichaperome is an integrated chaperome network that facilitates tumour survival. *Nature* **538**, 397-401

146. Whitesell, L., and Lindquist, S. L. (2005) HSP90 and the chaperoning of cancer. *Nature Reviews Cancer* **5**, 761-772
147. Soga, S., Neckers, L. M., Schulte, T. W., Shiotsu, Y., Akasaka, K., Narumi, H., Agatsuma, T., Ikuina, Y., Murakata, C., Tamaoki, T., and Akinaga, S. (1999) KF25706, a novel oxime derivative of radicicol, exhibits in vivo antitumor activity via selective depletion of Hsp90 binding signaling molecules. *Cancer Res* **59**, 2931-2938
148. An, W. G., Schulte, T. W., and Neckers, L. M. (2000) The heat shock protein 90 antagonist geldanamycin alters chaperone association with p210bcr-abl and v-src proteins before their degradation by the proteasome. *Cell Growth Differ* **11**, 355-360
149. Blagosklonny, M. V., Toretsky, J., and Neckers, L. (1995) Geldanamycin selectively destabilizes and conformationally alters mutated p53. *Oncogene* **11**, 933-939
150. Maroney, A. C., Marugan, J. J., Mezzasalma, T. M., Barnakov, A. N., Garrabrant, T. A., Weaner, L. E., Jones, W. J., Barnakova, L. A., Koblish, H. K., Todd, M. J., Masucci, J. A., Deckman, I. C., Galemmo, R. A., Jr., and Johnson, D. L. (2006) Dihydroquinone ansamycins: toward resolving the conflict between low in vitro affinity and high cellular potency of geldanamycin derivatives. *Biochemistry* **45**, 5678-5685
151. Onuoha, S. C., Mukund, S. R., Coulstock, E. T., Sengerovà, B., Shaw, J., McLaughlin, S. H., and Jackson, S. E. (2007) Mechanistic studies on Hsp90 inhibition by ansamycin derivatives. *J Mol Biol* **372**, 287-297
152. Patel, K., Piagentini, M., Rascher, A., Tian, Z. Q., Buchanan, G. O., Regentin, R., Hu, Z., Hutchinson, C. R., and McDaniel, R. (2004) Engineered biosynthesis of geldanamycin analogs for Hsp90 inhibition. *Chem Biol* **11**, 1625-1633
153. Day, J. E. H., Sharp, S. Y., Rowlands, M. G., Aherne, W., Hayes, A., Raynaud, F. I., Lewis, W., Roe, S. M., Prodromou, C., Pearl, L. H., Workman, P., and Moody, C. J. (2011) Targeting the Hsp90 Molecular Chaperone with Novel Macrolactams. Synthesis, Structural, Binding, and Cellular Studies. *ACS Chemical Biology* **6**, 1339-1347
154. Tran, P. L., Kim, S. A., Choi, H. S., Yoon, J. H., and Ahn, S. G. (2010) Epigallocatechin-3-gallate suppresses the expression of HSP70 and HSP90 and exhibits anti-tumor activity in vitro and in vivo. *BMC Cancer* **10**, 276
155. Yin, Z., Henry, E. C., and Gasiewicz, T. A. (2009) (-)-Epigallocatechin-3-gallate is a novel Hsp90 inhibitor. *Biochemistry* **48**, 336-345
156. Vasko, R. C., Rodriguez, R. A., Cunningham, C. N., Ardi, V. C., Agard, D. A., and McAlpine, S. R. (2010) Mechanistic Studies of Sansalvamide A-Amide: An Allosteric Modulator of Hsp90. *ACS Medicinal Chemistry Letters* **1**, 4-8
157. Chiosis, G., Lucas, B., Shtil, A., Huezo, H., and Rosen, N. (2002) Development of a purine-scaffold novel class of Hsp90 binders that inhibit the proliferation of cancer cells and induce the degradation of Her2 tyrosine kinase. *Bioorg Med Chem* **10**, 3555-3564
158. Speranza, G., Anderson, L., Chen, A. P., Do, K., Eugeni, M., Weil, M., Rubinstein, L., Majerova, E., Collins, J., Horneffer, Y., Juwara, L., Zlott, J., Bishop, R., Conley, B. A., Streicher, H., Tomaszewski, J., Doroshow, J. H., and Kummar, S. (2018) First-in-human study of the epichaperome inhibitor PU-H71: clinical results and metabolic profile. *Invest New Drugs* **36**, 230-239
159. Garg, G., Khandelwal, A., and Blagg, B. S. J. (2016) Anticancer Inhibitors of Hsp90 Function: Beyond the Usual Suspects. *Adv Cancer Res* **129**, 51-88

160. Butler, L. M., Ferraldeschi, R., Armstrong, H. K., Centenera, M. M., and Workman, P. (2015) Maximizing the Therapeutic Potential of HSP90 Inhibitors. *Mol Cancer Res* **13**, 1445-1451
161. Bagatell, R., Paine-Murrieta, G. D., Taylor, C. W., Pulcini, E. J., Akinaga, S., Benjamin, I. J., and Whitesell, L. (2000) Induction of a Heat Shock Factor 1-dependent Stress Response Alters the Cytotoxic Activity of Hsp90-binding Agents. *Clinical Cancer Research* **6**, 3312
162. Mak, O. W., Chand, R., Reynisson, J., and Leung, I. K. H. (2019) Identification of Isoform-Selective Ligands for the Middle Domain of Heat Shock Protein 90 (Hsp90). *Int J Mol Sci* **20**, 5333
163. Stothert, A. R., Suntharalingam, A., Tang, X., Crowley, V. M., Mishra, S. J., Webster, J. M., Nordhues, B. A., Huard, D. J. E., Passaglia, C. L., Lieberman, R. L., Blagg, B. S. J., Blair, L. J., Koren, J., 3rd, and Dickey, C. A. (2017) Isoform-selective Hsp90 inhibition rescues model of hereditary open-angle glaucoma. *Sci Rep* **7**, 17951
164. Gutiérrez-Vázquez, C., and Quintana, F. J. (2018) Regulation of the Immune Response by the Aryl Hydrocarbon Receptor. *Immunity* **48**, 19-33
165. Esser, C. (2016) The Aryl Hydrocarbon Receptor in Immunity: Tools and Potential. in *Suppression and Regulation of Immune Responses: Methods and Protocols, Volume II* (Cuturi, M. C., and Anegon, I. eds.), Springer New York, New York, NY. pp 239-257
166. Kawajiri, K., and Fujii-Kuriyama, Y. (2017) The aryl hydrocarbon receptor: a multifunctional chemical sensor for host defense and homeostatic maintenance. *Experimental Animals* **66**, 75-89
167. Vogel, C. F., Goth, S. R., Dong, B., Pessah, I. N., and Matsumura, F. (2008) Aryl hydrocarbon receptor signaling mediates expression of indoleamine 2,3-dioxygenase. *Biochem Biophys Res Commun* **375**, 331-335
168. Denis, M., Cuthill, S., Wikström, A. C., Poellinger, L., and Gustafsson, J. A. (1988) Association of the dioxin receptor with the Mr 90,000 heat shock protein: a structural kinship with the glucocorticoid receptor. *Biochem Biophys Res Commun* **155**, 801-807
169. Perdew, G. H. (1988) Association of the Ah receptor with the 90-kDa heat shock protein. *J Biol Chem* **263**, 13802-13805
170. Carver, L. A., and Bradfield, C. A. (1997) Ligand-dependent interaction of the aryl hydrocarbon receptor with a novel immunophilin homolog in vivo. *J Biol Chem* **272**, 11452-11456
171. Pongratz, I., Mason, G. G., and Poellinger, L. (1992) Dual roles of the 90-kDa heat shock protein hsp90 in modulating functional activities of the dioxin receptor. Evidence that the dioxin receptor functionally belongs to a subclass of nuclear receptors which require hsp90 both for ligand binding activity and repression of intrinsic DNA binding activity. *J Biol Chem* **267**, 13728-13734
172. Hankinson, O. (2005) Role of coactivators in transcriptional activation by the aryl hydrocarbon receptor. *Arch Biochem Biophys* **433**, 379-386
173. Schnekenburger, M., Peng, L., and Puga, A. (2007) HDAC1 bound to the Cyp1a1 promoter blocks histone acetylation associated with Ah receptor-mediated trans-activation. *Biochim Biophys Acta* **1769**, 569-578
174. Beischlag, T. V., Wang, S., Rose, D. W., Torchia, J., Reisz-Porszasz, S., Muhammad, K., Nelson, W. E., Probst, M. R., Rosenfeld, M. G., and Hankinson, O. (2002) Recruitment of the NCoA/SRC-1/p160 family of transcriptional coactivators by the aryl hydrocarbon receptor/aryl hydrocarbon receptor nuclear translocator complex. *Mol Cell Biol* **22**, 4319-4333

175. Ohtake, F., Baba, A., Takada, I., Okada, M., Iwasaki, K., Miki, H., Takahashi, S., Kouzmenko, A., Nohara, K., Chiba, T., Fujii-Kuriyama, Y., and Kato, S. (2007) Dioxin receptor is a ligand-dependent E3 ubiquitin ligase. *Nature* **446**, 562-566
176. Opitz, C. A., Litzenburger, U. M., Sahm, F., Ott, M., Tritschler, I., Trump, S., Schumacher, T., Jestaedt, L., Schrenk, D., Weller, M., Jugold, M., Guillemin, G. J., Miller, C. L., Lutz, C., Radlwimmer, B., Lehmann, I., von Deimling, A., Wick, W., and Platten, M. (2011) An endogenous tumour-promoting ligand of the human aryl hydrocarbon receptor. *Nature* **478**, 197-203
177. Gramatzki, D., Pantazis, G., Schittenhelm, J., Tabatabai, G., Köhle, C., Wick, W., Schwarz, M., Weller, M., and Tritschler, I. (2009) Aryl hydrocarbon receptor inhibition downregulates the TGF-beta/Smad pathway in human glioblastoma cells. *Oncogene* **28**, 2593-2605
178. Andersson, P., McGuire, J., Rubio, C., Gradin, K., Whitelaw, M. L., Pettersson, S., Hanberg, A., and Poellinger, L. (2002) A constitutively active dioxin/aryl hydrocarbon receptor induces stomach tumors. *Proceedings of the National Academy of Sciences* **99**, 9990
179. Moennikes, O., Loeppen, S., Buchmann, A., Andersson, P., Ittrich, C., Poellinger, L., and Schwarz, M. (2004) A constitutively active dioxin/aryl hydrocarbon receptor promotes hepatocarcinogenesis in mice. *Cancer Res* **64**, 4707-4710
180. Zudaire, E., Cuesta, N., Murty, V., Woodson, K., Adams, L., Gonzalez, N., Martínez, A., Narayan, G., Kirsch, I., Franklin, W., Hirsch, F., Birrer, M., and Cuttitta, F. (2008) The aryl hydrocarbon receptor repressor is a putative tumor suppressor gene in multiple human cancers. *J Clin Invest* **118**, 640-650
181. Gabriely, G., Wheeler, M. A., Takenaka, M. C., and Quintana, F. J. (2017) Role of AHR and HIF-1α in Glioblastoma Metabolism. *Trends Endocrinol Metab* **28**, 428-436
182. Haslbeck, V., Kaiser, C. J. O., and Richter, K. (2012) Hsp90 in non-mammalian metazoan model systems. *Biochimica et Biophysica Acta (BBA) - Molecular Cell Research* **1823**, 712-721
183. Richardson, J. M., Dornan, J., Opamawutthikul, M., Bruce, S., Page, A. P., and Walkinshaw, M. D. (2007) Cloning, expression and characterisation of FKB-6, the sole large TPR-containing immunophilin from C. elegans. *Biochem Biophys Res Commun* **360**, 566-572
184. Zhi, X., Zhou, X. E., Melcher, K., Motola, D. L., Gelmedin, V., Hawdon, J., Kliewer, S. A., Mangelsdorf, D. J., and Xu, H. E. (2012) Structural conservation of ligand binding reveals a bile acid-like signaling pathway in nematodes. *J Biol Chem* **287**, 4894-4903
185. Antebi, A. (2006) Nuclear hormone receptors in C. elegans. *WormBook : the online review of C. elegans biology*, 1-13
186. Hu, P. J. (2007) Dauer. *WormBook*, 1-19
187. Ludewig, A. H., Kober-Eisermann, C., Weitzel, C., Bethke, A., Neubert, K., Gerisch, B., Hutter, H., and Antebi, A. (2004) A novel nuclear receptor/coregulator complex controls C. elegans lipid metabolism, larval development, and aging. *Genes Dev* **18**, 2120-2133
188. Haslbeck, V., Eckl, J. M., Drazic, A., Rutz, D. A., Lorenz, O. R., Zimmermann, K., Kriehuber, T., Lindemann, C., Madl, T., and Richter, K. (2015) The activity of protein phosphatase 5 towards native clients is modulated by the middle- and C-terminal domains of Hsp90. *Sci Rep* **5**, 17058
189. Yang, J., Roe, S. M., Cliff, M. J., Williams, M. A., Ladbury, J. E., Cohen, P. T., and Barford, D. (2005) Molecular basis for TPR domain-mediated regulation of protein phosphatase 5. *Embo j* **24**, 1-10

190. Yang, J., Roe, S. M., Cliff, M. J., Williams, M. A., Ladbury, J. E., Cohen, P. T. W., and Barford, D. (2005) Molecular basis for TPR domain-mediated regulation of protein phosphatase 5. *The EMBO Journal* **24**, 1-10
191. Wandinger, S. K., Suhre, M. H., Wegele, H., and Buchner, J. (2006) The phosphatase Ppt1 is a dedicated regulator of the molecular chaperone Hsp90. *The EMBO Journal* **25**, 367-376
192. Melesse, M., Sloan, D. E., Benthal, J. T., Caylor, Q., Gosine, K., Bai, X., and Bembenek, J. N. (2018) Genetic Identification of Separase Regulators in Caenorhabditis elegans. *G3 (Bethesda)* **8**, 695-705
193. Richie, C. T., Bembenek, J. N., Chestnut, B., Furuta, T., Schumacher, J. M., Wallenfang, M., and Golden, A. (2011) Protein phosphatase 5 is a negative regulator of separase function during cortical granule exocytosis in <em>C. elegans</em&gt. *Journal of Cell Science* **124**, 2903
194. Lauwers, E., Wang, Y.-C., Gallardo, R., Van der Kant, R., Michiels, E., Swerts, J., Baatsen, P., Zaiter, S. S., McAlpine, S. R., Gounko, N. V., Rousseau, F., Schymkowitz, J., and Verstreken, P. (2018) Hsp90 Mediates Membrane Deformation and Exosome Release. *Molecular Cell* **71**, 689-702.e689
195. Moschou, P. N., Smertenko, A. P., Minina, E. A., Fukada, K., Savenkov, E. I., Robert, S., Hussey, P. J., and Bozhkov, P. V. (2013) The Caspase-Related Protease Separase (EXTRA SPINDLE POLES) Regulates Cell Polarity and Cytokinesis in <em>Arabidopsis</em&gt. *The Plant Cell* **25**, 2171
196. Studier, F. W. (2005) Protein production by auto-induction in high density shaking cultures. *Protein Expr Purif* **41**, 207-234
197. Xiong, S., Zhang, L., and He, Q.-Y. (2008) Fractionation of Proteins by Heparin Chromatography. in *2D PAGE: Sample Preparation and Fractionation* (Posch, A. ed.), Humana Press, Totowa, NJ. pp 213-221
198. Jussupow, A., Messias, A. C., Stehle, R., Geerlof, A., Solbak, S. M. Ø., Paissoni, C., Bach, A., Sattler, M., and Camilloni, C. (2020) The dynamics of linear polyubiquitin. *Science Advances* **6**, eabc3786
199. Hellman, L. M., and Fried, M. G. (2007) Electrophoretic mobility shift assay (EMSA) for detecting protein–nucleic acid interactions. *Nature Protocols* **2**, 1849-1861
200. Nørby, J. G. (1988) Coupled assay of Na+,K+-ATPase activity. *Methods Enzymol* **156**, 116-119
201. Ali, J. A., Jackson, A. P., Howells, A. J., and Maxwell, A. (1993) The 43-kilodalton N-terminal fragment of the DNA gyrase B protein hydrolyzes ATP and binds coumarin drugs. *Biochemistry* **32**, 2717-2724
202. Zhang, A., Hu, P., MacGregor, P., Xue, Y., Fan, H., Suchecki, P., Olszewski, L., and Liu, A. (2014) Understanding the Conformational Impact of Chemical Modifications on Monoclonal Antibodies with Diverse Sequence Variation Using Hydrogen/Deuterium Exchange Mass Spectrometry and Structural Modeling. *Analytical Chemistry* **86**, 3468-3475
203. Kazman, P., Vielberg, M. T., Pulido Cendales, M. D., Hunziger, L., Weber, B., Hegenbart, U., Zacharias, M., Köhler, R., Schönland, S., Groll, M., and Buchner, J. (2020) Fatal amyloid formation in a patient's antibody light chain is caused by a single point mutation. *Elife* **9**
204. Plum, S., Helling, S., Theiss, C., Leite, R. E. P., May, C., Jacob-Filho, W., Eisenacher, M., Kuhlmann, K., Meyer, H. E., Riederer, P., Grinberg, L. T., Gerlach, M., and Marcus, K. (2013) Combined enrichment of neuromelanin granules and synaptosomes from human substantia nigra pars compacta tissue for proteomic analysis. *J Proteomics* **94**, 202-206

205. Bracht, T., Schweinsberg, V., Trippler, M., Kohl, M., Ahrens, M., Padden, J., Naboulsi, W., Barkovits, K., Megger, D. A., Eisenacher, M., Borchers, C. H., Schlaak, J. F., Hoffmann, A.-C., Weber, F., Baba, H. A., Meyer, H. E., and Sitek, B. (2015) Analysis of Disease-Associated Protein Expression Using Quantitative Proteomics—Fibulin-5 Is Expressed in Association with Hepatic Fibrosis. *Journal of Proteome Research* **14**, 2278-2286
206. Cox, J., and Mann, M. (2008) MaxQuant enables high peptide identification rates, individualized p.p.b.-range mass accuracies and proteome-wide protein quantification. *Nat Biotechnol* **26**, 1367-1372
207. Yang, B., Wu, Y. J., Zhu, M., Fan, S. B., Lin, J., Zhang, K., Li, S., Chi, H., Li, Y. X., Chen, H. F., Luo, S. K., Ding, Y. H., Wang, L. H., Hao, Z., Xiu, L. Y., Chen, S., Ye, K., He, S. M., and Dong, M. Q. (2012) Identification of cross-linked peptides from complex samples. *Nat Methods* **9**, 904-906
208. Eswar, N., Webb, B., Marti-Renom, M. A., Madhusudhan, M. S., Eramian, D., Shen, M. Y., Pieper, U., and Sali, A. (2006) Comparative protein structure modeling using Modeller. *Curr Protoc Bioinformatics* **Chapter 5**, Unit-5.6
209. Pettersen, E. F., Goddard, T. D., Huang, C. C., Couch, G. S., Greenblatt, D. M., Meng, E. C., and Ferrin, T. E. (2004) UCSF Chimera--a visualization system for exploratory research and analysis. *J Comput Chem* **25**, 1605-1612
210. Kumar, R., Moche, M., Winblad, B., and Pavlov, P. F. (2017) Combined x-ray crystallography and computational modeling approach to investigate the Hsp90 C-terminal peptide binding to FKBP51. *Sci Rep* **7**, 14288
211. Haslbeck, V., Drazic, A., Eckl, J. M., Alte, F., Helmuth, M., Popowicz, G., Schmidt, W., Braun, F., Weiwad, M., Fischer, G., Gemmecker, G., Sattler, M., Striggow, F., Groll, M., and Richter, K. (2015) Selective activators of protein phosphatase 5 target the auto-inhibitory mechanism. *Biosci Rep* **35**
212. van Zundert, G. C. P., and Bonvin, A. M. J. J. (2015) DisVis: quantifying and visualizing accessible interaction space of distance-restrained biomolecular complexes. *Bioinformatics* **31**, 3222-3224
213. van Zundert, G. C. P., Trellet, M., Schaarschmidt, J., Kurkcuoglu, Z., David, M., Verlato, M., Rosato, A., and Bonvin, A. M. J. J. (2017) The DisVis and PowerFit Web Servers: Explorative and Integrative Modeling of Biomolecular Complexes. *Journal of Molecular Biology* **429**, 399-407
214. Irizarry, R. A., Hobbs, B., Collin, F., Beazer-Barclay, Y. D., Antonellis, K. J., Scherf, U., and Speed, T. P. (2003) Exploration, normalization, and summaries of high density oligonucleotide array probe level data. *Biostatistics* **4**, 249-264
215. Soroka, J., Wandinger, Sebastian K., Mäusbacher, N., Schreiber, T., Richter, K., Daub, H., and Buchner, J. (2012) Conformational Switching of the Molecular Chaperone Hsp90 via Regulated Phosphorylation. *Molecular Cell* **45**, 517-528
216. Grenert, J. P., Johnson, B. D., and Toft, D. O. (1999) The Importance of ATP Binding and Hydrolysis by Hsp90 in Formation and Function of Protein Heterocomplexes *. *Journal of Biological Chemistry* **274**, 17525-17533
217. Richter, K., Walter, S., and Buchner, J. (2004) The Co-chaperone Sba1 connects the ATPase reaction of Hsp90 to the progression of the chaperone cycle. *J Mol Biol* **342**, 1403-1413
218. Eckl, J. M., Drazic, A., Rutz, D. A., and Richter, K. (2014) Nematode Sgt1-homologue D1054.3 binds open and closed conformations of Hsp90 via distinct binding sites. *Biochemistry* **53**, 2505-2514

219. Sullivan, W. P., Owen, B. A. L., and Toft, D. O. (2002) The Influence of ATP and p23 on the Conformation of hsp90 *. *Journal of Biological Chemistry* **277**, 45942-45948
220. Smith, D. F. (1993) Dynamics of heat shock protein 90-progesterone receptor binding and the disactivation loop model for steroid receptor complexes. *Mol Endocrinol* **7**, 1418-1429
221. Hinds, T. D., Jr., and Sánchez, E. R. (2008) Protein phosphatase 5. *Int J Biochem Cell Biol* **40**, 2358-2362
222. Dominguez, C., Boelens, R., and Bonvin, A. M. (2003) HADDOCK: a protein-protein docking approach based on biochemical or biophysical information. *J Am Chem Soc* **125**, 1731-1737
223. van Zundert, G. C. P., Rodrigues, J. P. G. L. M., Trellet, M., Schmitz, C., Kastritis, P. L., Karaca, E., Melquiond, A. S. J., van Dijk, M., de Vries, S. J., and Bonvin, A. M. J. J. (2016) The HADDOCK2.2 Web Server: User-Friendly Integrative Modeling of Biomolecular Complexes. *Journal of Molecular Biology* **428**, 720-725
224. Denny, W. B., Valentine, D. L., Reynolds, P. D., Smith, D. F., and Scammell, J. G. (2000) Squirrel monkey immunophilin FKBP51 is a potent inhibitor of glucocorticoid receptor binding. *Endocrinology* **141**, 4107-4113
225. Richter, K., Soroka, J., Skalniak, L., Leskovar, A., Hessling, M., Reinstein, J., and Buchner, J. (2008) Conserved conformational changes in the ATPase cycle of human Hsp90. *J Biol Chem* **283**, 17757-17765
226. Gaiser, A. M., Brandt, F., and Richter, K. (2009) The non-canonical Hop protein from Caenorhabditis elegans exerts essential functions and forms binary complexes with either Hsc70 or Hsp90. *J Mol Biol* **391**, 621-634
227. Seitz, T., Thoma, R., Schoch, G. A., Stihle, M., Benz, J., D'Arcy, B., Wiget, A., Ruf, A., Hennig, M., and Sterner, R. (2010) Enhancing the stability and solubility of the glucocorticoid receptor ligand-binding domain by high-throughput library screening. *J Mol Biol* **403**, 562-577
228. Meijsing, S. H., Pufall, M. A., So, A. Y., Bates, D. L., Chen, L., and Yamamoto, K. R. (2009) DNA binding site sequence directs glucocorticoid receptor structure and activity. *Science* **324**, 407-410
229. Eckl, J., Sima, S., Marcus, K., Lindemann, C., and Richter, K. (2017) Hsp90-downregulation influences the heat-shock response, innate immune response and onset of oocyte development in nematodes. *PLoS One* **12**, e0186386
230. Papsdorf, K., Sima, S., Richter, G., and Richter, K. (2016) Construction and evaluation of yeast expression networks by database-guided predictions. *Microb Cell*. 10.15698/mic2016.06.505
231. Sima, S., Schmauder, L., and Richter, K. (2019) Genome-wide analysis of yeast expression data based on a priori generated co-regulation cliques. *Microb Cell* **6**, 160-176
232. Montojo, J., Zuberi, K., Rodriguez, H., Kazi, F., Wright, G., Donaldson, S. L., Morris, Q., and Bader, G. D. (2010) GeneMANIA Cytoscape plugin: fast gene function predictions on the desktop. *Bioinformatics* **26**, 2927-2928
233. He, X., Zhang, S., Chen, J., and Li, D. (2019) Increased LGALS3 expression independently predicts shorter overall survival in patients with the proneural subtype of glioblastoma. *Cancer Med* **8**, 2031-2040
234. Stancato, L. F., Hutchison, K. A., Krishna, P., and Pratt, W. B. (1996) Animal and plant cell lysates share a conserved chaperone system that assembles the glucocorticoid receptor into a functional heterocomplex with hsp90. *Biochemistry* **35**, 554-561

235. Reddy, T. E., Pauli, F., Sprouse, R. O., Neff, N. F., Newberry, K. M., Garabedian, M. J., and Myers, R. M. (2009) Genomic determination of the glucocorticoid response reveals unexpected mechanisms of gene regulation. *Genome Res* **19**, 2163-2171
236. Johnson, J. L. (2012) Evolution and function of diverse Hsp90 homologs and cochaperone proteins. *Biochimica et Biophysica Acta (BBA) - Molecular Cell Research* **1823**, 607-613
237. Polier, S., Samant, R. S., Clarke, P. A., Workman, P., Prodromou, C., and Pearl, L. H. (2013) ATP-competitive inhibitors block protein kinase recruitment to the Hsp90-Cdc37 system. *Nat Chem Biol* **9**, 307-312
238. Young, J. C., and Hartl, F. U. (2000) Polypeptide release by Hsp90 involves ATP hydrolysis and is enhanced by the co-chaperone p23. *Embo j* **19**, 5930-5940
239. Oroz, J., Chang, B. J., Wysoczanski, P., Lee, C. T., Pérez-Lara, Á., Chakraborty, P., Hofele, R. V., Baker, J. D., Blair, L. J., Biernat, J., Urlaub, H., Mandelkow, E., Dickey, C. A., and Zweckstetter, M. (2018) Structure and pro-toxic mechanism of the human Hsp90/PPIase/Tau complex. *Nat Commun* **9**, 4532
240. Zhang, J., Simisky, J., Tsai, F. T. F., and Geller, D. S. (2005) A critical role of helix 3–helix 5 interaction in steroid hormone receptor function. *Proceedings of the National Academy of Sciences of the United States of America* **102**, 2707-2712
241. Deng, Q., Waxse, B., Riquelme, D., Zhang, J., and Aguilera, G. (2015) Helix 8 of the ligand binding domain of the glucocorticoid receptor (GR) is essential for ligand binding. *Mol Cell Endocrinol* **408**, 23-32
242. Moffatt, N. S., Bruinsma, E., Uhl, C., Obermann, W. M., and Toft, D. (2008) Role of the cochaperone Tpr2 in Hsp90 chaperoning. *Biochemistry* **47**, 8203-8213
243. Farhan, S. M. K., Howrigan, D. P., Abbott, L. E., Klim, J. R., Topp, S. D., Byrnes, A. E., Churchhouse, C., Phatnani, H., Smith, B. N., Rampersaud, E., Wu, G., Wuu, J., Shatunov, A., Iacoangeli, A., Al Khleifat, A., Mordes, D. A., Ghosh, S., Eggan, K., Rademakers, R., McCauley, J. L., Schüle, R., Züchner, S., Benatar, M., Taylor, J. P., Nalls, M., Gotkine, M., Shaw, P. J., Morrison, K. E., Al-Chalabi, A., Traynor, B., Shaw, C. E., Goldstein, D. B., Harms, M. B., Daly, M. J., Neale, B. M., Consortium, A., Consortium, F., Project Min, E. C., and Consortium, C. R. (2019) Exome sequencing in amyotrophic lateral sclerosis implicates a novel gene, DNAJC7 , encoding a heat-shock protein. *Nature Neuroscience* **22**, 1966-1974
244. Kubo, N., Wu, D., Yoshihara, Y., Sang, M., Nakagawara, A., and Ozaki, T. (2013) Co-chaperon DnaJC7/TPR2 enhances p53 stability and activity through blocking the complex formation between p53 and MDM2. *Biochem Biophys Res Commun* **430**, 1034-1039
245. Xiang, S. L., Kumano, T., Iwasaki, S. I., Sun, X., Yoshioka, K., and Yamamoto, K. C. (2001) The J domain of Tpr2 regulates its interaction with the proapoptotic and cell-cycle checkpoint protein, Rad9. *Biochem Biophys Res Commun* **287**, 932-940
246. Diane, A., Mahmoud, N., Bensmail, I., Khattab, N., Abunada, H. A., and Dehbi, M. (2020) Alpha lipoic acid attenuates ER stress and improves glucose uptake through DNAJB3 cochaperone. *Sci Rep* **10**, 20482
247. Roosen, D. A., Blauwendraat, C., Cookson, M. R., and Lewis, P. A. (2019) DNAJC proteins and pathways to parkinsonism. *Febs j* **286**, 3080-3094
248. Brown, G. D., Willment, J. A., and Whitehead, L. (2018) C-type lectins in immunity and homeostasis. *Nat Rev Immunol* **18**, 374-389
249. Chiffoleau, E. (2018) C-Type Lectin-Like Receptors As Emerging Orchestrators of Sterile Inflammation Represent Potential Therapeutic Targets. *Front Immunol* **9**, 227

250. Idikio, H. A. (2011) Galectin-3 and Beclin1/Atg6 Genes In Human Cancers: Using cDNA Tissue Panel, qRT-PCR, and Logistic Regression Model to Identify Cancer Cell Biomarkers. *PLOS ONE* **6**, e26150
251. Chauhan, S., Kumar, S., Jain, A., Ponpuak, M., Mudd, M. H., Kimura, T., Choi, S. W., Peters, R., Mandell, M., Bruun, J. A., Johansen, T., and Deretic, V. (2016) TRIMs and Galectins Globally Cooperate and TRIM16 and Galectin-3 Co-direct Autophagy in Endomembrane Damage Homeostasis. *Dev Cell* **39**, 13-27
252. Hageman, J., and Kampinga, H. H. (2009) Computational analysis of the human HSPH/HSPA/DNAJ family and cloning of a human HSPH/HSPA/DNAJ expression library. *Cell Stress Chaperones* **14**, 1-21

7 Eidesstattliche Erklärung

Hiermit erkläre ich, Anna Kaziales, an Eides statt, dass ich die vorliegende Arbeit selbstständig verfasst und keine anderen als die angegebenen Quellen und Hilfsmittel verwendet habe. Aus fremden Quellen übernommene Gedanken sind als solche kenntlich gemacht. Die vorliegende Arbeit wurde noch keiner anderen Prüfungsbehörde vorgelegt. Teile dieser Arbeit wurden oder werden in wissenschaftlichen Journalen veröffentlicht.

Declaration

I, Anna Kaziales, hereby declare that this thesis was written by me independently and using only references and resources stated here. The work has so far not been submitted to any audit commission. Parts of this work are or will be published in scientific journals.

Datum, Unterschrift

8 Acknowledgements

I would first like to thank my PhD adviser, Klaus, for his guidance throughout this PhD, the opportunity to work on such fascinating topics and importantly, to learn by doing. I thank him for his trust and support. I would like to thank DFG and CIPSM for providing the funding for this work. I especially thank Johannes Buchner for the stimulating environment in Lehrstuhl Biotechnologie and for allowing me to use the JB labs and equipment.

I am very thankful to Martin Haslbeck, Margot Rubinstein and Marion Suttner for their support with running the Richter lab. Many thanks to Bettina Richter, Anja Osterauer, Gina Feind, Florian Rührnößl, Ruby Khan and Laura Meier for the excellent and friendly technical assistance throughout this work. Lukas Schmauder thank you for your precious help in running our Richter labs and the nice break and office times, it was great to have a colleague like you. Siyuan Sima thank you for introducing me to the lab and for diverse discussions. Furthermore, I would like to thank Philip, Lilly, Ben, Ruslana, Tobi and Jan for the excellent practical assistance and fun Mensa and lab times. A big thank you to all the current and former Buchner and Richter lab colleagues for sharing their knowledge, creating this nice atmosphere and celebrations to remember.

I wish to thank Florian Rührnößl, Adrian Drazic and the Arnesen lab, Katrin Marcus, Katalin Barkovits, Maike Krause, Christopher Möhle, Thomas Stempfl and Ralf Stehle for the fruitful collaborations and the fascinating measurements they made possible.

Last but not least I want to thank my family for their wonderful support throughout my studies and also my lovely friends that made this experience so much fun.